OUKA
The University of Osaka
Institutional Knowledge Archive

Title	Phase-Averaged SPIV Wake Field Measuremet for KVLCC2 Propeller Plane in Waves
Author(s)	Kim, Ho
Citation	大阪大学, 2014, 博士論文
Version Type	VoR
URL	https://doi.org/10.18910/50513
rights	
Note	

The University of Osaka Institutional Knowledge Archive : OUKA

https://ir.library.osaka-u.ac.jp/

The University of Osaka

Doctoral Dissertation

Phase-Averaged SPIV Wake Field Measurement for KVLCC2 Propeller Plane in Waves

Kim Ho

July 2014

Department of Naval Architecture and Ocean Engineering Graduate School of Engineering

Osaka University Japan

TABLE OF CONTENTS

List of tables ---- 4

List of figures ---- 5

CHAPTER 1: INTRODUCTION ---- 10

CHAPTER 2: TEST DESIGN ---- 14

2.1 Facility and coordinate system ---- 14

2.1.1 Towing tank ---- 14

2.1.2 Coordinate system ---- 16

2.2 Ship geometry ---- 16

2.3 EFD setup and conditions with free surge ---- ---- 18

2.4 Stereo PIV system ---- 21

2.4.1 Stereo PIV set up ---- 21

2.5 New measurement technique ---- 27

2.6 Application result of phase synchronizer system ---- 29

CHAPTER 3: SHIP MOTION AND ADDED RESISTANCE ---- 31

3.1 Calm water result ---- 31

3.2 Fully – loaded condition ---- 32

3.2.1 Time history study ---- 32

3.2.2 RAOs of added resistance and ship motions ---------- 33

3.3 Ballast condition ---------- 39

3.3.1 RAOs of added resistance and ship motions. ---------- 39

CHAPTER 4: STEREO PIV MEASUREMENT RESULTS ---------- 43

4.1 Velocity distribution at propeller plane in fully-loaded condition ---------- 43

4.1.1 Velocity distribution at propeller plane in calm water condition --------- 43

4.1.2 Velocity distribution at propeller plane, λ/L=0.6 ---------- 44

4.1.3 Velocity distribution at propeller plane, λ/L=1.1 ---------- 53

4.1.4Velocity distribution at propeller plane, λ/L=1.6 ---------- 66

4.2 Velocity distribution at propeller plane in ballast condition ---------- 73

4.2.1 Velocity distribution at propeller plane in ballast condition ---------- 73

4.2.2 Velocity distribution at propeller plane in ballast condition ---------- 74

4.2.3 Velocity distribution at propeller plane, λ/L=0.6 ---------- 76

4.2.4 Velocity distribution at propeller plane, λ/L=0.9 ---------- 84

4.2.5 Velocity distribution at propeller plane, λ/L=1.5 ---------- 92

CHAPTER 5: CONCLUSIOM AND FUTURE WORK ---------- 98

Reference ---------- 100

Acknowledgement ---------- 104

Appendix ---------- 105

List of publications ---------- 115

Curriculum vitae ---------- 116

List of tables

Table 2-1 Principal particular of ship model ---------- 17

Table 2-2 Experimental conditions ---------- 19

Table 2.3 Camera angle and Standoff distance ---------- 23

Table 2.4 Principal particular of SPIV system ---------- 25

Table 3-1 Comparison of CFD and EFD resistance force and motions for resistance test in calm water. ---------- 31

Table 3-2 Running mean and running RMS of EFD and CFD time histories. ---- 32

Table 3-3. Symbols used in figures ---------- 39

List of figures

Fig. 2-1 Osaka University towing tank facility ---------- 14

Fig. 2-2 Coordinate system ---------- 16

Fig. 2-3 KVLCC2 body plan and hull form ---------- 17

Fig. 2-4 EFD set up for free surge condition ---------- 18

Fig. 2-5 LaVision Stereo PIV System ---------- 22

Fig. 2-6 Schematic view of camera angle with distance ---------- 23

Fig. 2-7 Stereo PIV system installed on the towing carriage ---------- 24

Fig. 2-8 Schematic view of seeding ejection system ---------- 26

Fig. 2-9 Arrangement of Total experimental setup ---------- 27

Fig. 2-10 Phase synchronizer system ---------- 28

Fig. 2-11 Time history of wave elevation, force and motions ---------- 29

Fig. 2-12 Example of TTL signal and heave motion ---------- 29

Fig. 2-13 Particle images example (camera1, first exploration) ---------- 30

Fig. 3-1 The RAOs of heave amplitude and phase at Fr=0.142 ---------- 35

Fig. 3-2 The RAOs of pitch amplitude and phase at Fr=0.142 ---------- 36

Fig. 3-3 The RAOs of surge amplitude and phase at Fr=0.142 ---------- 37

Fig. 3-4 RAOs of added resistance at Fr=0.142 ---------- 38

Fig. 3-5 The RAOs of Heave amplitude ---------- 40

Fig. 3-6 The RAOs of Pitch amplitude ---------- 40

Fig. 3-7 The RAOs of Surge amplitude ---------- 41

Fig. 3-8 Added resistance for Ballast condition ---------- 41

Fig. 4-1 Velocity distribution in calm water ---------- 43

Fig. 4-2 Wave elevation and motions in one period (λ/L=0.6) ---------- 44

Fig. 4-3 Velocity distribution (λ/L=0.6), t/T=0.026 ---------- 45

Fig. 4-4 Velocity distribution (λ/L=0.6), t/T=0.149 ---------- 46

Fig. 4-5 Velocity distribution (λ/L=0.6), t/T=0.274 ---------- 47

Fig. 4-6 Velocity distribution (λ/L=0.6), t/T=0.398 ---------- 48

Fig. 4-7 Velocity distribution (λ/L=0.6), t/T=0.532 ---------- 49

Fig. 4-8 Velocity distribution (λ/L=0.6), t/T=0.656 ---------- 50

Fig. 4-9 Velocity distribution (λ/L=0.6), t/T=0.780 ---------- 51

Fig. 4-10 Velocity distribution (λ/L=0.6), t/T=0.905 ---------- 52

Fig. 4-11 Wave elevation and motion in one period (λ/L=1.1) ---------- 53

Fig. 4-12 Velocity distribution (λ/L=1.1), t/T=0.041 ---------- 54

Fig. 4-13 Velocity distribution (λ/L=1.1), t/T=0.130 ---------- 55

Fig. 4-14 Velocity distribution (λ/L=1.1), t/T=0.220 ---------- 56

Fig. 4-15 Velocity distribution (λ/L=1.1), t/T=0.309 ---------- 57

Fig. 4-16 Velocity distribution (λ/L=1.1), t/T=0.380 ---------- 58

Fig. 4-17 Velocity distribution (λ/L=1.1), t/T=0.469 ---------- 59

Fig. 4-18 Velocity distribution (λ/L=1.1), t/T=0.541 ---------- 60

Fig. 4-19 Velocity distribution (λ/L=1.1), t/T=0.630 ---------- 61

Fig. 4-20 Velocity distribution (λ/L=1.1), t/T=0.720 ---------- 62

Fig. 4-21 Velocity distribution (λ/L=1.1), t/T=0.809 ---------- 63

Fig. 4-22 Velocity distribution (λ/L=1.1), t/T=0.881 ---------- 64

Fig. 4-23 Velocity distribution (λ/L=1.1), t/T=0.970 ---------- 65

Fig. 4-24 Wave elevation and motion in one period (λ/L=1.6) ---------- 66

Fig. 4-25 Velocity distribution (λ/L=1.6), t/T=0.079 ---------- 67

Fig. 4-26 Velocity distribution (λ/L=1.6), t/T=0.235 ---------- 68

Fig. 4-27 Velocity distribution (λ/L=1.6), t/T=0.418 ---------- 69

Fig. 4-28 Velocity distribution (λ/L=1.6), t/T=0.574 ---------- 70

Fig. 4-29 Velocity distribution (λ/L=1.6), t/T=0.727 ---------- 71

Fig. 4-30 Velocity distribution (λ/L=1.6), t/T=0.926 ---------- 72

Fig. 4-31 Velocity distribution in calm water ---------- 73

Fig. 4-32 Velocity distribution (λ/L=0.6), t/T=0.034 ---------- 76

Fig. 4-33 Velocity distribution (λ/L=0.6), t/T=0.159 ---------- 77

Fig. 4-34 Velocity distribution (λ/L=0.6), t/T=0.284 ---------- 78

Fig. 4-35 Velocity distribution (λ/L=0.6), t/T=0.409 ---------- 79

Fig. 4-36 Velocity distribution (λ/L=0.6), t/T=0.534 ---------- 80

Fig. 4-37 Velocity distribution (λ/L=0.6), t/T=0.659 ---------- 81

Fig. 4-38 Velocity distribution (λ/L=0.6), t/T=0.784 ---------- 82

Fig. 4-39 Velocity distribution (λ/L=0.6), t/T=0.909 ---------- 83

Fig. 4-40 Velocity distribution (λ/L=0.9), t/T=0.0358 ---------- 84

Fig. 4-41 Velocity distribution (λ/L=0.9), t/T=0.1608 ---------- 85

Fig. 4-42 Velocity distribution (λ/L=0.9), t/T=0.2858 ---------- 86

Fig. 4-43 Velocity distribution (λ/L=0.9), t/T=0.4108 ---------- 87

Fig. 4-44 Velocity distribution (λ/L=0.9), t/T=0.5358 ---------- 88

Fig. 4-45 Velocity distribution (λ/L=0.9), t/T=0.6608 ---------- 89

Fig. 4-46 Velocity distribution (λ/L=0.9), t/T=0.7858 ---------- 90

Fig. 4-47 Velocity distribution (λ/L=0.9), t/T=0.9108 ---------- 91

Fig. 4-48 Velocity distribution (λ/L=1.5), t/T=0.074 ---------- 92

Fig. 4-49 Velocity distribution (λ/L=1.5), t/T=0.241 ---------- 93

Fig. 4-50 Velocity distribution (λ/L=1.5), t/T=0.407 ---------- 94

Fig. 4-51 Velocity distribution (λ/L=1.5), t/T=0.574 ---------- 95

Fig. 4-52 Velocity distribution (λ/L=1.5), t/T=0.741 ---------- 96

Fig. 4-53 Velocity distribution (λ/L=1.5), t/T=0.9071 ---------- 97

CHAPTER 1: INTRODUCTION

In the ship design process, the study of behavior and performance of the ships in sea waves are very important. Prediction of ship propulsion performance and ship motions represents an important challenge for ship-owners due to economic operation in terms of choice of fuel consumption and route-time evaluation. Therefore, these problems should be considered already in the early stages of the ship design. Many researchers have investigated the ship propulsion performance in waves (Nakamura et al., 1975). conducted with a model of single screw high speed container ship, resistance and self-propulsion tests in regular and irregular waves. Moreover, in order to clarify the characteristics of self-propulsion factors in waves, it seems to be necessary to measure the inflow velocity distribution into the propeller disk. So, Nakamura et al.(1975) measured the radial distribution of inflow velocity in propeller disk by use of a circular ring type wake meter. Nominal wake field in waves were measured by a few researchers using five holes Pitot tube. O'Dea et al. (1992) studied experimentally heave and pitch motions for a model of the S-175 containership advancing in head regular waves and identified nonlinear effects on the vertical motions. Adegeest (1995) carried out experiments for two Wigley hulls, the original and a modified one with different bow and significant flare. Adegeest (1995) presented heave and pitch motions of the models advancing in head regular waves, as well as vertical shear forces and bending moments at midship. The results showed negligible nonlinearity in heave and pitch motions. Ogiwara and Yamashita (1996) conducted an experimental study on added resistance in regular short-length head waves. They found that the resistance owing to diffraction of waves on the bow is attributed to a pressure increase on a very narrow area of hull

surface along the wave profile in steady state. Naito et al. (1996) studied the impact of above-water bow shape on added resistance in waves. Two above-water bow shapes were introduced for the reduction of added resistance in waves. They explained the mechanism of the reduction of added resistance with changing the above-water bow shape. The effects of above-water bow shape is also confirmed by Matsumoto et al. (1998) and Hirota et al. (2005) such that the added resistance can be reduced by 20-30% by modifying the shape of above-water of the bow. Kim (1998) presented experimental and computational results of added resistance of the FFG-7 class frigate in waves. Experiments were also performed for self-propulsion model and it was found that self-propulsion did not have a strong effect on the measured added resistance. Nonlinear effects of the waves loads were studied experimentally by Mizokami et al. (2001) for a container ship and strong nonlinearity were found for vertical bending moment and wave-induced pressure. Tsukada et al. (1997) measured the unsteady ship wakes in regular waves by a five Pitot tube for understanding fluctuation of mean wake and circulation in propeller disk. Using five holes tube or ring velocity meter, it seems that the response time or resolution may be a problem to get the second harmonic or higher harmonic of velocity field. Some studies exist on prediction of inflow by direct measurement of thrust force or torque. Ueno et al. (2013) conducted for free running test using a 4m container ship model in regular and irregular waves. From the thrust or torque measurement, they predicted the effective inflow velocity using thrust or torque identity method for time history of thrust or torque. The relative longitudinal flow velocity at the sides of the propeller in regular and irregular waves measured using vane-wheel current meters and compared with the predicted effective inflow velocity. However, some problems regarding measurement phase may occur due to the gravity

gradient component of the shaft and propeller that affects thrust measurements and response of spring-mass system. For the prediction of inflow velocity to the propeller, the orbital velocity and ship motion were mainly considered in the previous studies. The velocity distribution at propeller plane has not been measured for many ship shapes due to the difficulty of experiment.

On the contrary, by the rapid advances in computational fluid dynamics (CFD) technique, the flow field around a moving ship in waves can be computed by many researchers or commercial code and the complicated phenomena has been shown. But the validation data for detailed flow field is not fully available. In parallel, PIV studies for ship velocity fields have been conducted for various specialized purposes, as reviewed by Longo et al. (2004). Fu et al. (2002) apply digital PIV and the auto-correlation evaluation method in a rotating arm basin to study dominant cross-flow separation induced by a 5.18 m submarine model in a turn. Calcagno et al. (2002) use 3D, stereoscopic PIV in a circulating water tunnel to investigate the turbulent propeller wake flow of a 6.096 m ship model equipped with a 0.222 m diameter, 5-bladed propeller. The phase-averaged data highlights the interactions of the turbulent wake of the hull and propulsor, tip vortex system, slipstream contraction, and strong diffusion and dissipation of the propeller blade wakes. Cotroni et al. (2000) and Di Felice et al. (2000) investigate the phase-averaged wake flow of two, 4-bladed propellers in a cavitation tunnel using digital PIV, the cross-correlation evaluation method, and uncertainty assessment. The phase averaged flow measurements were done for diffraction problems by Gui L et al. (2002) by rotating 2D PIV of 90 degree to measure the three velocity components. It includes the unsteady resistance, heave force, pitch moment and free-surface elevations for DTMB 5512 at steady forward speed in

regular head waves in the IIHR towing tank. Paik et al., (2004) successfully used PIV to study a ship model's wake, their study was still a fixed PIV system in a relatively smaller test facility. This implies that a ship model's complete characteristics could only be known either by a resistance/motion test in a towing tank using a larger scaled model plus a flow field test in an open channel using a smaller model, or by doing all tests using the same smaller model in an open channel with larger uncertainty of the important resistance–velocity relationship due to scale effect. Experiments using a moving PIV system in a towing tank have rarely been reported. J, Longo et al. (2006) performed for a surface combatant advancing in calm water as it undergoes planar motion mechanism maneuver in the towing tank. But the detailed flow field around a ship with motion in waves is not available.

So, in this study, phase-averaged flow fields in waves were measured in the towing tank around the KVLCC2 ship model which has propeller dummy hub by using stereo PIV system and phase synchronizer with heave motion. The model tests have been carried out for fully-loaded condition and ballast condition in the condition of surge, heave and pitch free at forward speed Fr=0.142 (Re=2.55×106) in various head waves and one calm water condition. Some repeated tests are also performed to check the repeatability. The fluctuation of propeller plane wake is discussed based on the measured results. Although some preliminary results were already compared with CFD computation (Sadat Hosseini et al. 2013), the measurement system for phase averaged flow field for the free heave, serge and pitch motion and results are shown in this paper. The motion and force measurement was reported in Sadat-Hosseini et al. (2010).

CHAPTER 2: TEST DESIGN

2.1 FACILITY AND COODINATE SYSTEM

2.1.1 Towing tank



Towing tank



Towing carriage



Wave generator

Fig. 2-1 Osaka University towing tank facility

Tests are conducted at Osaka University towing tank shown in Fig. 2-1. The tank is 100 m long, 7.8 m wide and 4.35 m deep, and equipped with a drive carriage (7.4m in

length, 7.8m in width, and 6.4 m height) running from 0.01 to 3.5 m/s, automated wave damper system, and wave-dampening beach. It is also equipped with plunger-type wave maker generating regular and irregular waves up to 500 mm wave height and wave length of 0.5 to 15m. The wave absorber is a small fixed gridiron beach. The drive carriage is instrumented with several data-acquisition computers, speed circuit, and signal conditioning for analog voltage measurements of such as forces and moments, ship motions, and carriage speed. Wave dampeners and the wave-dampening beach enable fifteen-minute intervals between one carriage runs that is determined sufficient based on visual inspection of the free surface.

2.1.2 Coordinate system

Fig. 2-2 show the coordinate system and It is fixed on the constant speed towing carriage and the origin is located at center of gravity in calm water before the carriage run, x is flow direction (opposite to forward direction), y is horizontal in starboard direction and z is in vertical upward direction, respectively.

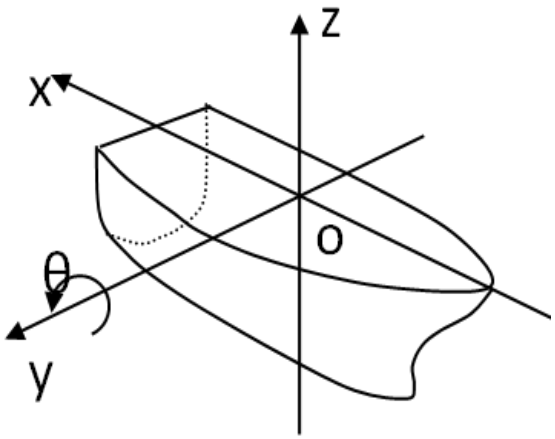


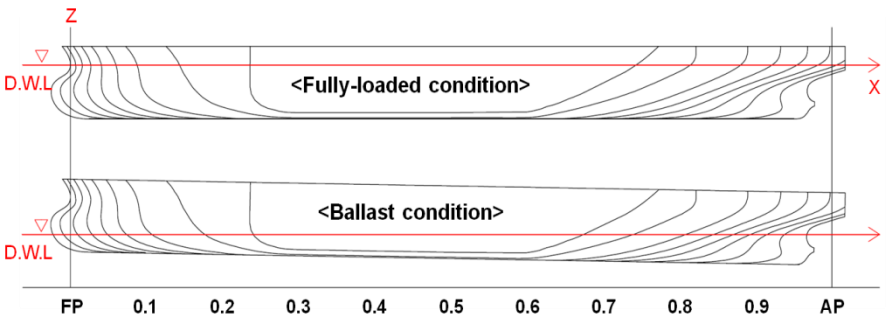
Fig. 2-2 Coordinate system

2.2 SHIP GEOMETRY

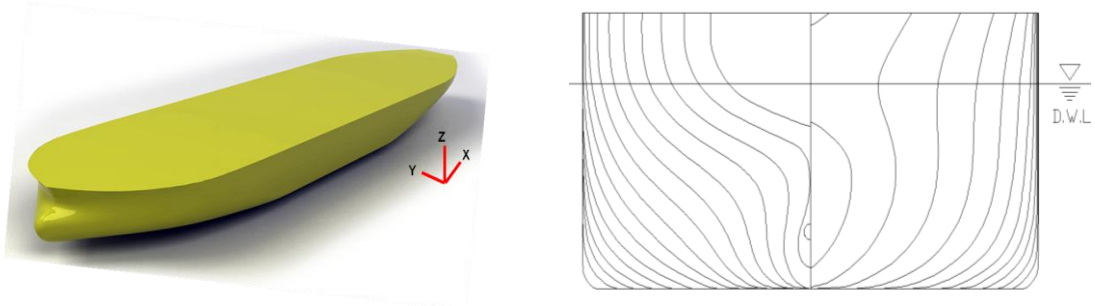
The experiments were conducted for bare hull KVLCC2 ship model appended with propeller shaft, dummy boss and boss cap which is a modern commercial tanker ship. The model was manufactured of wood with scale ratio of 1/100. Principal particular and hull form are shown in Fig. 2-3 and Table 2-1, respectively.

Table 2-1 Principal particular of ship model

		Fully-loaded cond.	Ballast cond.
Length between perpendiculars	L_{PP} (m)	3.200	
Beam	B_{WL} (m)	0.580	
Depth	(m)	0.30	
Draft	T (m)	0.208	T_F=0.067 T_A=0.119
Displacement	∇ (m^3)	0.313	0.126
Longitudinal center of buoyancy	LCB(%L_{PP}), fwd+	3.48	-0.923
Vertical Center of Gravity (from keel)	KG (m)	0.186=KG_D	0.75KG_D
Radius of gyration	K_{XX} (m)	0.4B	
	K_{YY} (m)	0.25Lpp	
	K_{ZZ} (m)	0.25Lpp	
Block coefficient	C_B	0.8098	0.5725
Mid-ship section coefficient	C_M	0.9980	0.8245
Water plane area coefficient	C_W	0.9000	0.8218



KVLCC2 side view drawing for ballast condition



3-D view of ship model Body plan

Fig. 2-3 KVLCC2 body plan and hull form

2.3 EFD SETUP AND CONDITIONS WITH FREE SURGE

The free surge tests were conducted for a 1/100 scaled model. The experimental condition is shown in Table 2-2. The model were towed with light weight carriage connected to main carriage by mean of a spring to allow the model to be free in surge motion while it is free to heave and pitch, as shown in Fig. 2-4. The external force F_0 was used to avoid large stretch for spring. The mass of the model including hull and pitch free gimbals (shown by red color in Fig. 2-4) was m_1=306.2 Kg. The mass of dynamometer (blue part) and light weight carriage (green part) were m_2=6.4 Kg and m_3=2.5 Kg, respectively.

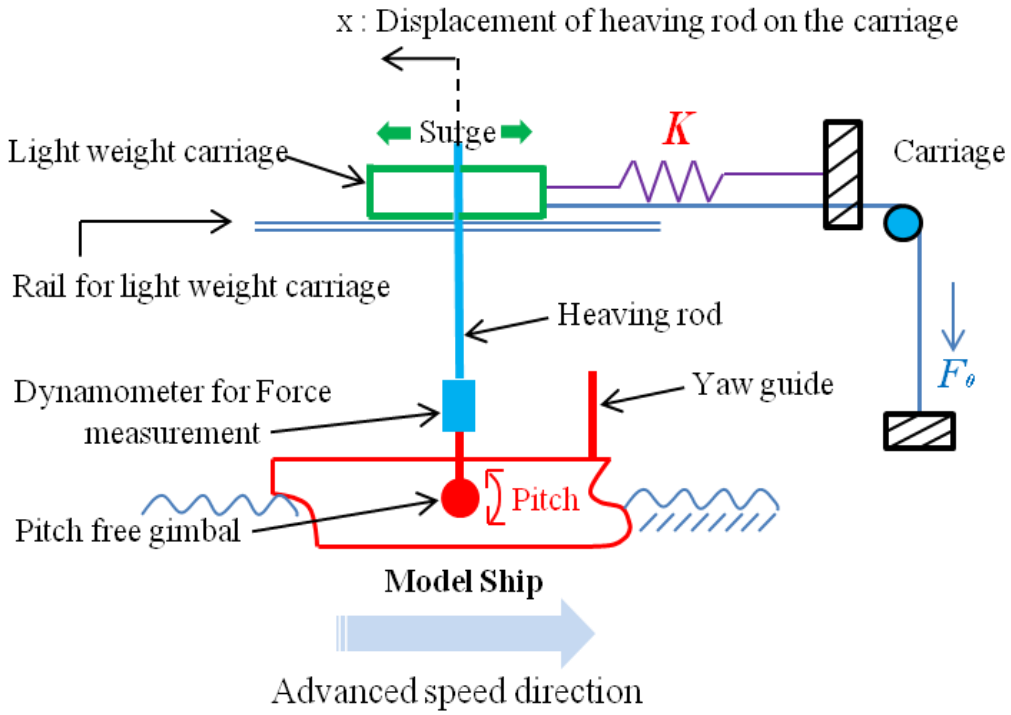


Fig. 2-4 EFD set up for free surge condition

Table 2-2 Experimental conditions

Fully-loaded condition		Ballast condition	
EFD	OU	**EFD**	OU
Model scale	1/100	**Model scale**	1/100
DOF*	3	**DOF***	3
Fr	0.1422	**Fr**	0.1422
Re×10⁶	2.546	**Re×10⁶**	2.546
λ/L	Calm 0.6 0.7 0.9 1.1 1.2 1.4 1.6 1.8 2	**λ/L**	Calm a:0.3 b:0.4 c:0.5 d: 0.6 0.7 0.9 1.1 1.2 1.4 1.6 1.8 2
A×10⁻³/L	9.375	**A×10⁻³/L**	a:5.0 b:6.719 c:8.281 d:9.375

Under the heaving rod, a load cell was installed to measure the longitudinal force (it is not hydrodynamic force acting on the ship). Under the load cell, the pitch free mount gimbal was installed at center of gravity. The pitch, heave and surge motions were measured by potentiometers. The very weak spring connected to light weight carriage and constant towing force acting to the very light carriage are mimicked by servo motor. The constant force is adjusted by preliminary tests to keep the mean surge is 0 (mean position on the light weight carriage is same). Wave elevation was measured in the front of the bows of a ship model to know the incident wave by servo type probe. Force and motion measurement results are shown in previous paper, Sadat-Hosseini et al. (2010).

But in the results in Sadat –Hosseini et al.,(2010) the mean surge is not zero due to the slight difference of constant force because the force is estimated before carriage run. So, for SPIV measurement, the force was adjusted by some preliminary carriage runs. But the low frequency (long period) surge motion due to mass weak spring system could not be eliminated. The amplitude of this surge motion was within 4mm, but the measurement plane for one phase move a little bit in x direction.

In the test, incident waves are 180degree heading waves. The experimental conditions for SPIV measurement were for various wave length (λ) ship length (L_{pp}) ratio, λ/L_{pp}=0.6, 1.1, 1.6(fully-loaded condition) and λ/L_{pp}=0.6, 0.9, 1.5(ballast condition). Incident wave height was set to be h=0.06m, but the real wave height vary a little bit.

The appropriate spring stiffness and external force F_0 were found based on the analytical solution of following 1DOF surge equation:

$$m\ddot{x} = F_x - Kx - F_0 \quad \text{---------- (1)}$$

where m is $m_1+m_2+m_3$, F_x is hydrodynamic force, and x is surge motion. The hydrodynamic force F_x can be assumed a linear superposition of added mass force ($-m_x\ddot{x}$), resistance in calm water (R_C), added resistance in waves (R_A), and wave force ($A\cos(\omega_e t)$).

Since the surge velocity is very close to carriage speed U_0, resistance force can be evaluated from resistance coefficient (C_T) at carriage speed:

$$\begin{aligned} R_C &= 1/2\rho S(-U_0 - \dot{x})^2 C_T \\ &\cong \underbrace{1/2\rho S U_0^2 C_T}_{R_{C_0}} + \rho S U_0 \dot{x} C_T \end{aligned} \quad \text{---------- (2)}$$

where R_{C0} is the resistance in calm water for the model advancing at U_0. Then, Eq. (1) and its solution can be written as follow:

$$(m+m_x)\ddot{x}+\rho SU_0\dot{x}+Kx=F'+A\cos\omega_e t \quad \text{---------- (3)}$$

$$x=\frac{F'}{K}-\frac{\omega_e{}^2(m+m_x)-K}{(\omega_e^2(m+m_x)-K)^2+(\rho SU_0)^2}A\cos\omega_e t+\frac{\rho SU_0}{(\omega_e^2(m+m_x)-K)^2+(\rho SU_0)^2}A\sin\omega_e t$$
$$+C_1e^{-\alpha t}\sin\sqrt{\omega_s{}^2-\alpha^2}\,t+C_2e^{-\alpha t}\cos\sqrt{\omega_s{}^2-\alpha^2}\,t \quad \text{---------- (4)}$$

where $F'=R_{C_0}+R_A-F_0$, $\alpha=-\rho SU_0/2(m+m_x)$, and $\omega_s=K/(m+m_x)$.

To avoid interfere of spring with surge motion due to waves, a weak spring compared with $(m+m_x)\omega_e{}^2$ has to be used, as shown in Eq. (4). The spring stiffness of K=98 N/m was used to satisfy $K<<(m+m_x)\omega_e{}^2$. The external force F_0 for each case was chosen close to $R_{C_0}+R_A$ (resistance + added resistance), which reduces the stretch of the spring by shifting mean value of surge motion around zero.

2.4 STEREO PIV SYSTEM

2.4.1 Stereo PIV set up

The stereo PIV is a LaVision Inc. custom-designed and built measurement system (Fig. 2-5). Shown camera sections are discontinued. All new camera sections have the camera above the mirror section. It consists of a 135 mJ double-pulsed YAG laser, submerged lightsheet generator, two sensor CCD cameras and computer and software for data acquisition and reduction of PIV recordings. The lenses are equipped with

motors for automatic remote focusing and aperture adjustments. The camera bodies are equipped with motors for automatic remote Scheimpflug angle adjustments. Both cameras are arranged asymmetrically in submerged enclosures downstream of the lightsheet to minimize wave and flow field effects of the enclosures at the measurement area. The laser, lightsheet generator, and camera enclosures are assembled on a lightweight matrix of aluminum extrusions for adjustability and rigidity. The SPIV system is calibrated in situ by submerging and fixing a two-tier LaVision calibration plate in the plane of the lightsheet where both camera field of views overlap.

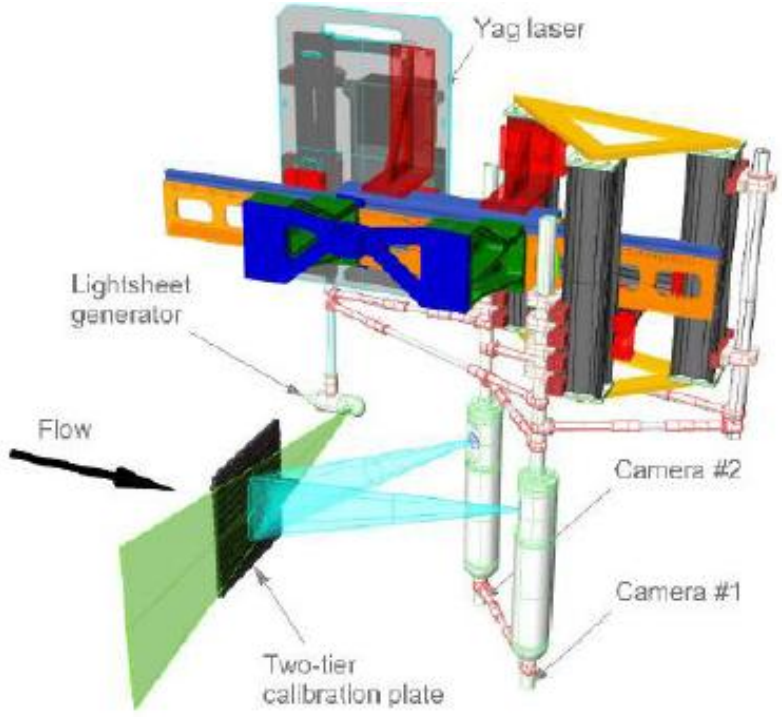


Fig. 2-5 LaVision Stereo PIV System

Single images from each camera are used to create a mapping function of the plate markers which is used later to reconstruct 3D velocity vectors from particle image pairs. The original calibration is refined iteratively with a self-calibration procedure to account for translational or rotational misalignment of the calibration plate in the lightsheet plane. The schematic view of camera angle with distance is as shown in fig. 2-6 and Table 2.3.

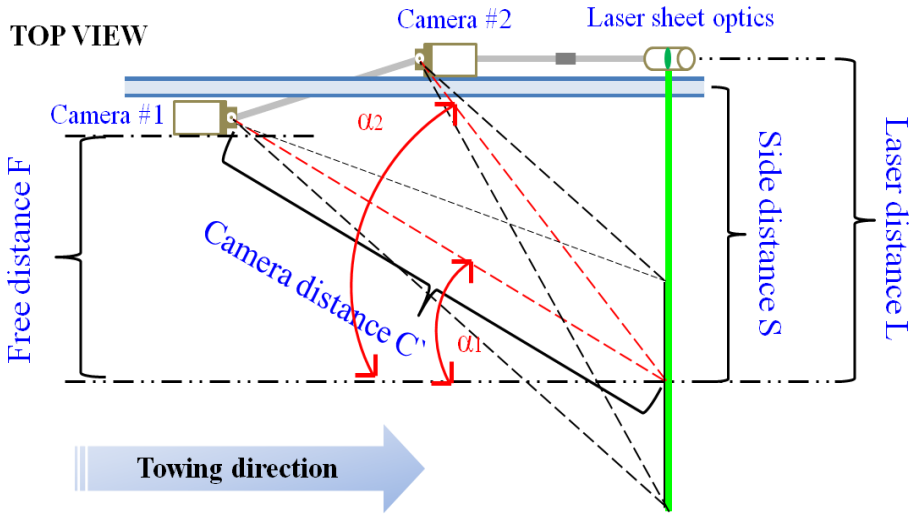


Fig. 2-6 Schematic view of camera angle with distance

Table 2.3 Camera angle and Standoff distance

Camera angle and Standoff distance	Symbol	Value
Camera 1 view angle	α1	22°
Camera 2 view angle	α2	55°
Camera to measurement center	C	890mm
Laser to measurement center	L	714mm
Side distance	S	614mm
Free distance	F	288mm

The cameras were mounted in surface piercing vertical pods (Diameter 90mm) with the glass window and 45 degree mirror. Cameras were in the pod looking downward and looking perpendicular to the glass window using mirror to avoid the large refractive index effect (the center of measurement section can be seen in air and water to adjust the camera). The CCD camera lenses are equipped with motors for automatic remote focusing and aperture adjustments. The camera bodies are equipped with motors for automatic remote Scheimpflug angle adjustments.

Total system installed in towing tank is shown in Fig. 2-7. The camera pod and pod for laser sheet object and arrangement of laser sheet and ship model can be seen in the figure. As shown in the figure, SPIV system was fixed on the carriage and the model moves around the original position by first harmonic (wave encounter frequency) and low frequency (natural frequency of weak spring and mass system). So, the measurement plane is not fixed on ship coordinate. Table 2.4 shows the principal particular of SPIV system.

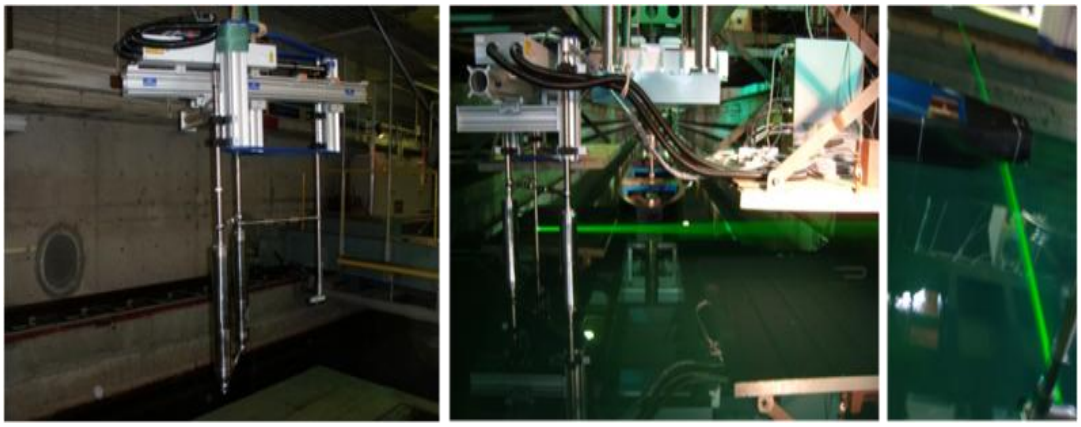


Fig. 2-7 Stereo PIV system installed on the towing carriage

Table 2.4 Principal particular of SPIV system

Field of view	120mm X 120mm
Camera resolution and model	1600 X 1600pixel, Image pro 2M
Laser and power	YAG Laser double pulse, Max 135 mJ
Frame rate	30 Hz
Max towing speed	2m/sec
Camera senor size	1.8 X 8.9mm
Seeding particle	Silver coated glass spheres Gravity : 1.7 g/ml, Diameter : 14μm
Software	LaVision DaVis 7.2

The seeding ejection " T " shape tubes with 14 holes in bottom tubing for SPIV measurement was constructed to distribute the seeding particle across a complete measurement area, as shown in Fig. 2-8. Conduct-O-FIL brand silver-coated hollow glass spheres produced by Potter Industries Inc, with a mean diameter of 14μm, gravity of approximately 1.7g/ml were used for seeding particles.

In the same time with SPIV measurement, force, heave, pitch, surge and wave elevation at several points were recorded. In this record, the TTL signal from phase synchronizer was also recorded. SPIV recordings are processed with LaVision DaVis v7.2 software in batch process. Laser light sheet measurement section was in the propeller plane for the original model position and the measurement plane can be shifted three-axis (x,y,z) by automated traverse system.

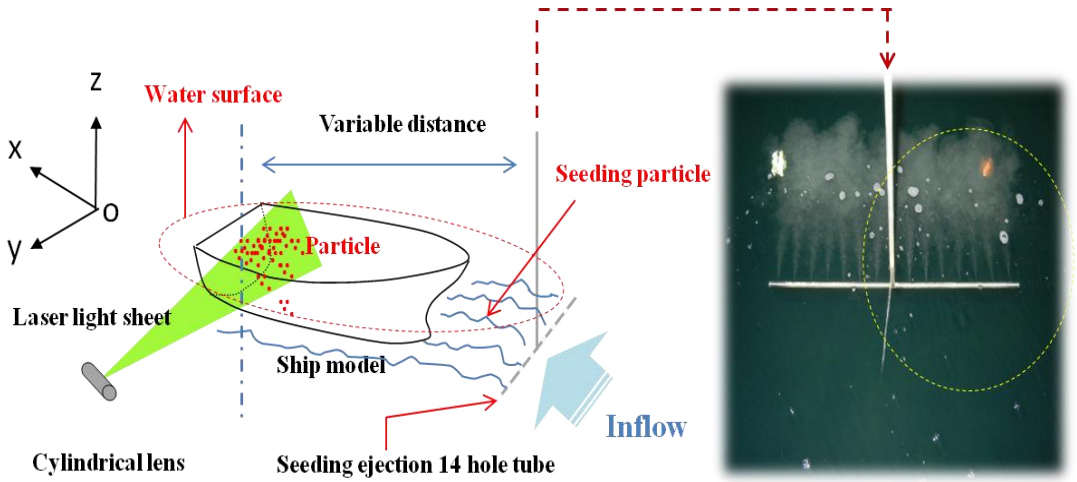


Fig. 2-8 Schematic view of seeding ejection system

In some measurement with large motion, the three measurement planes were used to know the flow characteristics. The SPIV system was installed on the towing carriage, so the velocity components measured in this paper are in the inertia coordinate fixed advancing with constant speed on the towing carriage, as shown in Fig. 2-9. So, the relative velocity to the propeller should be corrected considering ship motion. But in present experimental condition, the surge velocity due to motion was small. So, the measured values are shown in this paper. It should be noted that the long period surge due to mass-spring system exists and the measurement plane is shifted for each wave. In this paper, this effect is considered to be small due to longitudinal gradient in boundary layer is small and long period surge was kept to be small by careful release. Effect to axial velocity component considered to be very small, but the effect to the cross section components to the propeller should be modified using pitch motion effect. These correction and mean value in the propeller plane will be discussed in next stage.

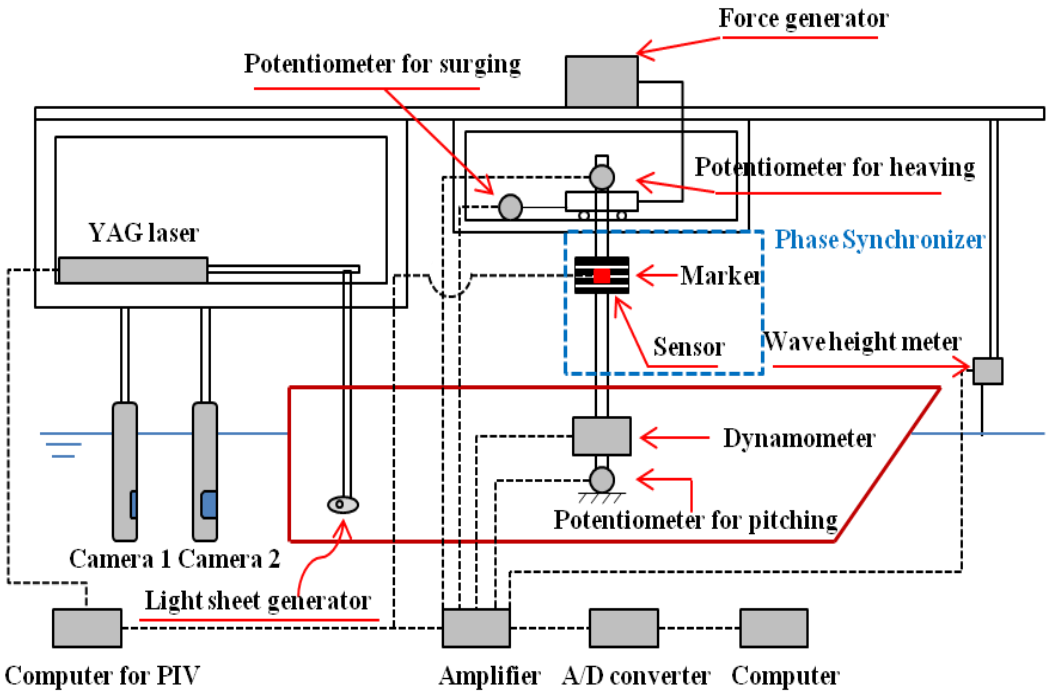


Fig. 2-9 Arrangement of Total experimental setup

2.5 NEW MEASUREMENT TECHNIQUE

The stereo PIV system can take particle image not only at a certain interval but at a certain moment by using external trigger signals. If the signal can be made at one phase in one encounter period, PIV system can take the images at one phase for many periods. In this study, a Laser sensor and a marker plate have been installed as a Phase synchronizer system aimed to send TTL signal to the PIV system according to heave motion. The heave motion was selected as a synchronization parameter because the heave motion was stable for all results in preliminary experiments and it was convenient for installation. To the maker plate fixed on the heaving rod, silver lines are

indicated at the same interval against the background black color. The silver lines are read by a laser sensor fixed on the towing carriage, and whenever the sensor goes through the line, TTL signal is sent to PIV system. The center line was set to capture the mean value of heave. The mean sinkage value and amplitude of heave motion was measured by preliminary experiments. The multiple lines could be used to measure multiple phase and the delay time from signal can be assigned in PIV program and used to shift the phase in real motion.

Phase synchronizer system is shown in Fig. 7. In the figure, three lines are used to measure for 6 phases. (0, 60, 120, 180, 240, 300 degree in one encounter period)

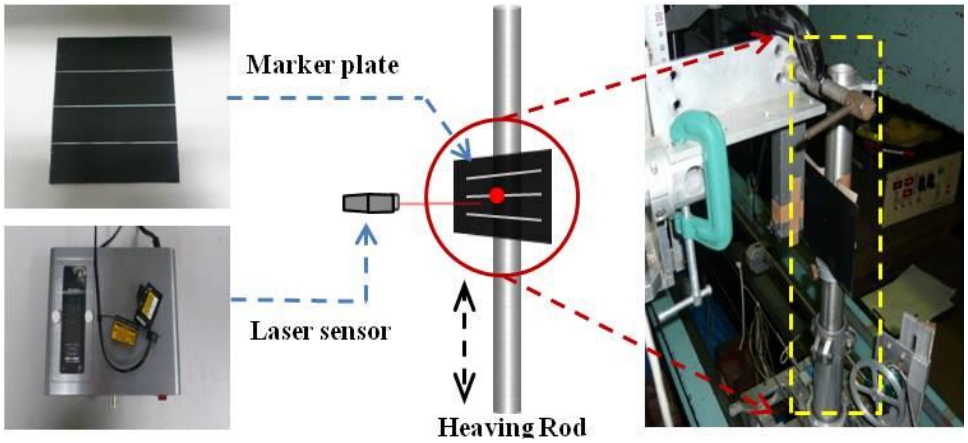


Fig. 2-10 Phase synchronizer system

2.6 APPLICATION RESULT OF PHASE SYNCHRONIZER SYSTEM

The example time history of force and motions is shown in Fig. 2-11(a). As shown in figure, in some region, wave amplitude can be considered constant.

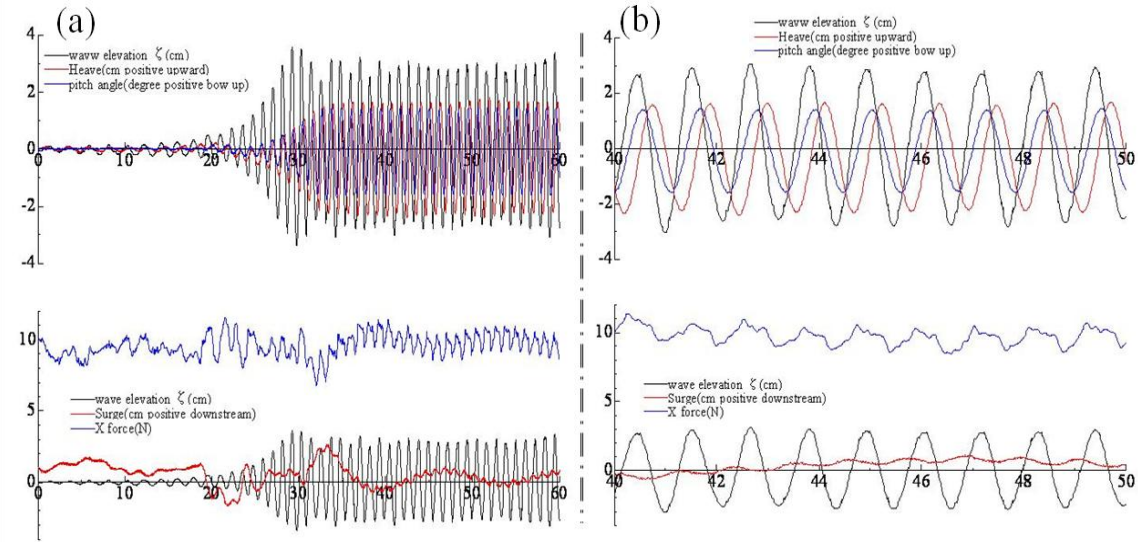


Fig. 2-11 Time history of wave elevation, force and motions

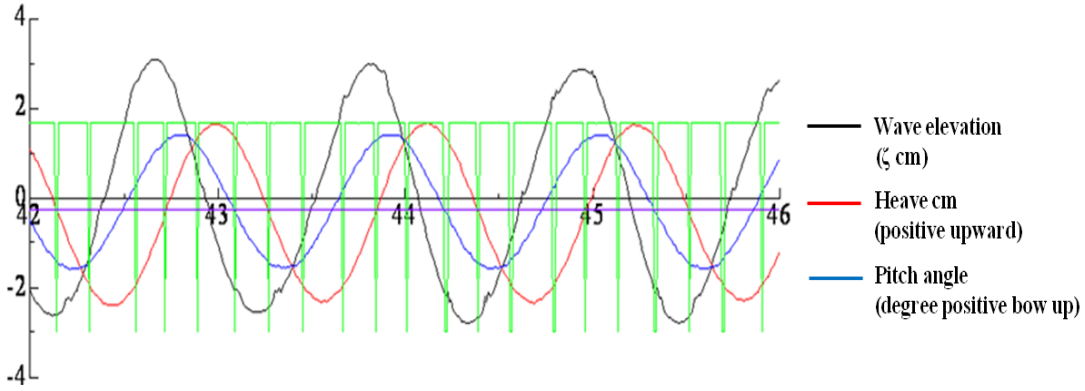


Fig. 2-12 Example of TTL signal and heave motion

So, the measurement was done in this region. The time history in measurement region is shown in Fig. 2-11 and Fig. 2-12 shows the heave and pitch motion with TTL signal from synchronizer. From the figure, it can be seen that the image was taken at same phase of heave motion. Fig. 2-13 shows actual images taken by the PIV system. In those images, it can be seen that the boss cap is moving vertically and every 6 images, the boss position was almost same for all images used to get the one phase averaged velocity field. It is noted that the instantaneous velocity analysis was done for two camera image pair for double pulse and averaged.

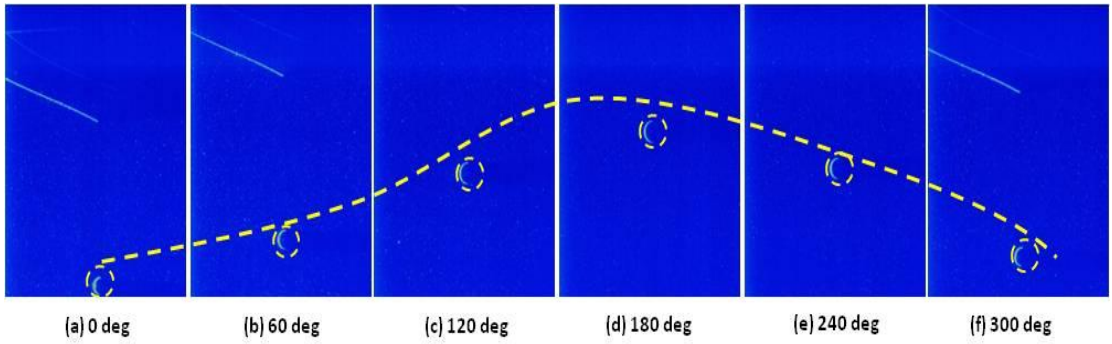


Fig. 2-13 Particle images example (camera1, first exploration)

CHAPTER 3: SHIP MOTION AND ADDED RESISTANCE

3.1 CALM WATER RESULT

Table 3-1 Comparison of CFD and EFD resistance force and motions for resistance test in calm water.

	EFD (Free Surge)	EFD (Fixed Surge)	CFD (Free Surge)	E%D
Sinkage (cm)	-0.3178	-0.259	-0.3246	-2.13
Trim (deg)	-0.1290	-0.142	-0.1238	4.04
x (cm)	1.2426	-	1.2992	-4.55
X (N)	4.3844	4.425	4.7268	-7.8

Table 3-1 shows the EFD and CFD comparison for calm water case with free surge. The CFD prediction of surge motion provides very good agreement with EFD data. EFD dynamic sinkage and trim are -0.31783 cm and -0.129 deg, respectively. The EFD resistance is about 4.38 N, corresponding to resistance coefficient of C_T=0.0051. The EFD surge is 1.24 cm, suggesting that the external force F_0=3.16 N was used in the calm water experiment, as $x = (R - F_0)/K$. EFD data for fixed surge is also given in Table 3-2. The free and fixed condition should not change the steady state values of motions and resistance but the transient values. EFD for fixed surge shows fairly similar value for resistance but sinkage and trim are different most probably due to discrepancy in the static condition. CFD predicts sinkage and trim by E=-2.13%D and 4.04 %D, respectively. The error is in the same order of previous CFD simulations errors reported

by Sadat-Hosseini et al. (2010). Nevertheless, the surge motion has fairy well agreement with EFD such that the comparison error is about -4.5%D.

3.2 FULLY-LOADED CONDITION

3.2.1 Time history study

As shown in Table 3-2. The EFD surge motion has the maximum convergence error, suggesting x is not converged very well. The x oscillates at both f_e and spring natural frequency $f_s = \frac{1}{2\pi}\sqrt{K/m}$=0.09HZ with amplitudes of 0.055A and 0.18A, respectively.

Table 3-2 Running mean and running RMS of EFD and CFD time histories.

		x (cm)		z (cm)		θ (deg.)		X (N)		Ave.	
	U_I %Ave	*Running mean*	*Running RMS*	*Running mean*	*Running RMS*	*Running mean*	*Running RMS*	*Running mean*	*Running RMS*	*Running mean*	*Running RMS*
λ/L=0.6	EFD Free	4.2	2.6	1.16	0.33	2.02	0.43	-	-	2.46	1.12
	CFD Fixed	-	-	0.32	0.19	1.47	0.81	2.74	0.20	1.51	0.40
	CFD Free	2.0	0.8	0.12	0.11	1.60	0.16	1.05	0.11	1.19	0.30
λ/L=1.1	EFD Fixed	-	-	3.92	0.18	10.0	0.22	2.12	0.18	5.35	0.19
	EFD Free	2.2	2.8	2.64	0.55	5.55	0.23	-	-	3.46	1.19
	CFD Fixed	-	-	3.25	0.17	7.10	0.18	1.83	0.36	4.06	0.24
	CFD Free	2.1	1.4	2.01	0.10	4.14	0.12	0.71	0.46	2.24	0.52
λ/L=1.6	EFD Fixed	-	-	6.91	0.27	14.2	0.31	9.10	0.47	10.07	0.35
	EFD Free	3.1	1.8	3.79	0.39	4.48	0.39	-	-	3.79	0.86
	CFD Fixed	-	-	5.63	0.40	5.85	0.39	5.25	0.57	5.58	0.45
	CFD Free	2.5	1.6	3.46	0.21	3.59	0.17	3.3	0.23	3.21	0.55

The mean value of x cannot be discussed as it is shifted by an arbitrary F_0 used in the experiment. EFD z and θ show sinusoidal response with frequency of f_e with amplitudes of 0.06A and 0.017Ak, respectively, with about 100 deg phase lag between them. The mean values of z (-0.3147 cm) and θ (-0.124 deg) are nearly close to the values for calm water. For axial force, there is no EFD data for X time history as $X' = X - m\ddot{x}$ was recorded which could only be used to estimate the mean value of X since $\overline{X'} = \bar{X}$. The mean value of EFD axial force is 6.85 N which is 2.47 N larger that for calm water representing the added resistance.

3.2.2 RAOs of added resistance and ship motions

Fig.3-1 shows RAOs of heave amplitude and phase for CFD compared with EFD data for both free and fixed surge. EFD data for free surge condition are available for 0.6< λ/L <2 and include repeated tests and fixed surge data is presented for only λ/L=1.1 and 1.6. For free surge condition, the EFD heave amplitude is fairly small for short waves and reaches to about wave amplitude A for long waves as the ship just moves up and down with the amplitude of wave at large wave length. The heave response increases dramatically for λ/L >1 and the maximum response is observed for λ/L =1.4, where wave encounter frequency is f_e=0.768 close to heave natural frequency. The heave phase indicates no phase lag between heave response and wave at large wave length underlining that heave is synchronized with incident wave. The maximum phase lag is 90 deg which occurs at λ/L =1 i.e. the heave response is close to zero when wave crest is located on center of gravity and λ/L =1. The average CFD prediction error for heave amplitude is 7.06%D for the whole range of wave length. The maximum error is for the

shortest wave length and is 1.5 times the average error. To avoid the meaningless large phase errors for phases close to zero, the phases are added by 180 deg before being used to evaluate the error of CFD phase prediction.

The RAOs of pitch amplitude and phase are plotted in Fig. 3-2. For free surge condition, the pitch amplitude increases with wave length to slightly more than 1.0 at long waves. The rate of pitch amplitude increase is fairly constant (=1.34) from λ /L=0.9 to λ /L=1.4. The pitch phase indicates that the ship reaches to asymptotic behavior at long waves, where the pitch response has 90 deg phase with incoming waves i.e. zero degree of phase lag respect to wave slope. The minimum phase lag is -90 deg observed for λ /L=0.7. This means that the ship is in bow up position while the center gravity of ship is located on wave downslope. CFD illustrates very good agreement with EFD. The average error of pitch amplitude prediction is 4.2%D for the current range of wave length. The maximum prediction error is for maximum wave length with 13%D. The CFD for RAO of phase also shows good prediction with the average error of 5.29%D and maximum of 17.6%D for λ /L=0.7. For fixed surge condition, CFD and EFD show similar results to free surge condition except that the EFD pitch for λ /L=1.6 is notably different.

The RAOs of surge amplitude and phase are shown in Fig. 3-3. The RAO of surge amplitude indicates that the surge is fairly constant for λ /L<1.2 and then starts increasing. The maximum sure response is for the largest wave in which surge amplitude is about 50% of the wave amplitude. The RAO of surge phase shows that the surge amplitude is maximum when the ship is located on wave downslope in long waves or on wave upslope in short waves. CFD predicts similar trend for surge amplitude and phase. The average error of CFD simulation is 12.3 and 3.5%D for amplitude and phase,

respectively. The maximum errors are about twice the average errors which take place at λ /L=1.4 for amplitude and λ /L=0.6 for phase.

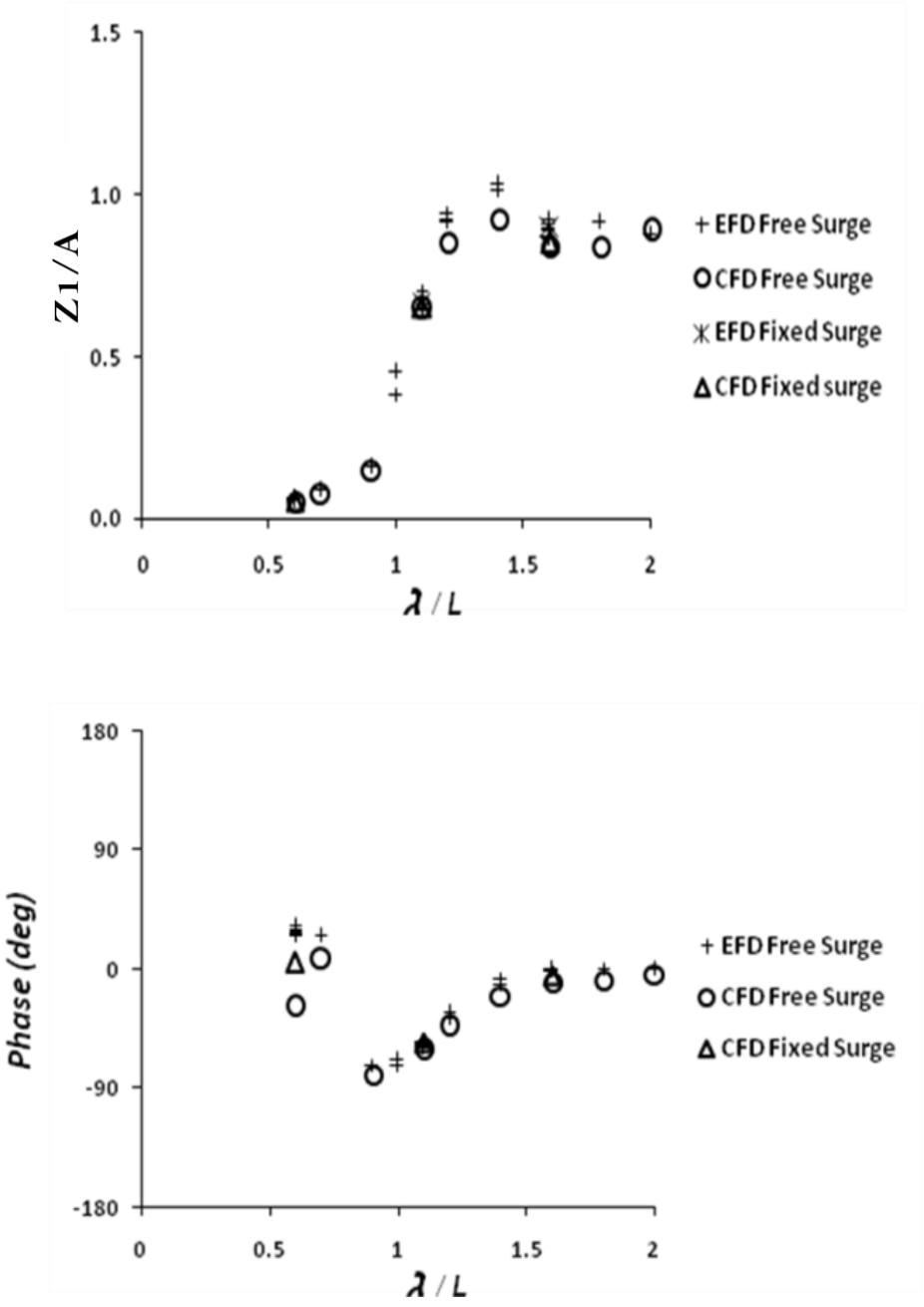


Fig. 3-1 The RAOs of heave amplitude and phase at Fr=0.142

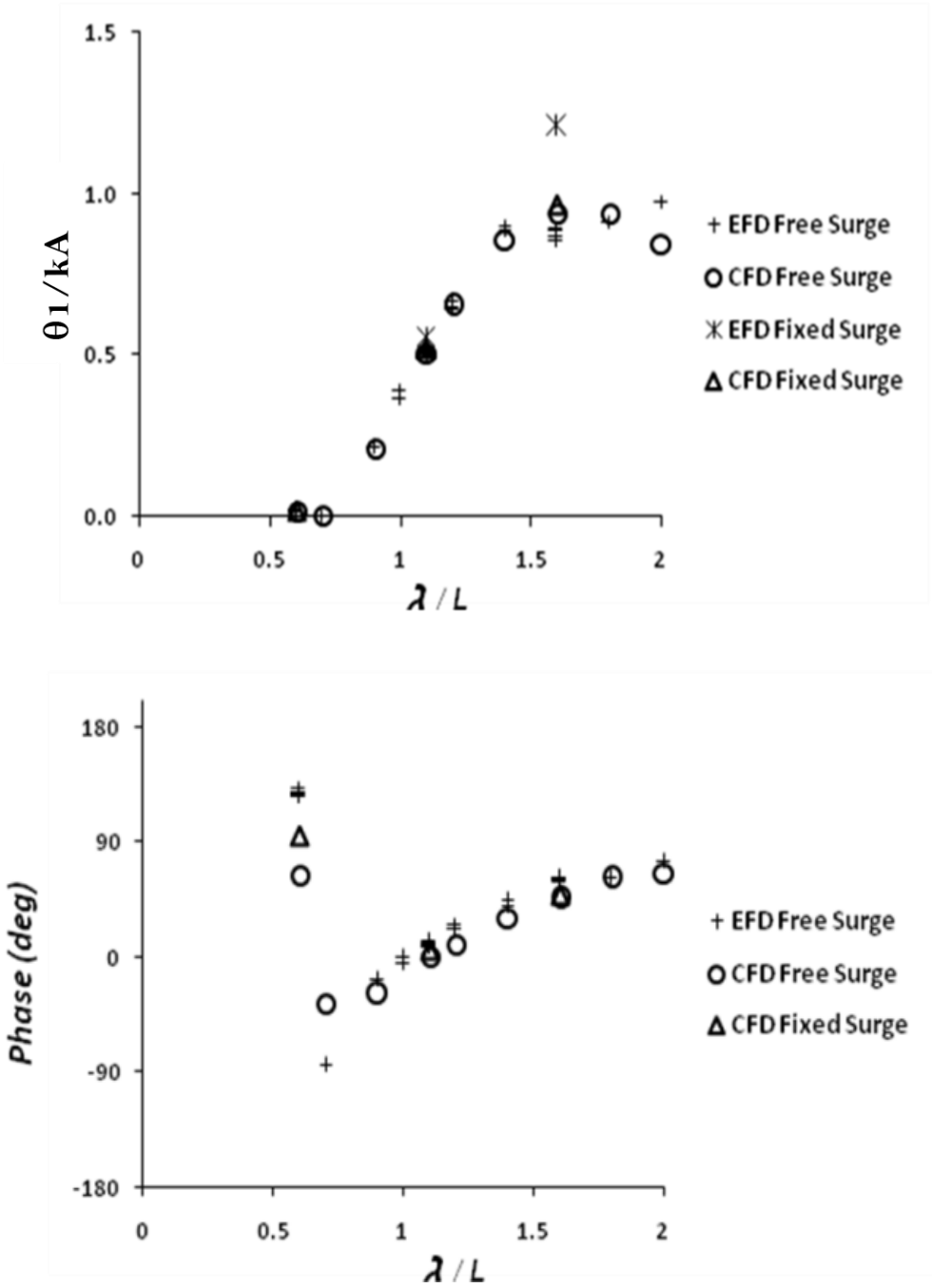


Fig. 3-2 The RAOs of pitch amplitude and phase at Fr=0.142

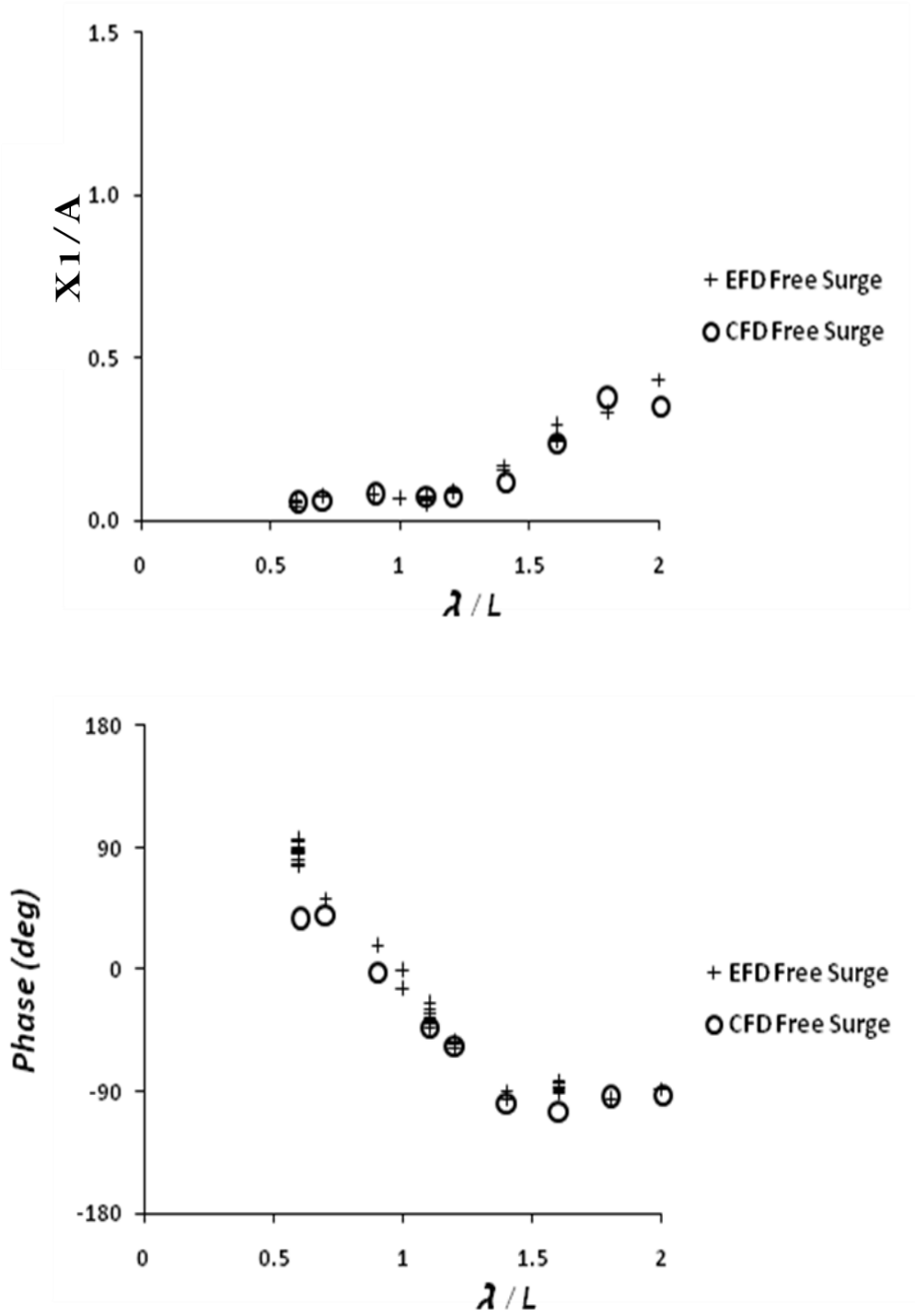


Fig. 3-3 The RAOs of surge amplitude and phase at Fr=0.142

The RAO of added resistance is shown in Fig. 3-4. The EFD repeated tests do not show good repeatability such that the data are scattered for most of wave conditions. In particular, the added resistance at λ /L=1.1 is scattered around ±10% its average value. The maximum added resistance occurs around λ /L=1.1. The CFD simulation under predicts the added resistance for short waves and over predicts for long waves. The average error is 42%D with maximum error for longest wave. Fixed surge condition results illustrate fairly similar value for λ /L=1.1 but slightly different for λ /L=1.6.

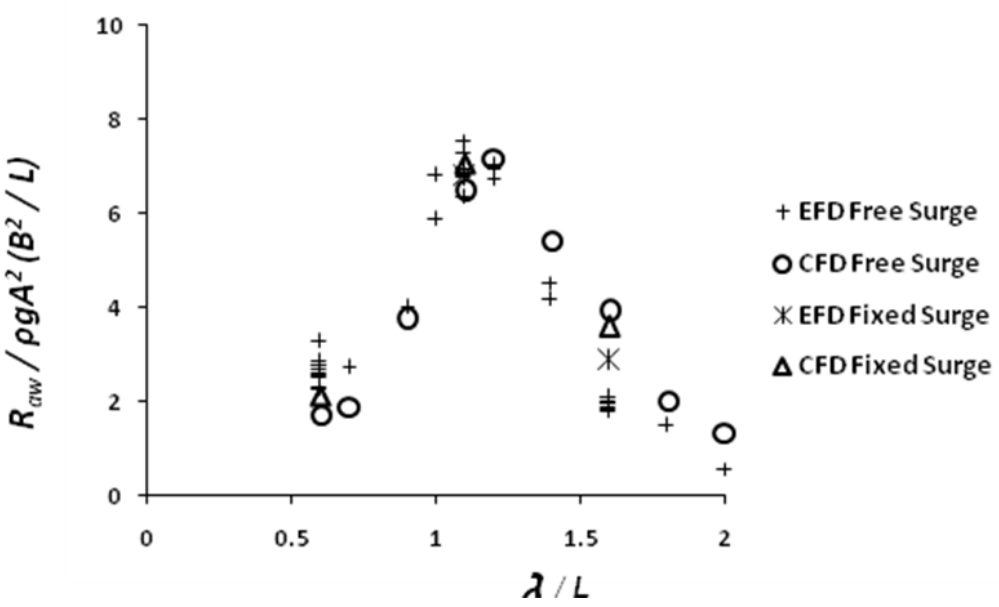


Fig. 3-4 RAOs of added resistance at Fr=0.142

3.3 BALLAST CONDITION

3.3.1 RAOs of added resistance and ship motions.

Table 3-3 shows the symbols used in figures. Although it is worst case of wave amplitude fluctuation due to wave making performance for short waves, wave amplitude can be considered constant in some region. So, the measurement was done in this region. The results of motion response and added resistance are shown from Fig. 3-5 to Fig.3-7. The CFD results (Wu (2013)) are also shown in the figures. In Wu (2013), the detailed comparison including phase is available.

Table 3-3 Symbols used in figures

Rw	Wave resistance	(N)
Rc	Calm water resistance	(N)
A	Wave amplitude	(m)
B	Breadth	(m)
L_{PP}	Ship length between perpendicular	(m)
g	Gravity	N/kg
ρ	Water density	Kg/m^3
Z1	1^{st} harmonic amplitude of ship motion ,Heave	(m)
X1	1^{st} harmonic amplitude of ship motion ,Surge	(m)
θ1	1^{st} harmonic amplitude of ship motion ,Pitch	(rad)
k	wave number (rad/m) $k=2\pi/\lambda$ λ:wave length	(m)

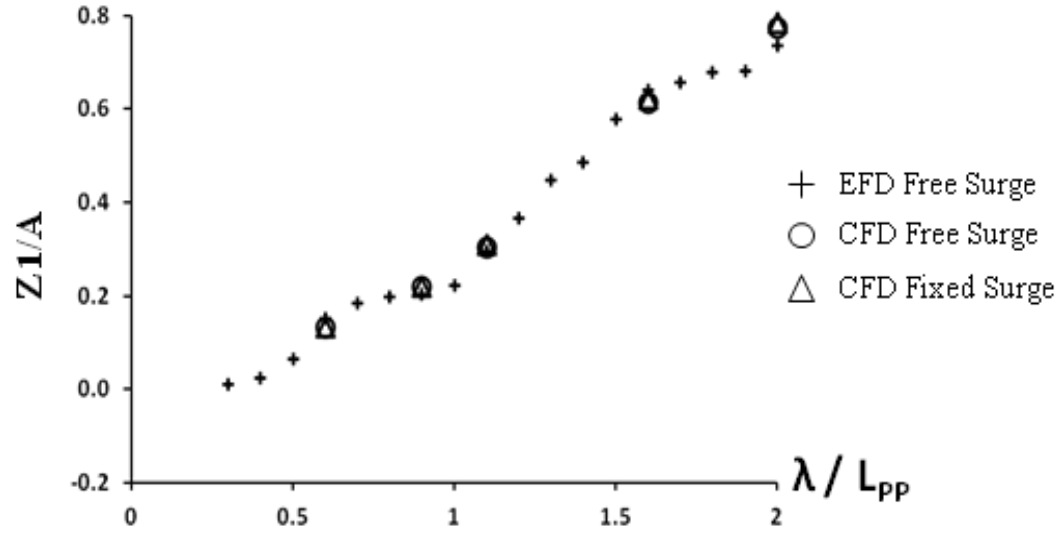


Fig. 3-5 The RAOs of Heave amplitude

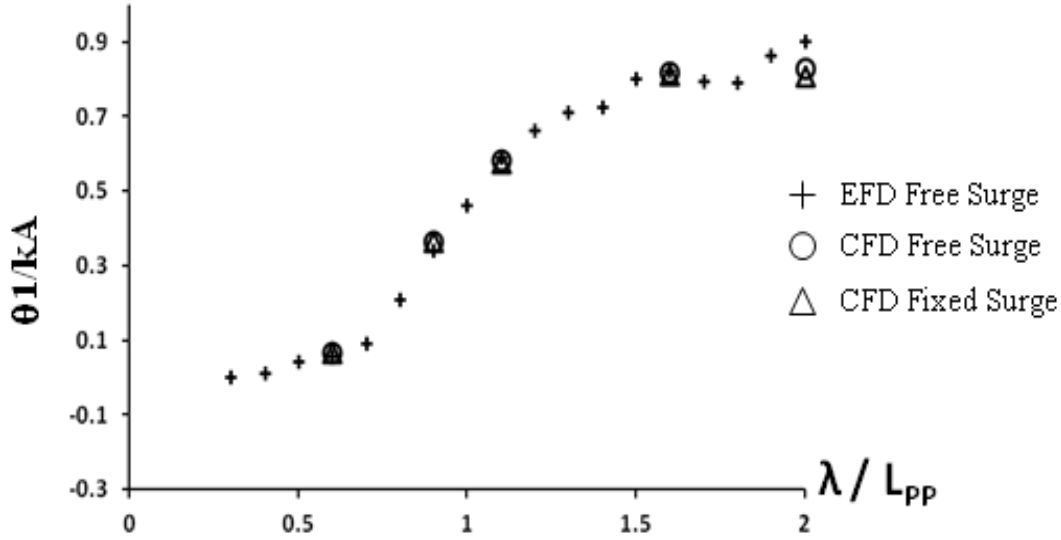


Fig. 3-6 The RAOs of Pitch amplitude

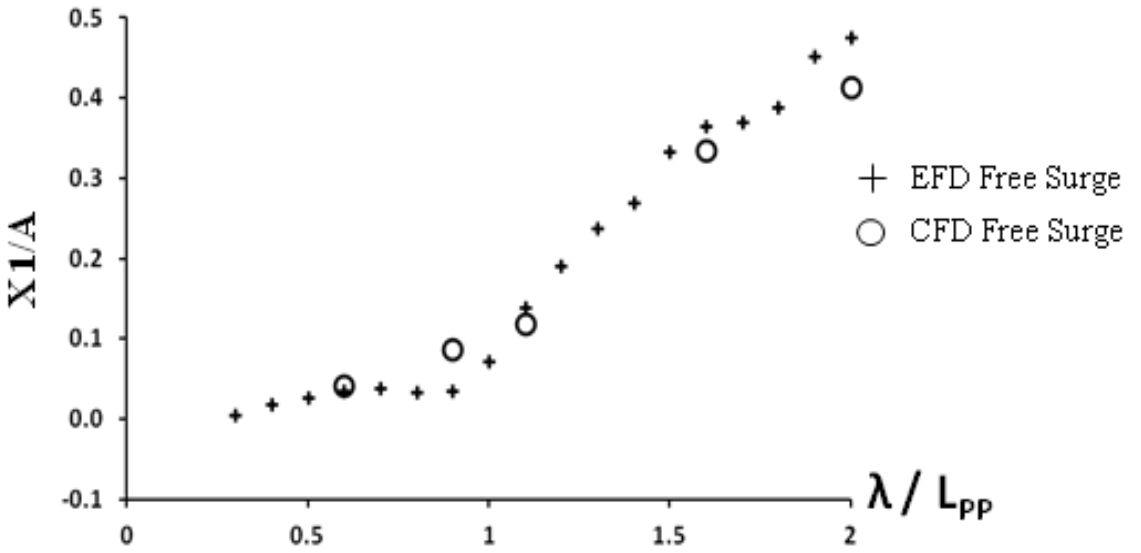


Fig. 3-7 The RAOs of Surge amplitude

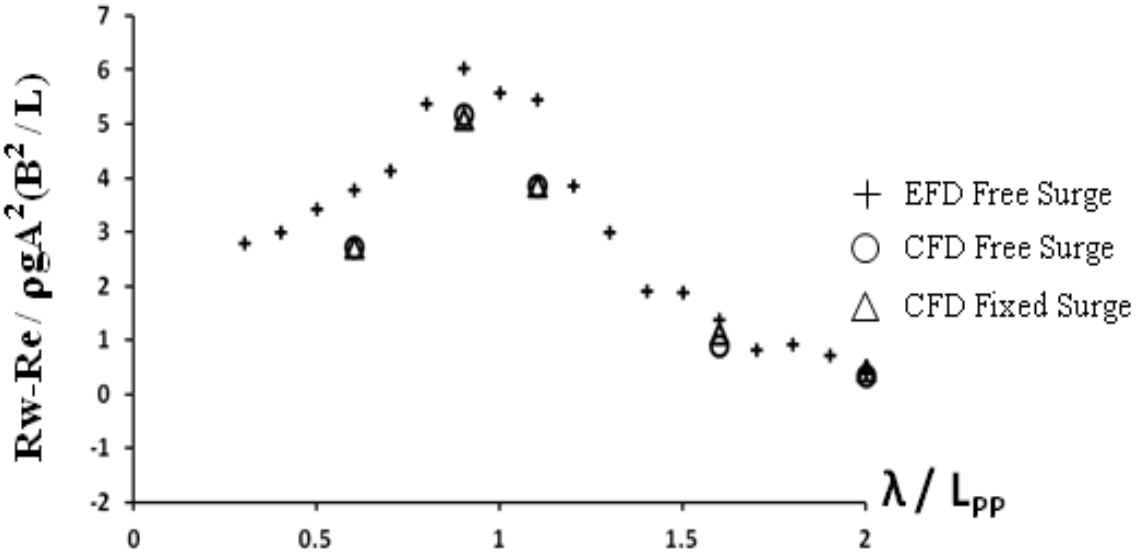


Fig. 3-8 Added resistance for Ballast condition

The data for heave first harmonic amplitude are shown for $0.3< \lambda/L <2.0$ in Fig. 3-5. The heave amplitude is fairly small for short wave and gradually increases as λ/L increases to the value that is a little bit smaller than wave amplitude A for long waves. The results of pitch first harmonic amplitude are plotted in Fig. 3-6. The amplitude increases as λ/L increases from 0.7 to 1.6, fairly small in short wave region and almost constant in long wave region. The results for surge first harmonic response are shown in Fig.3-7. The surge amplitude is small in the region $\lambda/L<0.9$ and it gradually increases in the region $0.9<\lambda/L$. From the figures, CFD can predict the motion response fairly well. For the added resistance coefficient as shown in Fig. 3-8, the peak is observed at $\lambda/L=0.9$ and at that point, the heave and pitch response is not maximum, but the phase is different from the long wave region. Except for the long wave region, CFD predicted slightly lower than the EFD result. The discrepancy of added resistance prediction may be solved by refinement of grid around bulbous bow piercing the free surface. After these measurements, the constant force F_0 is adjusted to keep the mean surge is 0 for the velocity measurement. From Fig. 3-7, the surge amplitude is not small for long waves, so the measurement plane is not exactly at propeller plane even though the mean and long period surge motion due to the mas and weak spring system was made small by adjustment.

CHAPTER 4: STEREO PIV MEASUREMENT RESULTS

4.1 VELOCITY DISTRIBUTION AT PROPELLER PLANE IN FULLY-LOADED CONDITION

4.1.1 Velocity distribution at propeller plane in calm water condition

Fig. 4-1 shows the measurement results in calm water condition. The coordinates of the results shown below were made non dimensional by using L_{pp} and towing carriage speed U. For a numerical algorithm, the cross-correlation method was used. Finally, 32×32 pixel was selected as the inspection area and for the interrogation area; a 50% overlap was allowed between adjacent measurement areas. Number of data sets for averaging is 200 frames for in waves, and 1000 frames for in calm water condition. From the calm water measurement, the PIV system can measure the flow field around KVLCC2 model from the comparison with previous results by five-hole pitot tube.

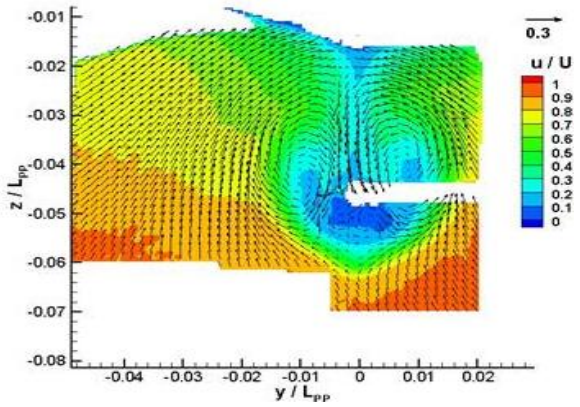


Fig. 4-1 Velocity distribution in calm water

4.1.2 Velocity distribution at propeller plane, λ/L=0.6

The Fourier analysis in measurement region, the pitch, heave and surge motion and incident wave elevation at FP and propeller plane (converted from the wave elevation in front of bow) for λ / L_{pp} =0.6 are shown in Fig. 4-2. This is the example for short wave condition with small motion. Vertical lines show the phase in one encounter period when the velocity field was measured. The reference to phase is the time when the incident wave crest is at FP plane. T denotes the encounter period and t is time from reference. As shown in figure, the motion is very small in this case. Fig.4-3 to Fig. 4-10 shows the velocity distribution for each phase at propeller plane. Since the ship motion is rather small, pressure gradient effect and orbital velocity effect to the stretching of vortex sheet are dominant in the velocity distribution. From Fig. 4-2, the wave height at the propeller plane is maximum at phase5, t/T=0.656, so the axial velocity in outer invisid region is large due to the orbital motion velocity in wave. The boundary layer thickness is changed by pressure gradient and the outer invicid flow. Near the propeller boss cap, the velocity fluctuation of low momentum fluid is larger than outer part and the phase is a little bit different.

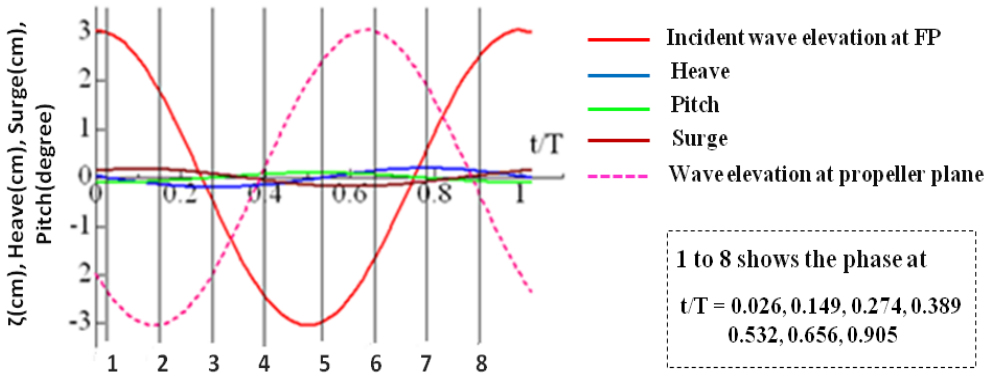
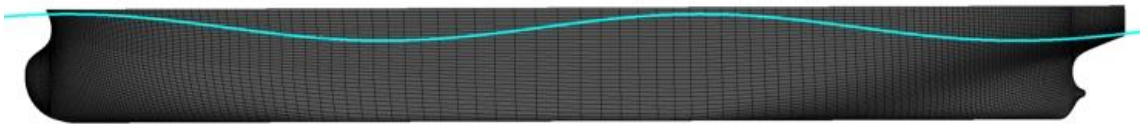
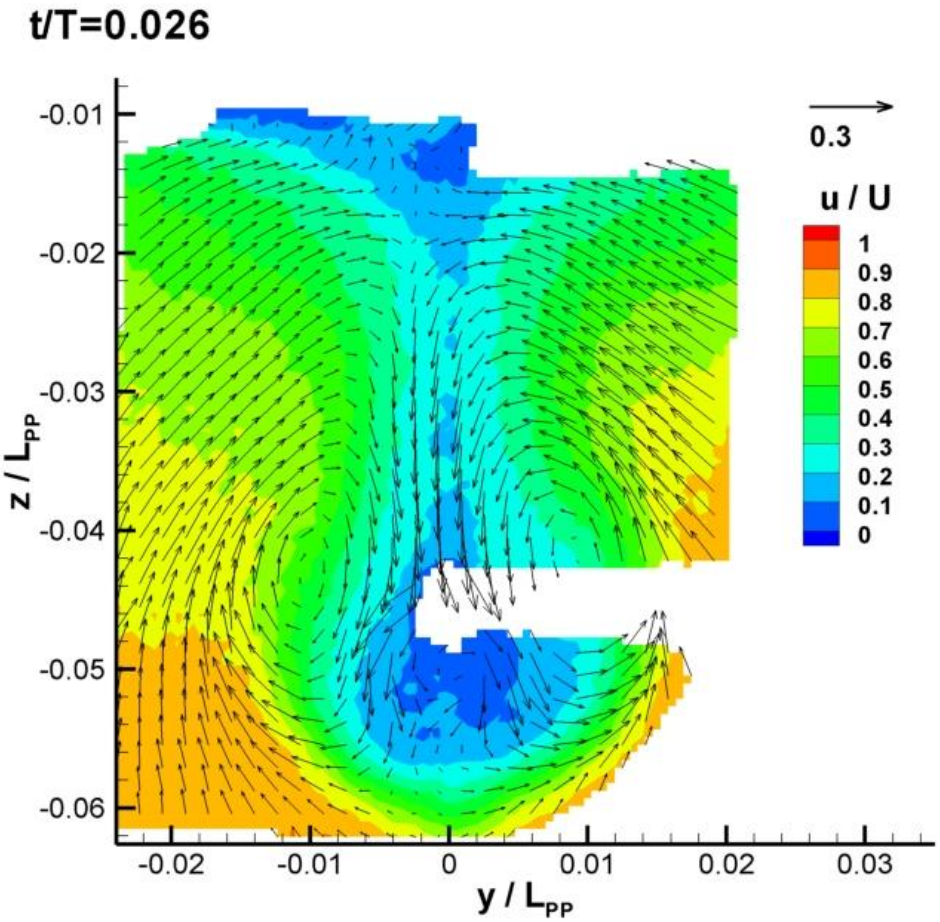


Fig. 4-2 Wave elevation and motions in one period (λ/L=0.6)

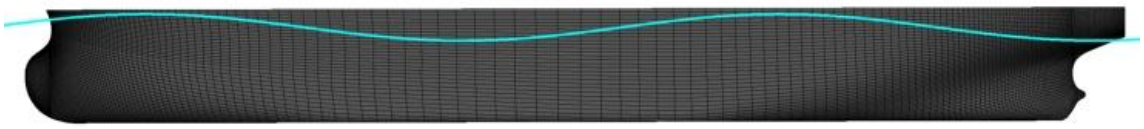


(a) Schematic view of wave and model ship

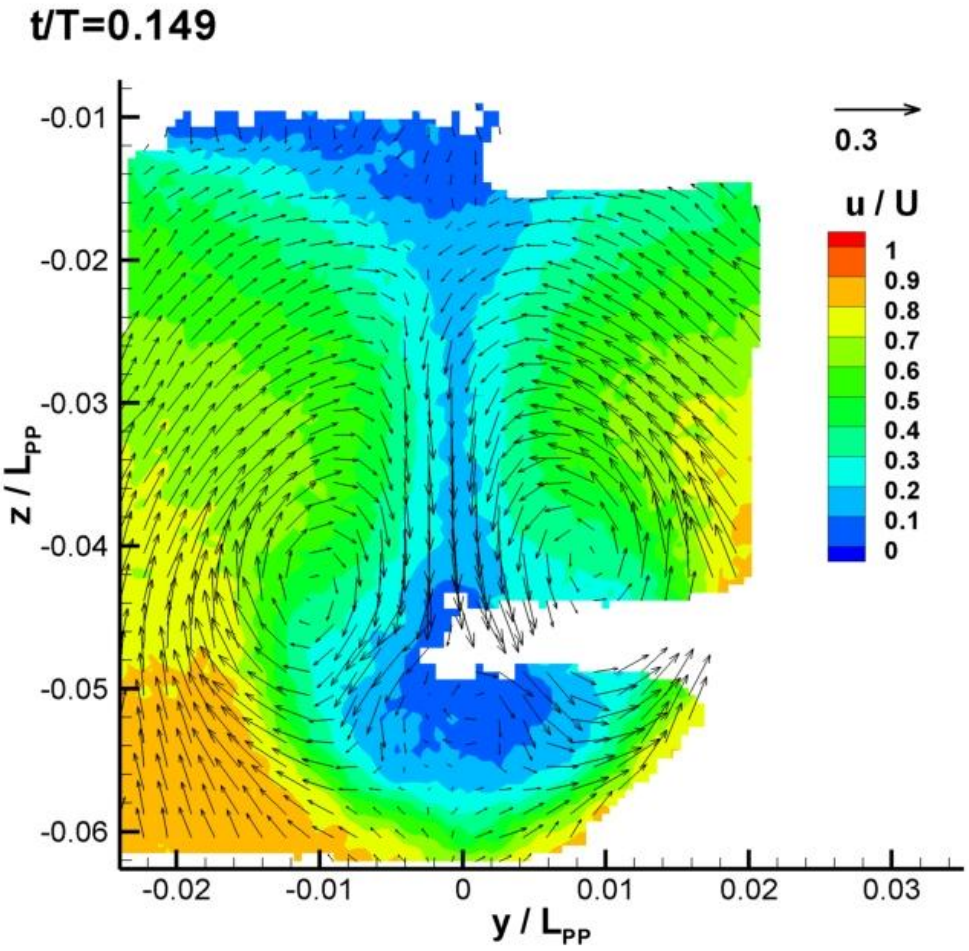


(b) Velocity distribution

Fig. 4-3 Velocity distribution (λ/L=0.6), t/T=0.026

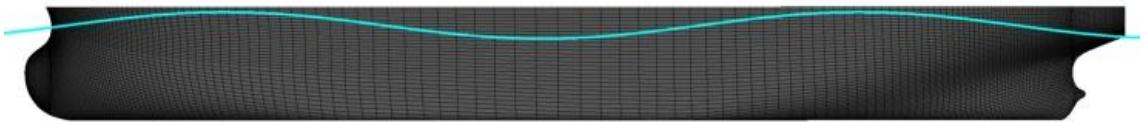


(a) Schematic view of wave and model ship

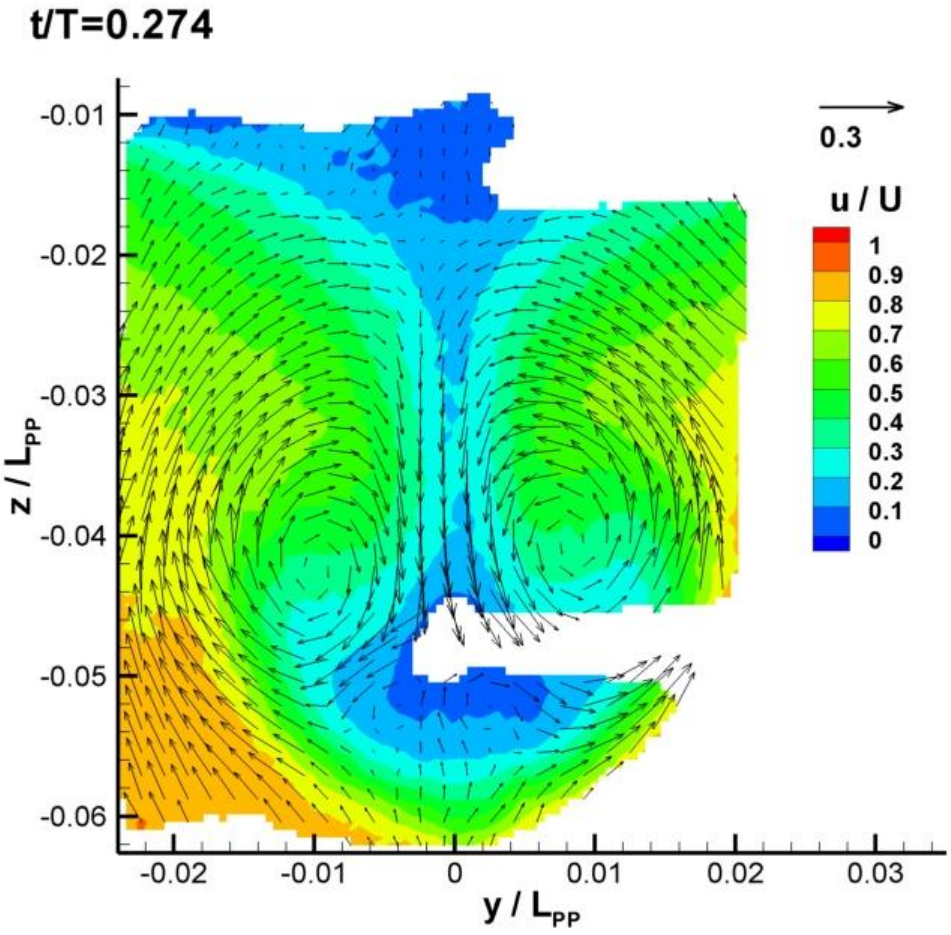


(b) Velocity distribution

Fig. 4-4 Velocity distribution (λ/L=0.6), t/T=0.149

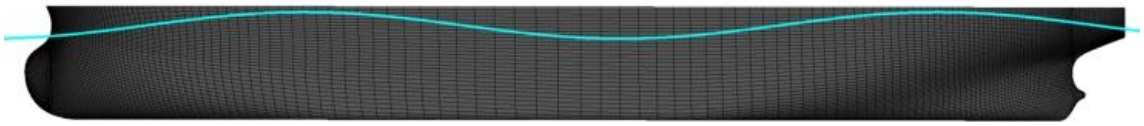


(a) Schematic view of wave and model ship

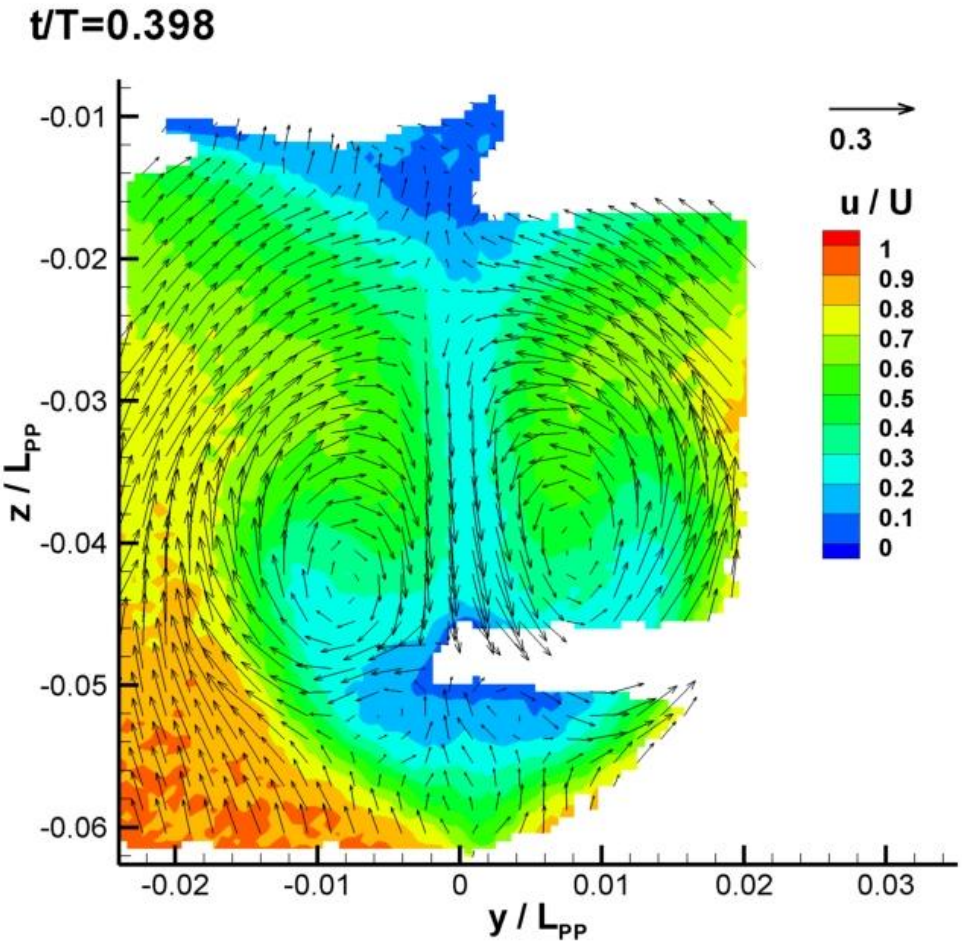


(b) Velocity distribution

Fig. 4-5 Velocity distribution (λ/L=0.6), t/T=0.274

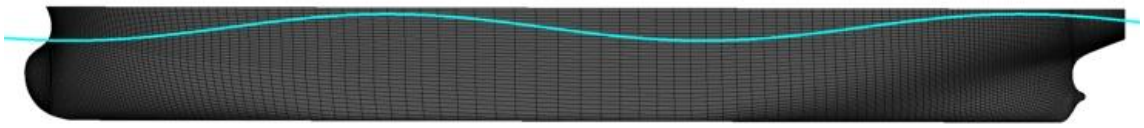


(a) Schematic view of wave and model ship

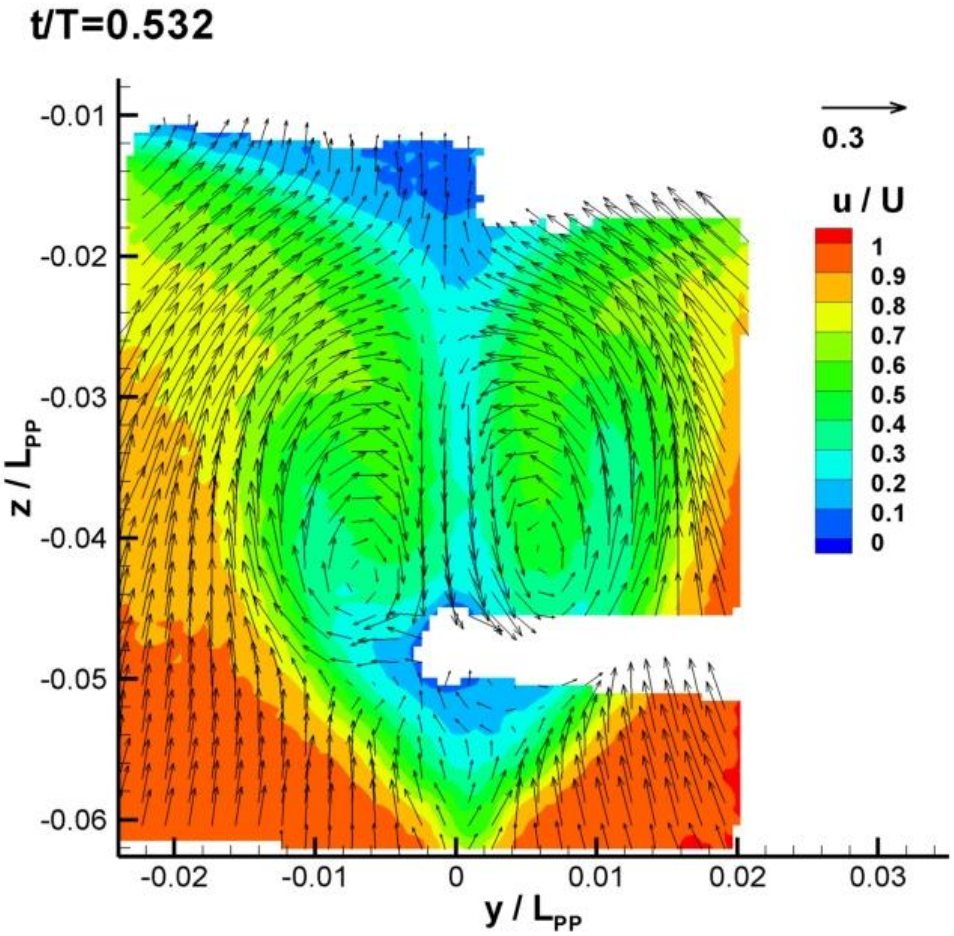


(b) Velocity distribution

Fig. 4-6 Velocity distribution (λ/L=0.6), t/T=0.398

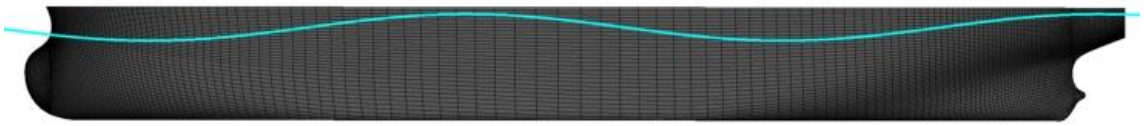


(a) Schematic view of wave and model ship

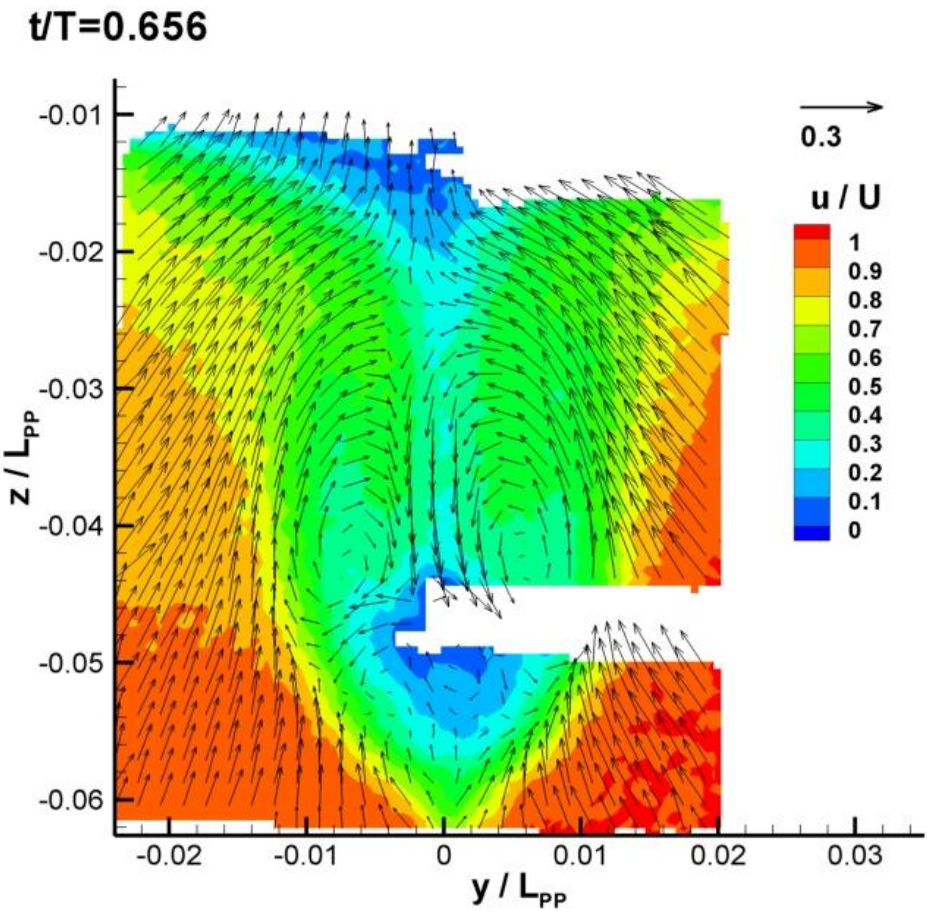


(b) Velocity distribution

Fig. 4-7 Velocity distribution (λ/L=0.6), t/T=0.532

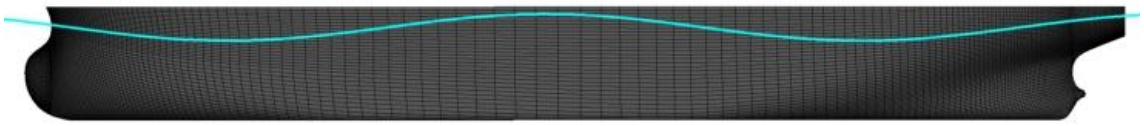


(a) Schematic view of wave and model ship

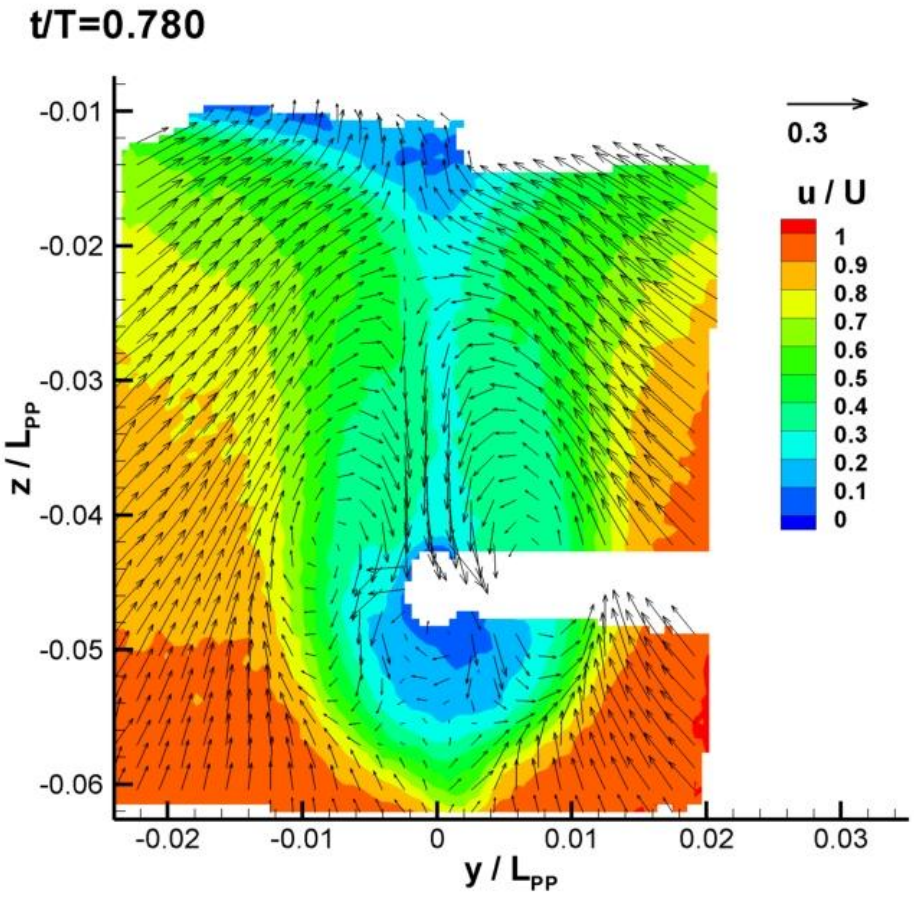


(b) Velocity distribution

Fig. 4-8 Velocity distribution (λ/L=0.6), t/T=0.656

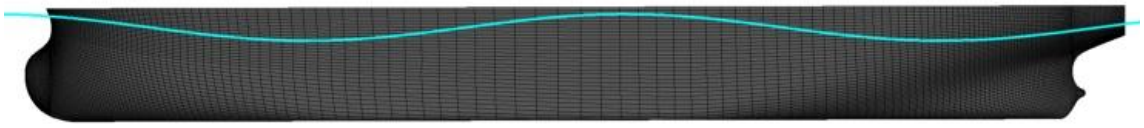


(a) Schematic view of wave and model ship

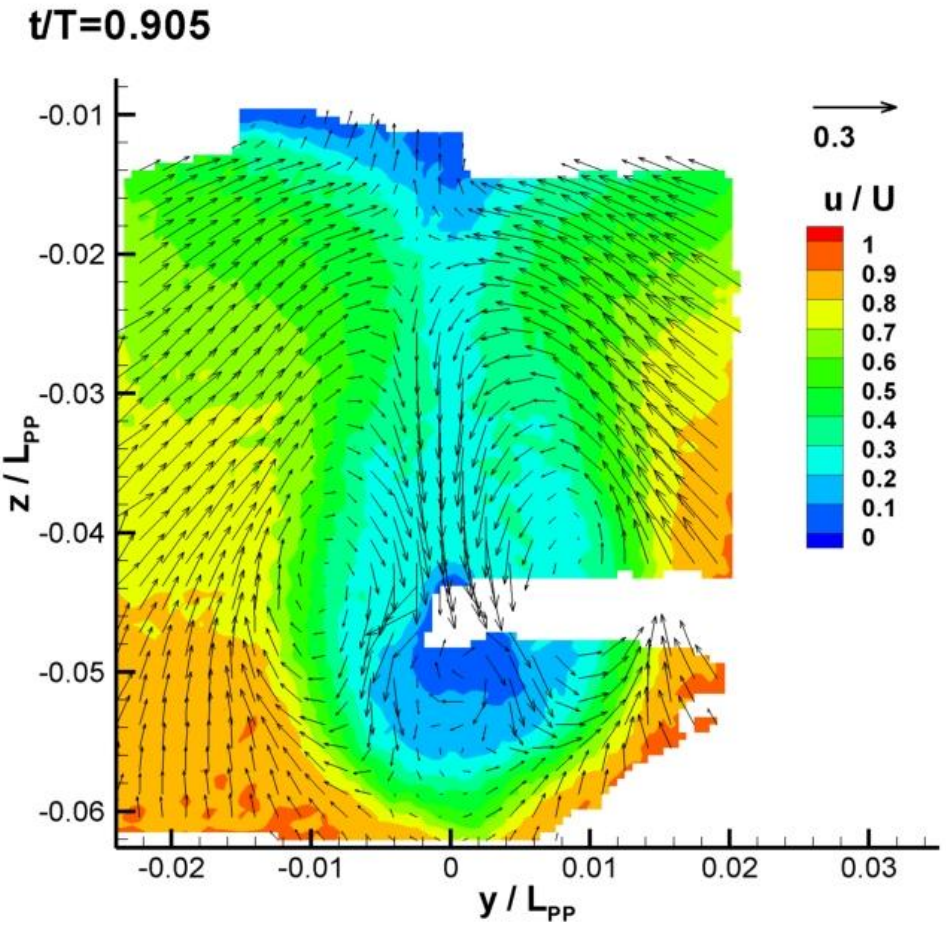


(b) Velocity distribution

Fig. 4-9 Velocity distribution (λ/L=0.6), t/T=0.780



(a) Schematic view of wave and model ship



(b) Velocity distribution

Fig. 4-10 Velocity distribution (λ/L=0.6), t/T=0.905

4.1.3 Velocity distribution at propeller plane, λ/L=1.1

Fig. 4-11 shows the pitch, heave and surge motion and incident wave elevation at FP and propeller plane for λ / L_{pp}=1.1. This condition was chosen as a point of maximum added resistance. From this figure, the heave and pitch motion is large. From the phase, the relative gradient between wave and ship is large. Fig. 4-12 to Fig. 4-23 shows the velocity distribution for each phase at propeller plane. The orbital motion effect and pressure gradient effect are also seen in the figure. In this case, the bilge vortices are moved vertically due to ship motion. The vortices from the propeller boss are also seen in the figure. So, the low velocity region due to bilge vortices is also moved vertically. In some phase, the high velocity region outside the boundary layer exists in propeller disk. The phase of the velocity fluctuation in inner part is different from outer flow.

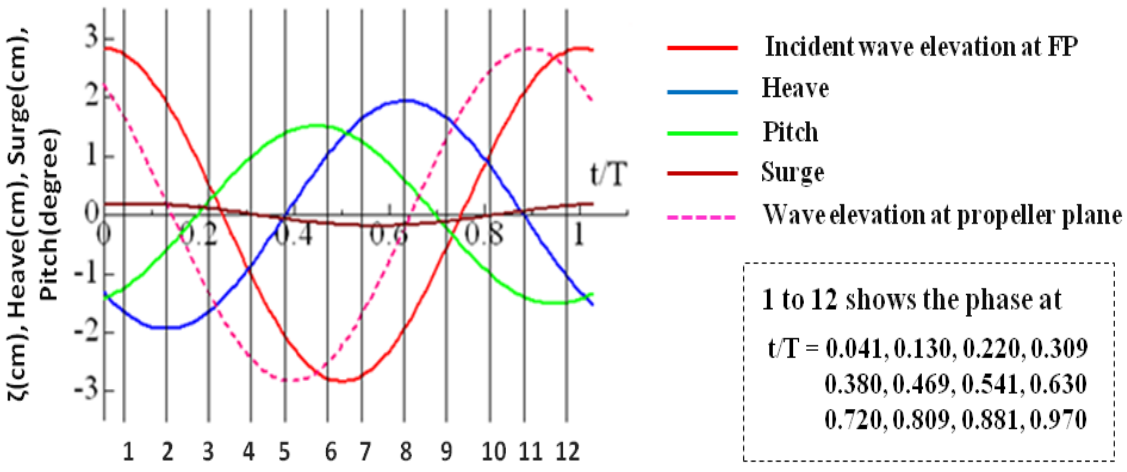
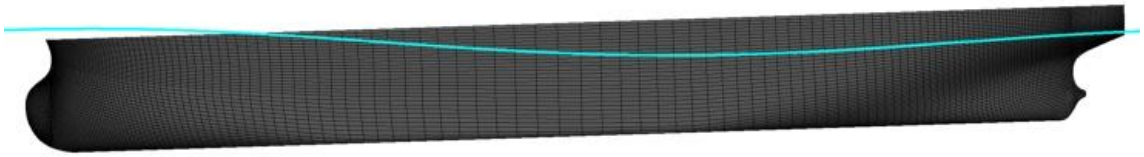
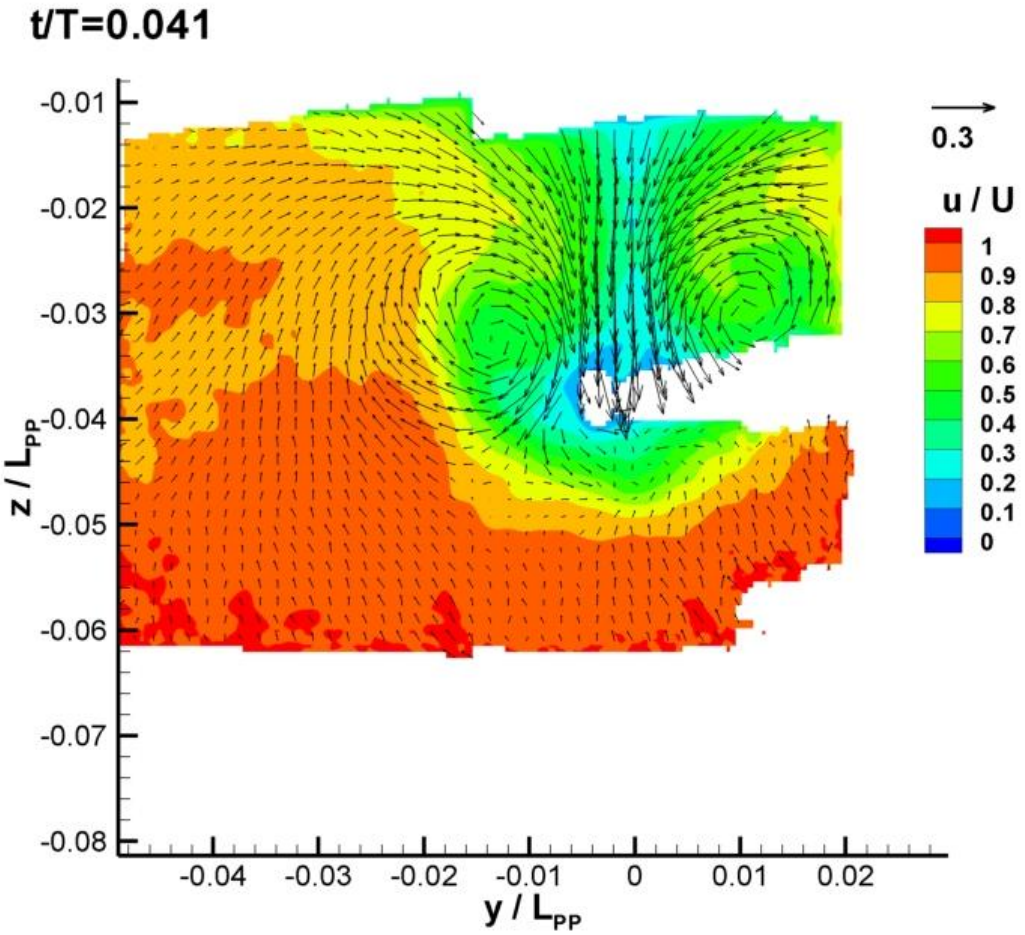


Fig. 4-11 Wave elevation and motion in one period (λ/L=1.1)

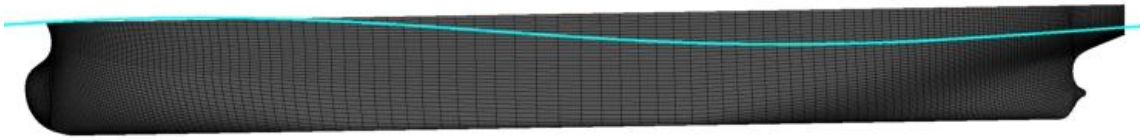


(a) Schematic view of wave and model ship

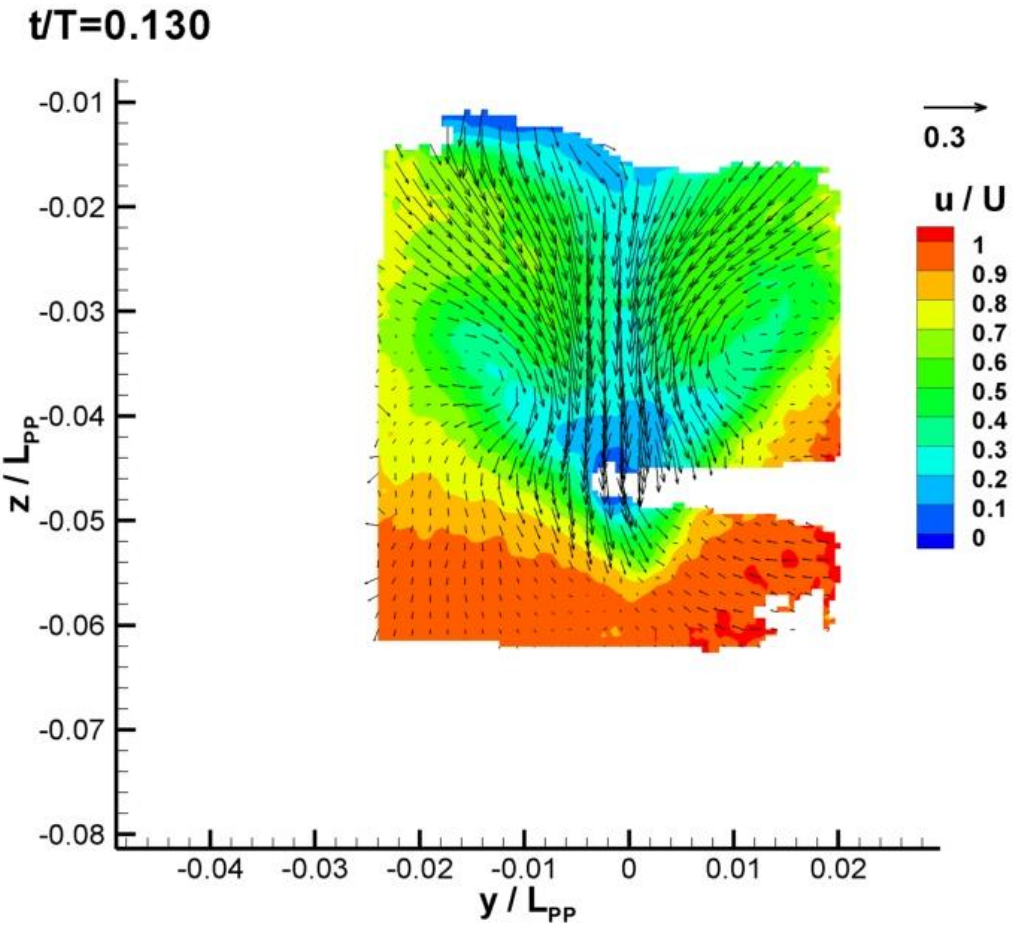


(b) Velocity distribution

Fig. 4-12 Velocity distribution (λ/L=1.1), t/T=0.041

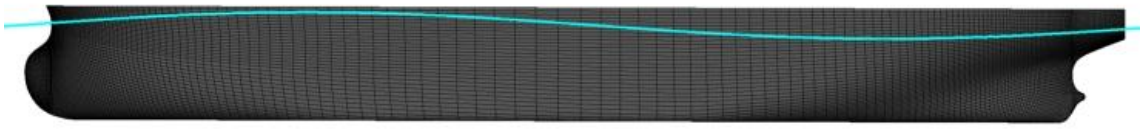


(a) Schematic view of wave and model ship

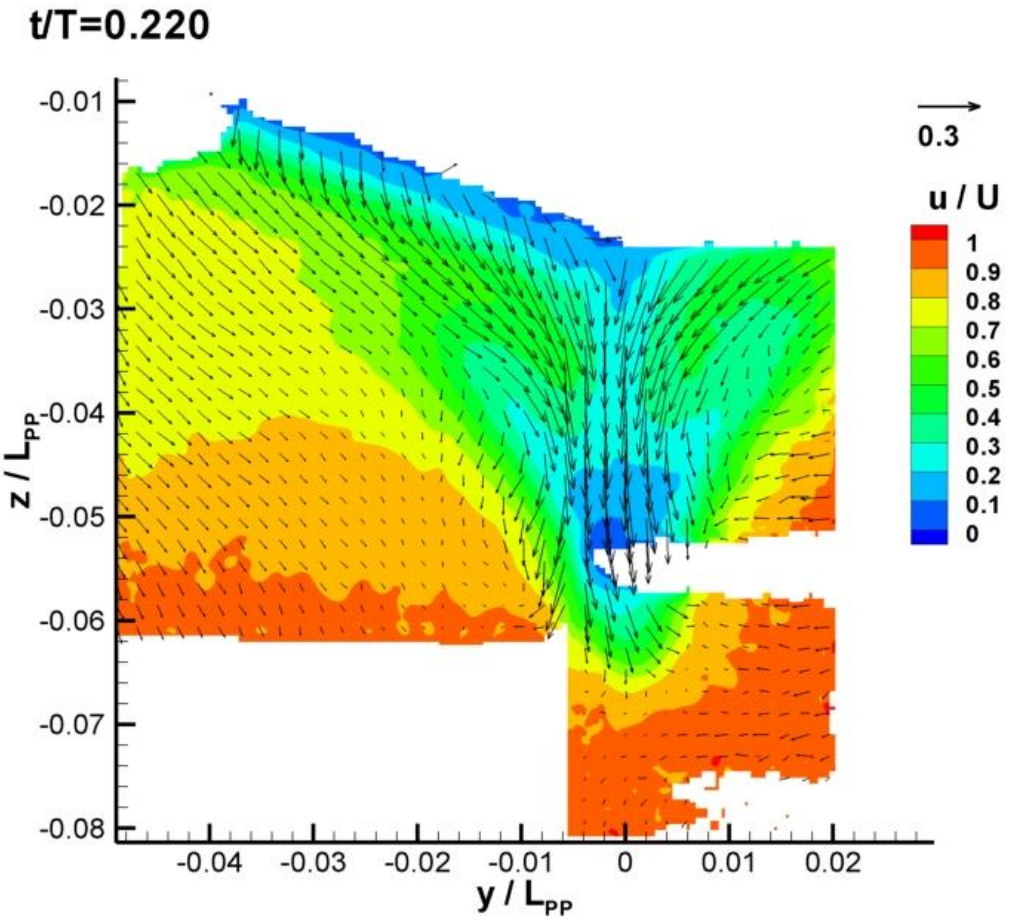


(b) Velocity distribution

Fig. 4-13 Velocity distribution (λ/L=1.1), t/T=0.130

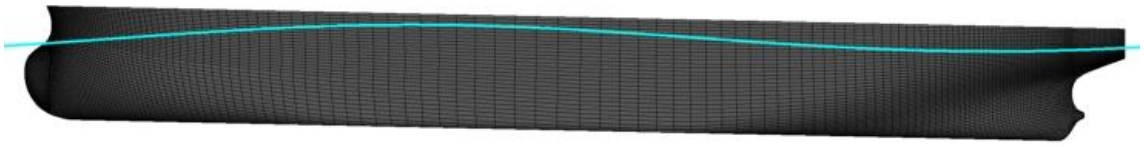


(a) Schematic view of wave and model ship

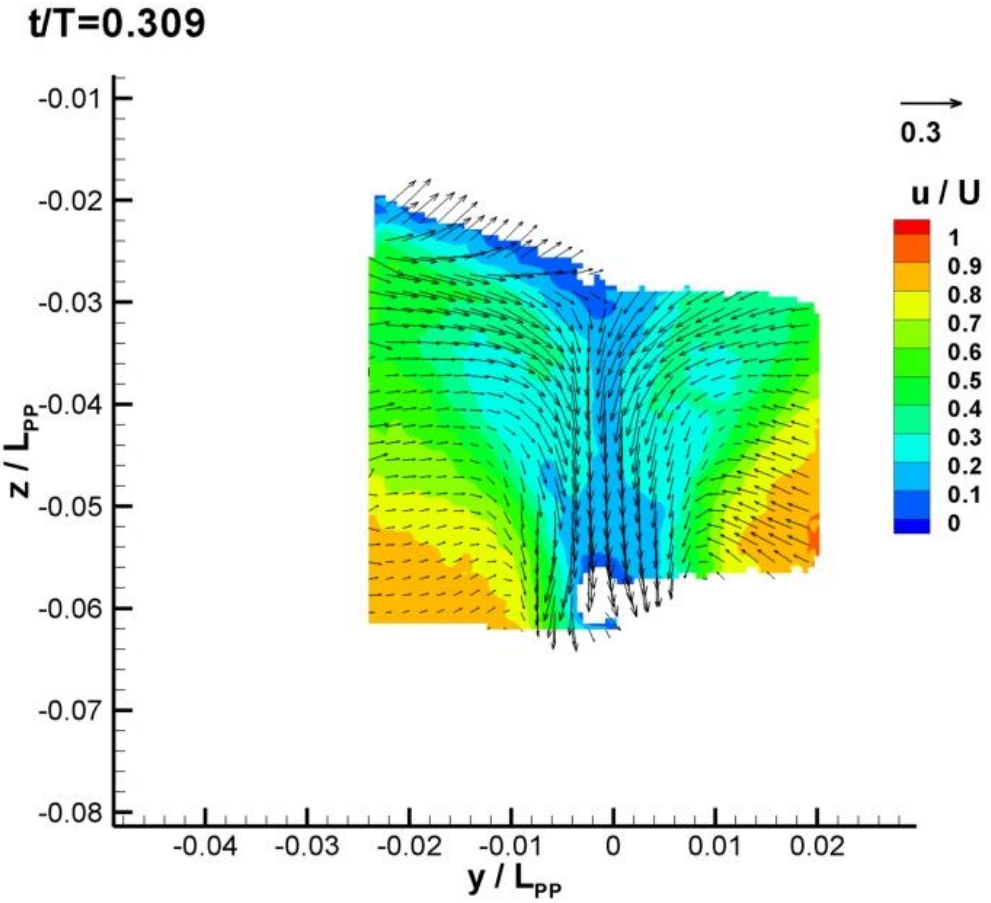


(b) Velocity distribution

Fig. 4-14 Velocity distribution (λ/L=1.1), t/T=0.220

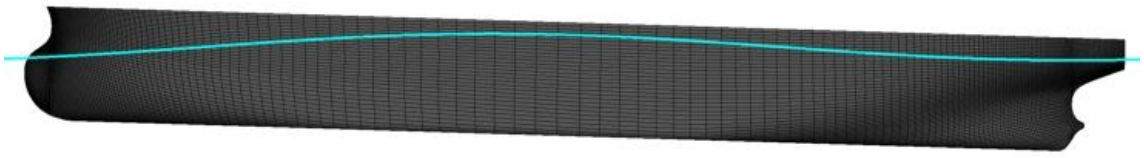


(a) Schematic view of wave and model ship

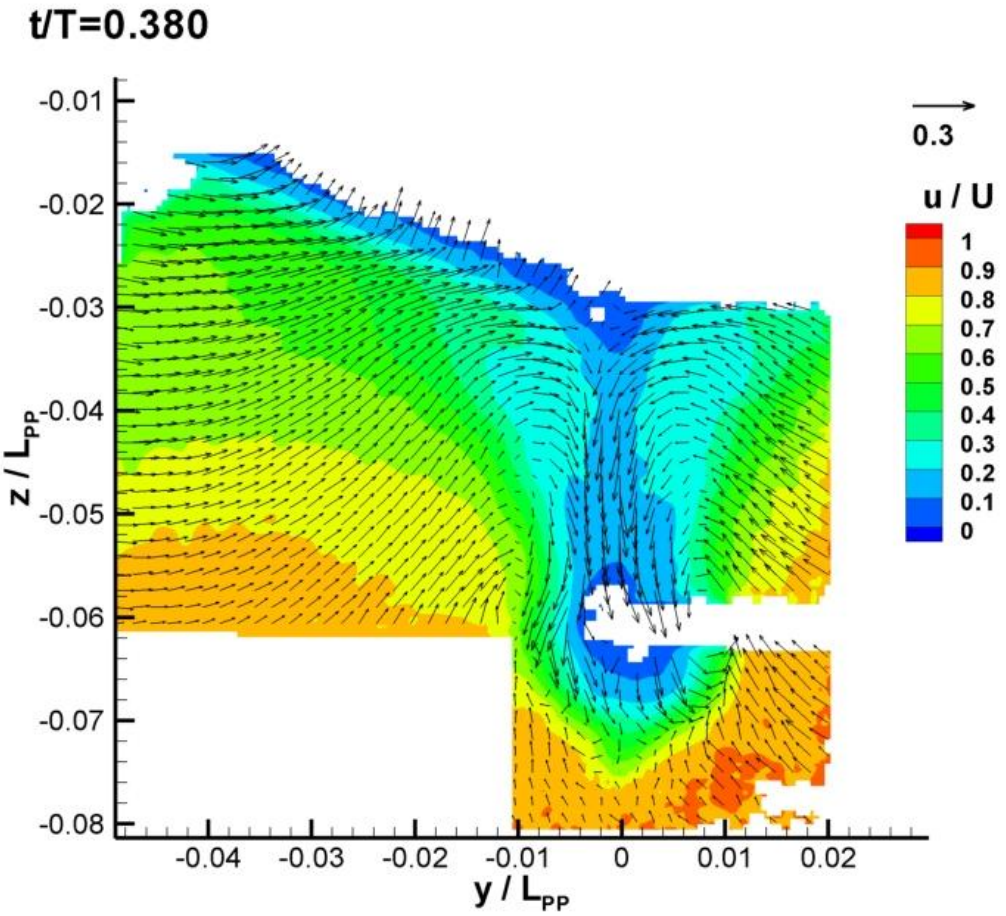


(b) Velocity distribution

Fig. 4-15 Velocity distribution (λ/L=1.1), t/T=0.309

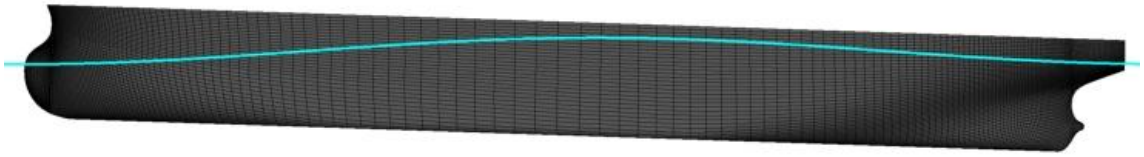


(a) Schematic view of wave and model ship

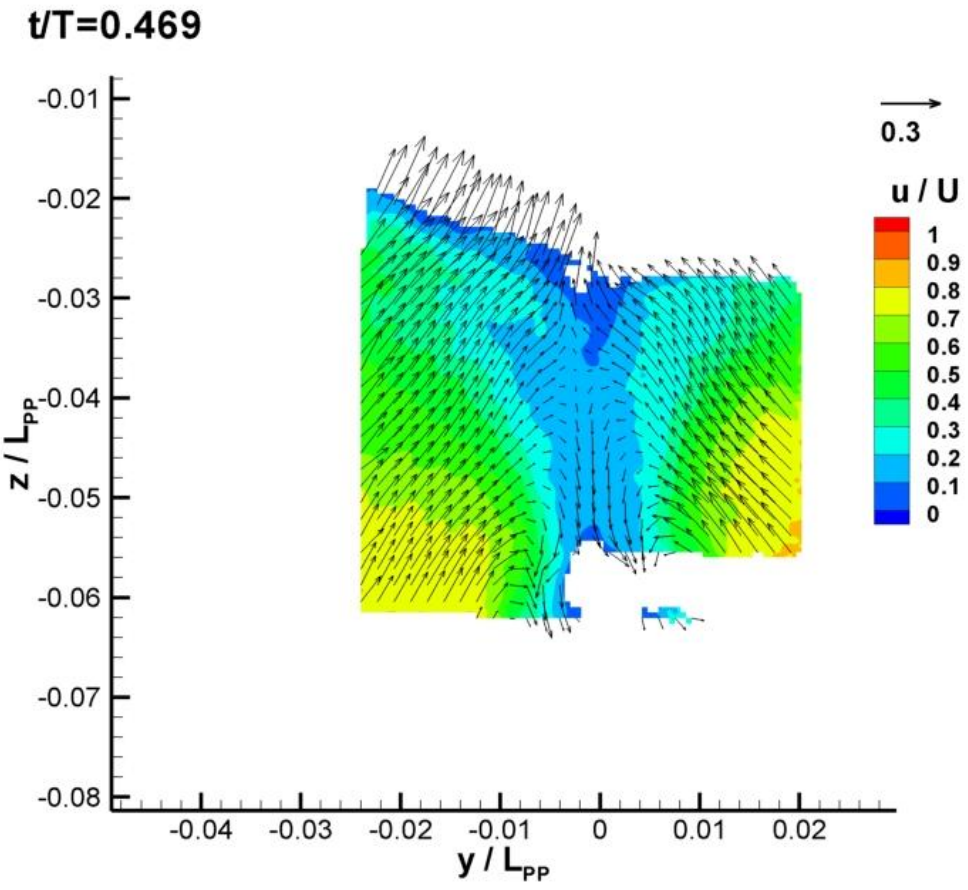


(b) Velocity distribution

Fig. 4-16 Velocity distribution (λ/L=1.1), t/T=0.380

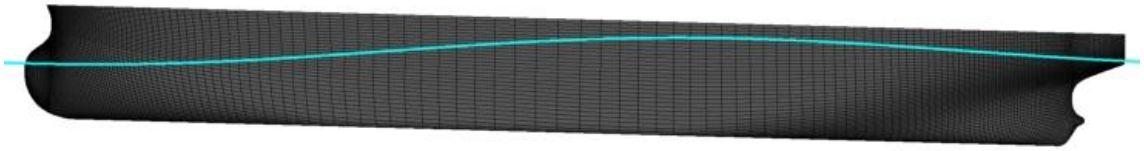


(a) Schematic view of wave and model ship

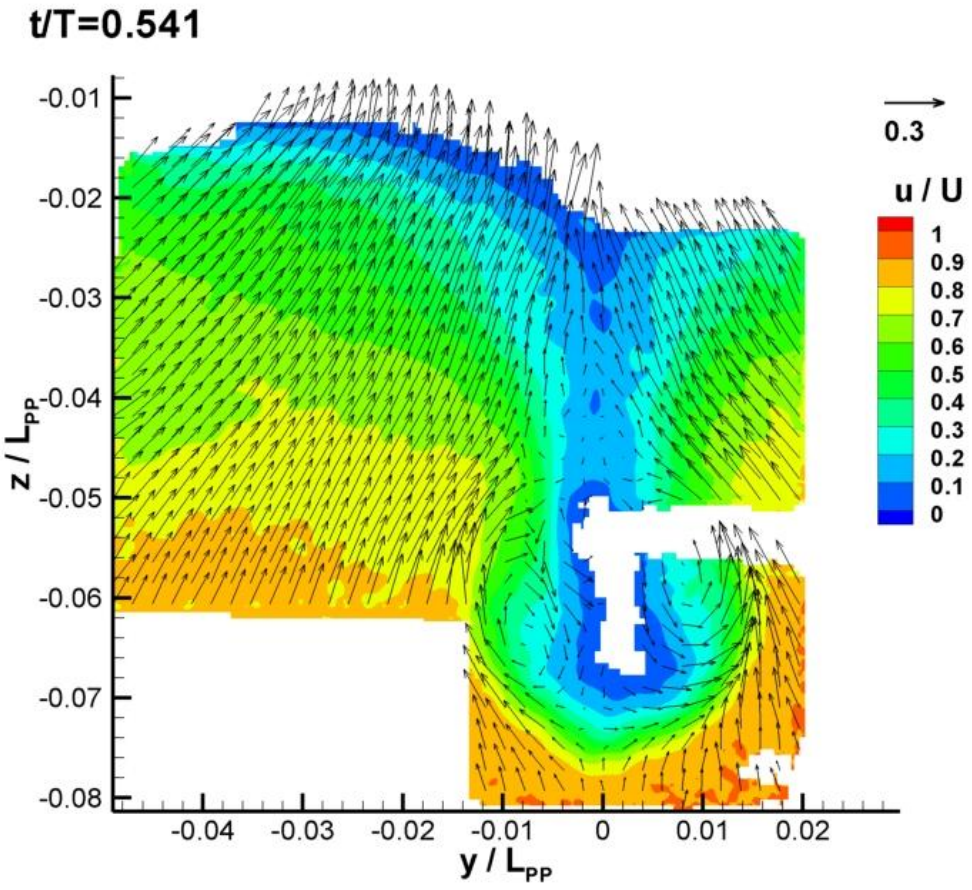


(b) Velocity distribution

Fig. 4-17 Velocity distribution (λ/L=1.1), t/T=0.469

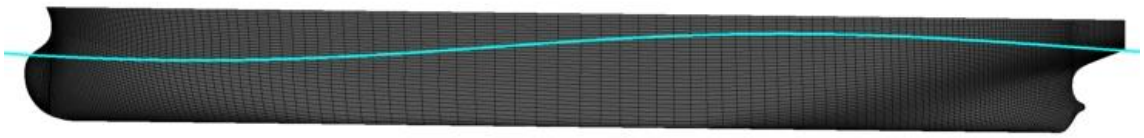


(a) Schematic view of wave and model ship

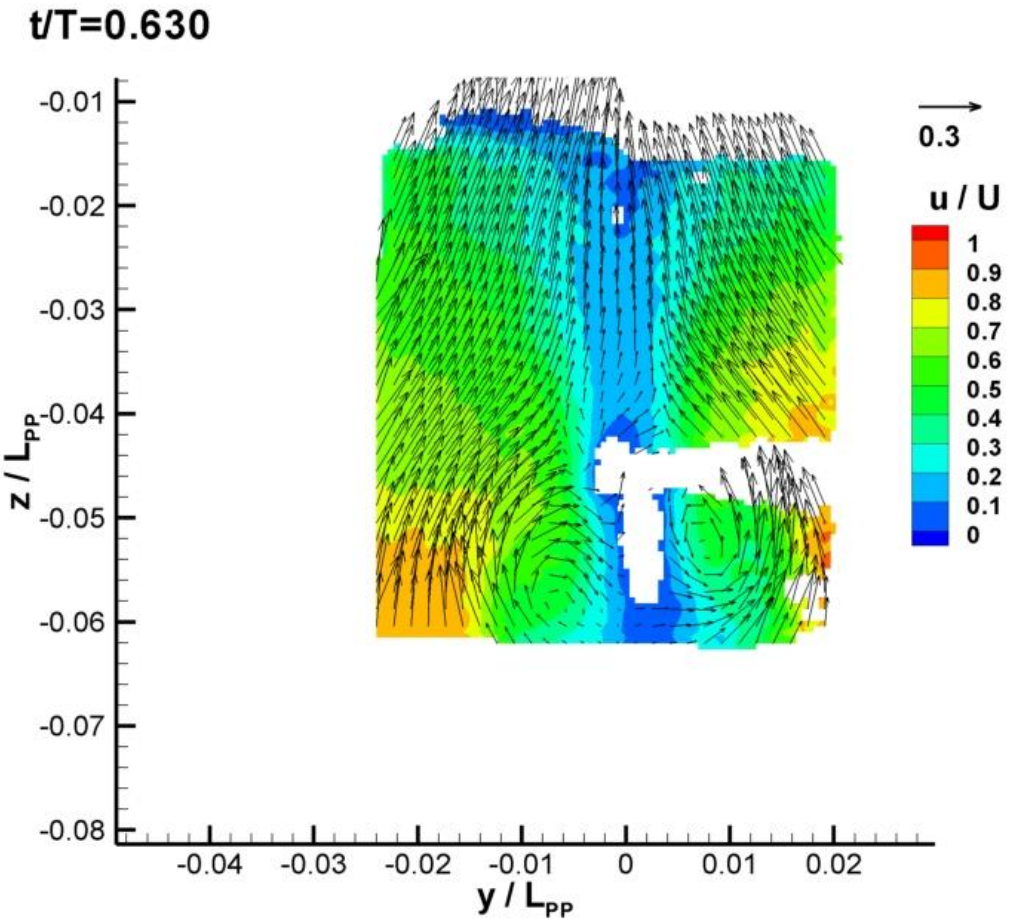


(b) Velocity distribution

Fig. 4-18 Velocity distribution (λ/L=1.1), t/T=0.541

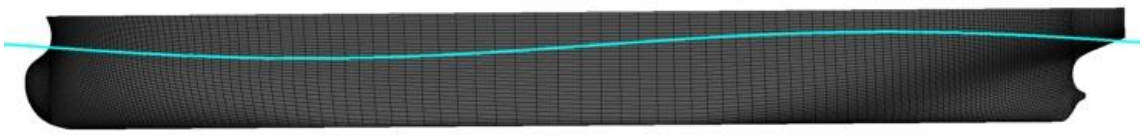


(a) Schematic view of wave and model ship

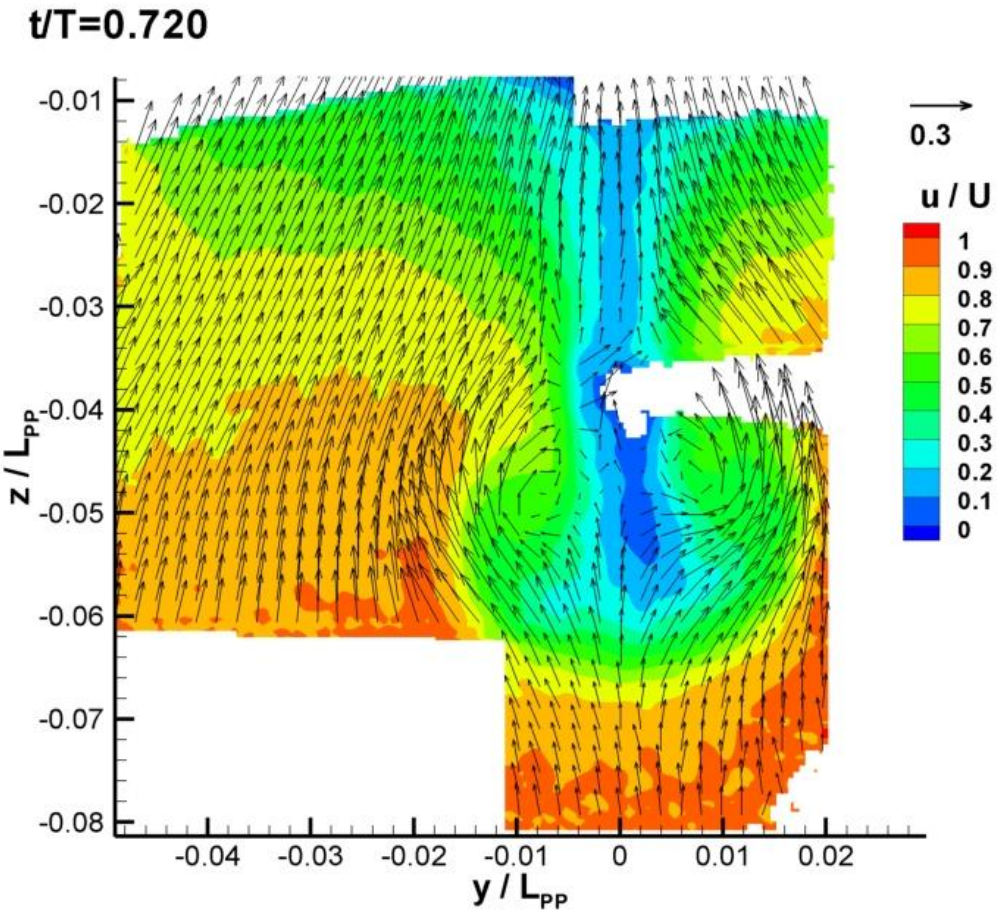


(b) Velocity distribution

Fig. 4-19 Velocity distribution (λ/L=1.1), t/T=0.630

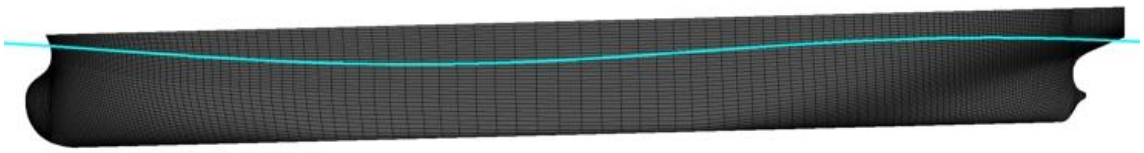


(a) Schematic view of wave and model ship

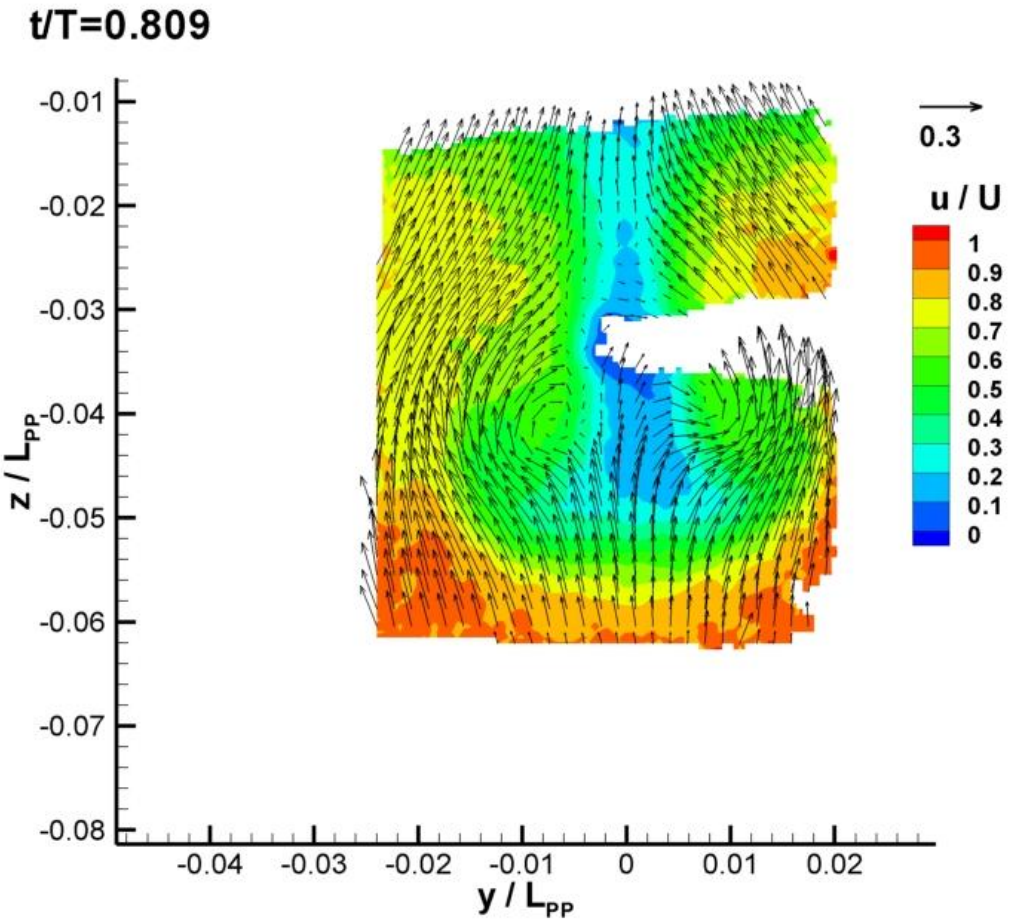


(b) Velocity distribution

Fig. 4-20 Velocity distribution (λ/L=1.1), t/T=0.720

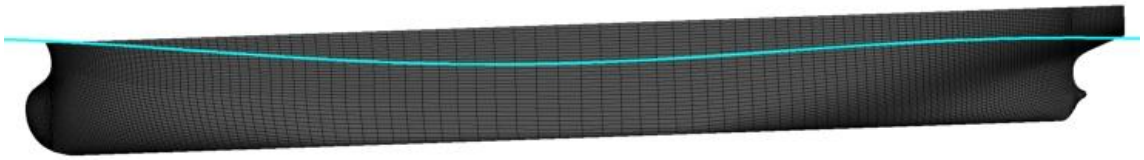


(a) Schematic view of wave and model ship

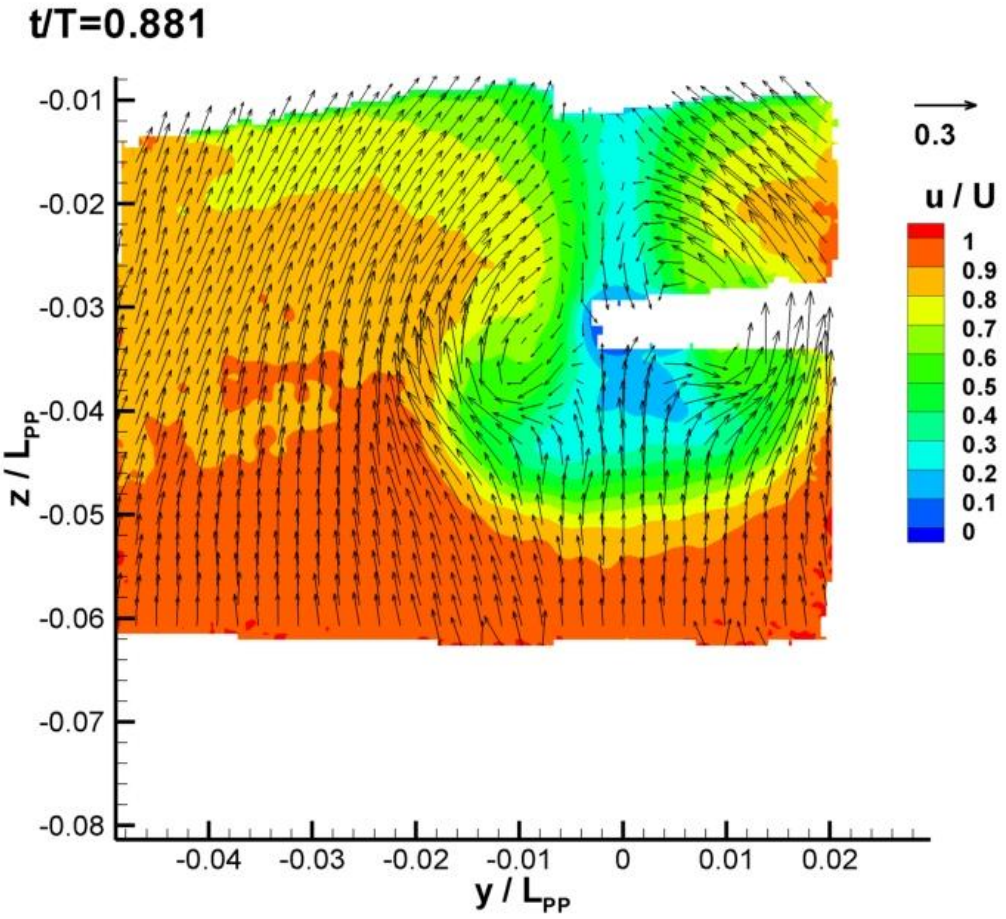


(b) Velocity distribution

Fig. 4-21 Velocity distribution (λ/L=1.1), t/T=0.809

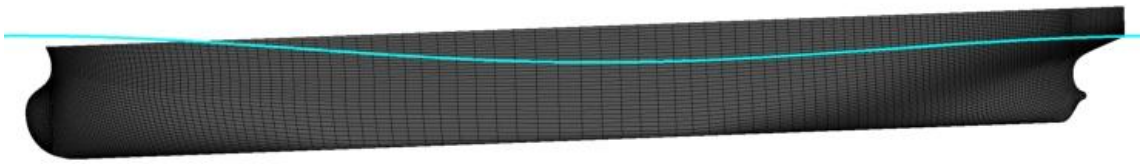


(a) Schematic view of wave and model ship

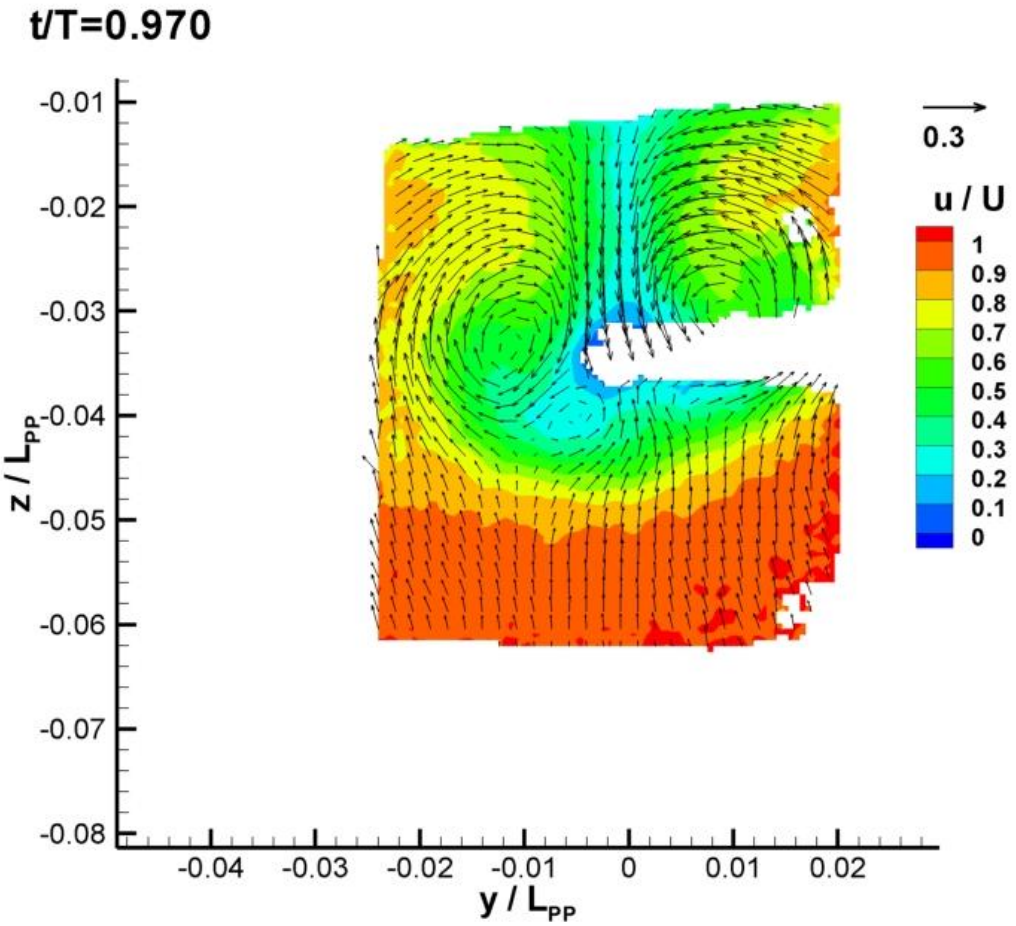


(b) Velocity distribution

Fig. 4-22 Velocity distribution (λ/L=1.1), t/T=0.881



(a) Schematic view of wave and model ship



(b) Velocity distribution

Fig. 4-23 Velocity distribution (λ/L=1.1), t/T=0.970

4.1.4Velocity distribution at propeller plane, λ/L=1.6

Fig. 4-24 shows the pitch, heave and surge motion with incident wave elevation at FP and propeller plane for λ / L_{pp}=1.6. The pitch and heave motion are large, but the added resistance is small. Fig. 4-25 to Fig. 4-30 shows the velocity distribution for each phase at propeller plane. The phase velocity fluctuation inside the boundary layer is different from the outside. Detailed discussion is next step using the comparison with CFD, because the measurement area is small.

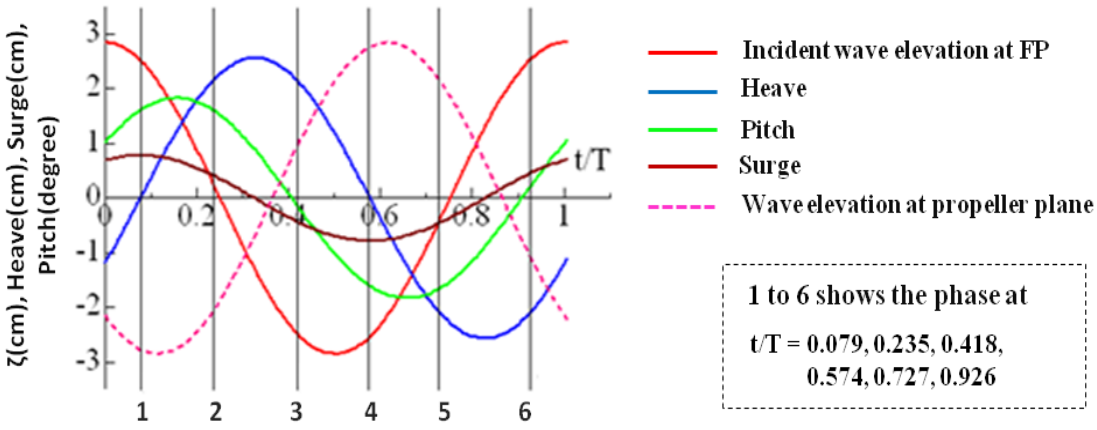
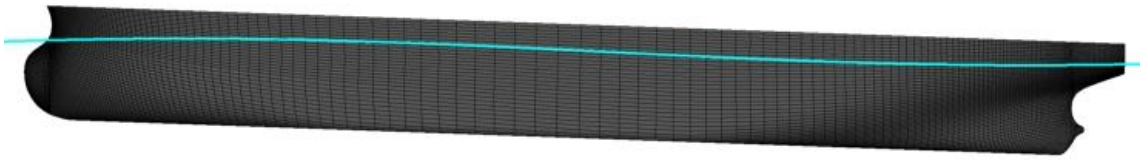
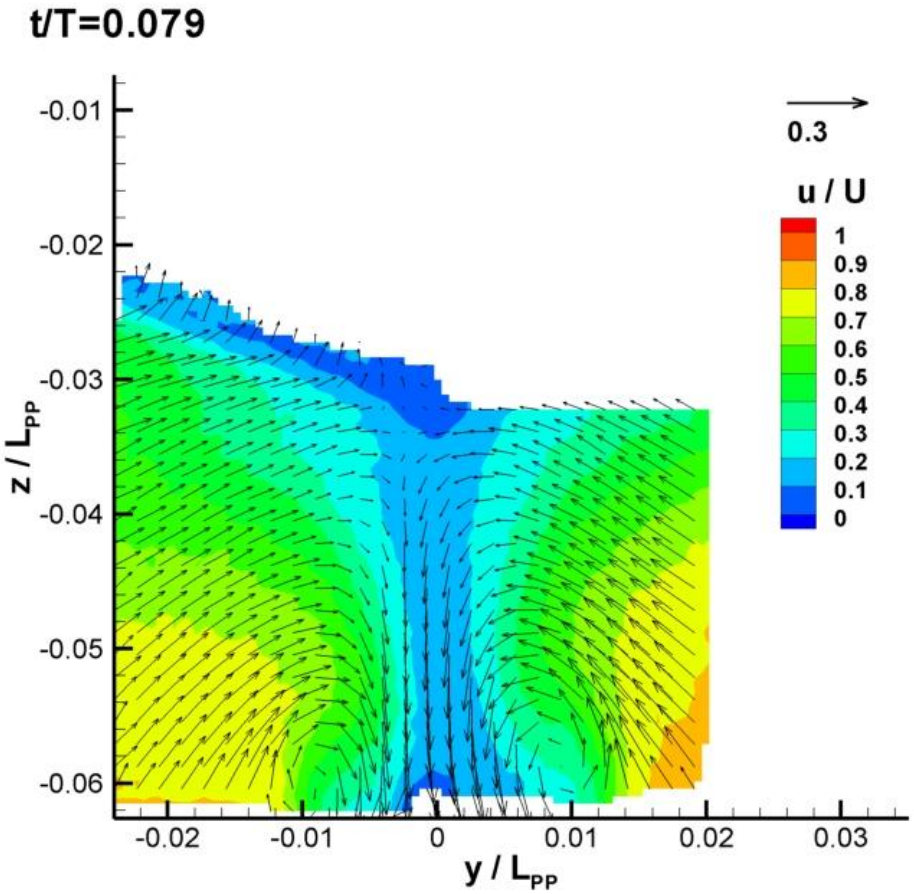


Fig. 4-24 Wave elevation and motion in one period (λ/L=1.6)

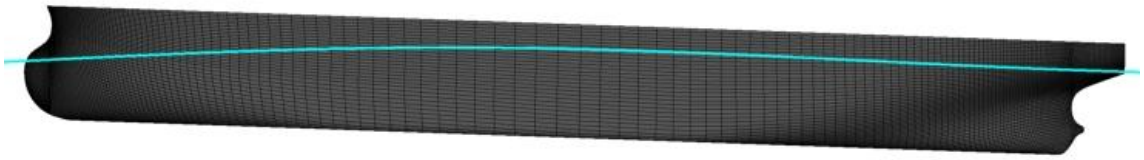


(a) Schematic view of wave and model ship

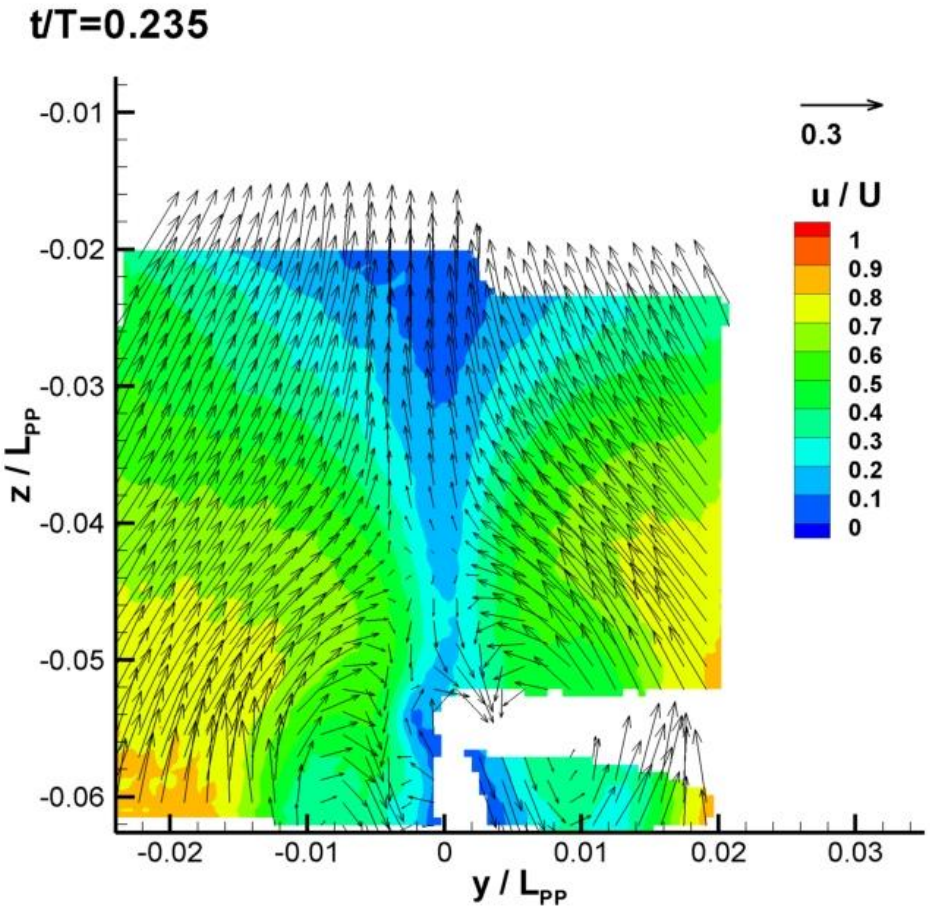


(b) Velocity distribution

Fig. 4-25 Velocity distribution (λ/L=1.6), t/T=0.079

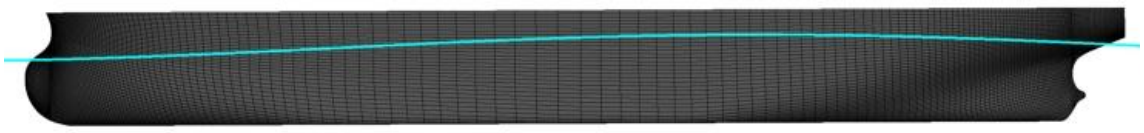


(a) Schematic view of wave and model ship

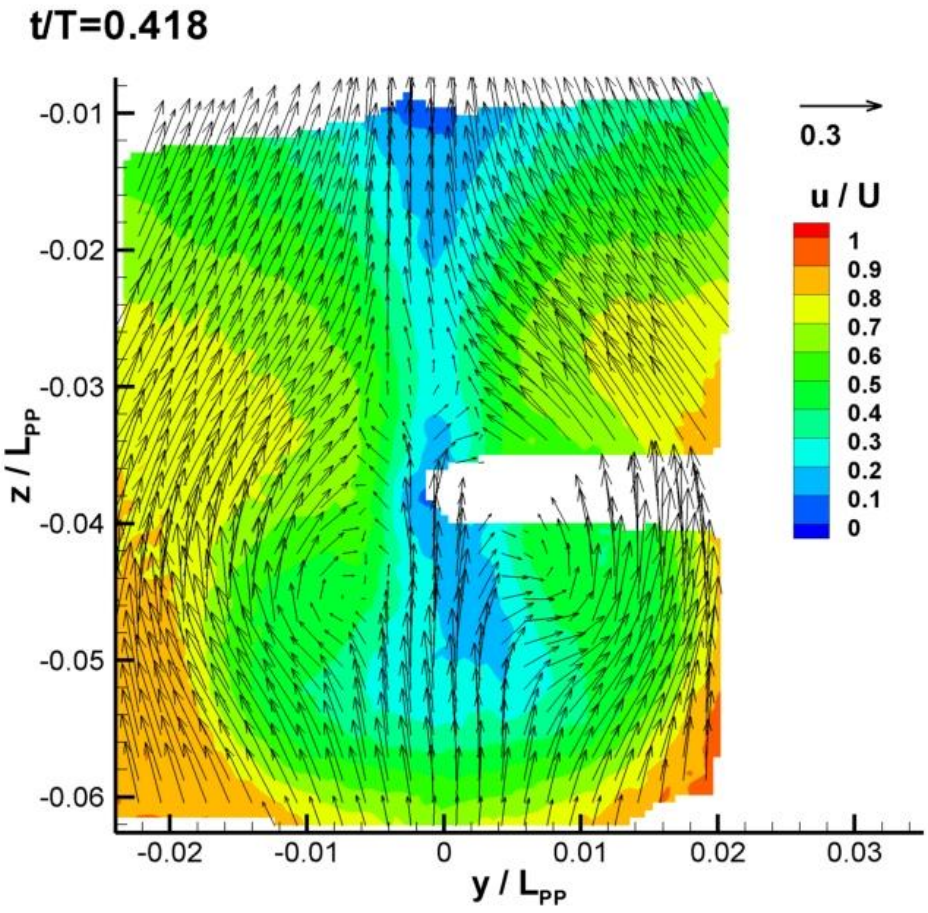


(b) Velocity distribution

Fig. 4-26 Velocity distribution (λ/L=1.6), t/T=0.235

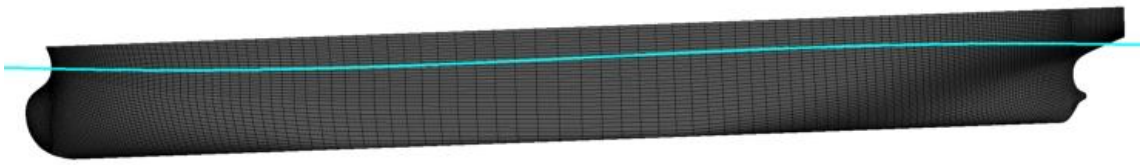


(a) Schematic view of wave and model ship

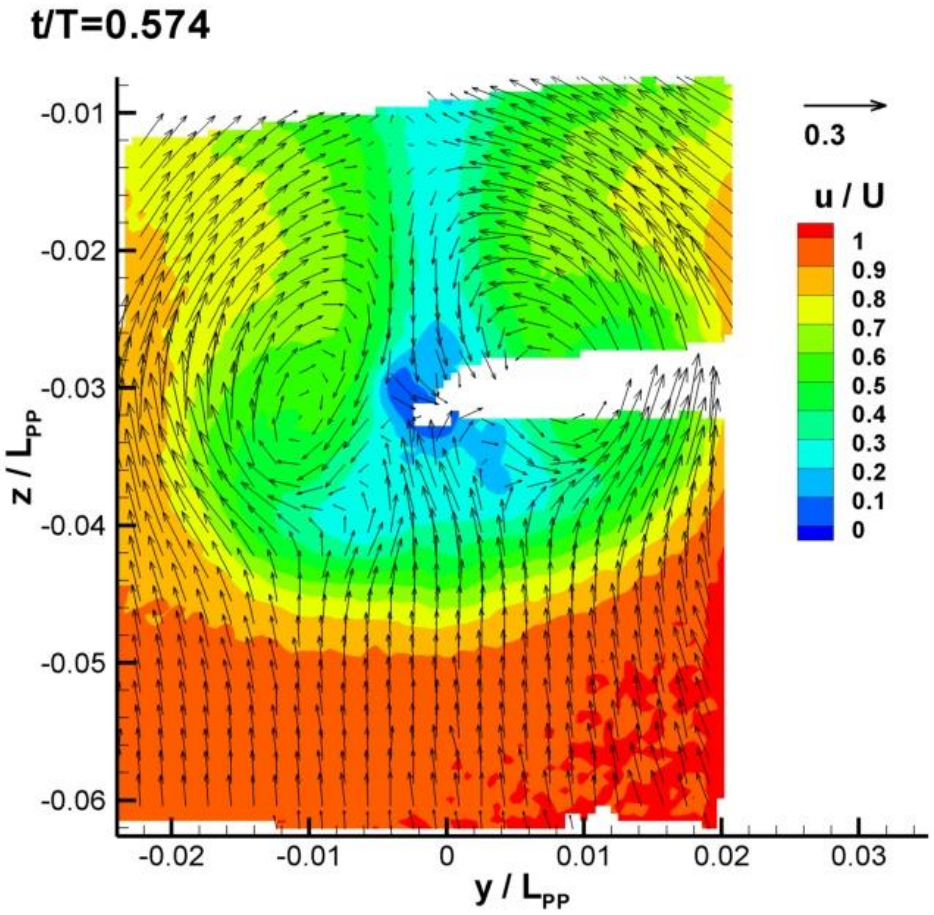


(b) Velocity distribution

Fig. 4-27 Velocity distribution (λ/L=1.6), t/T=0.418

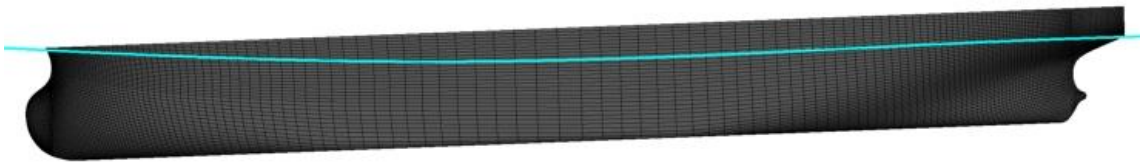


(a) Schematic view of wave and model ship

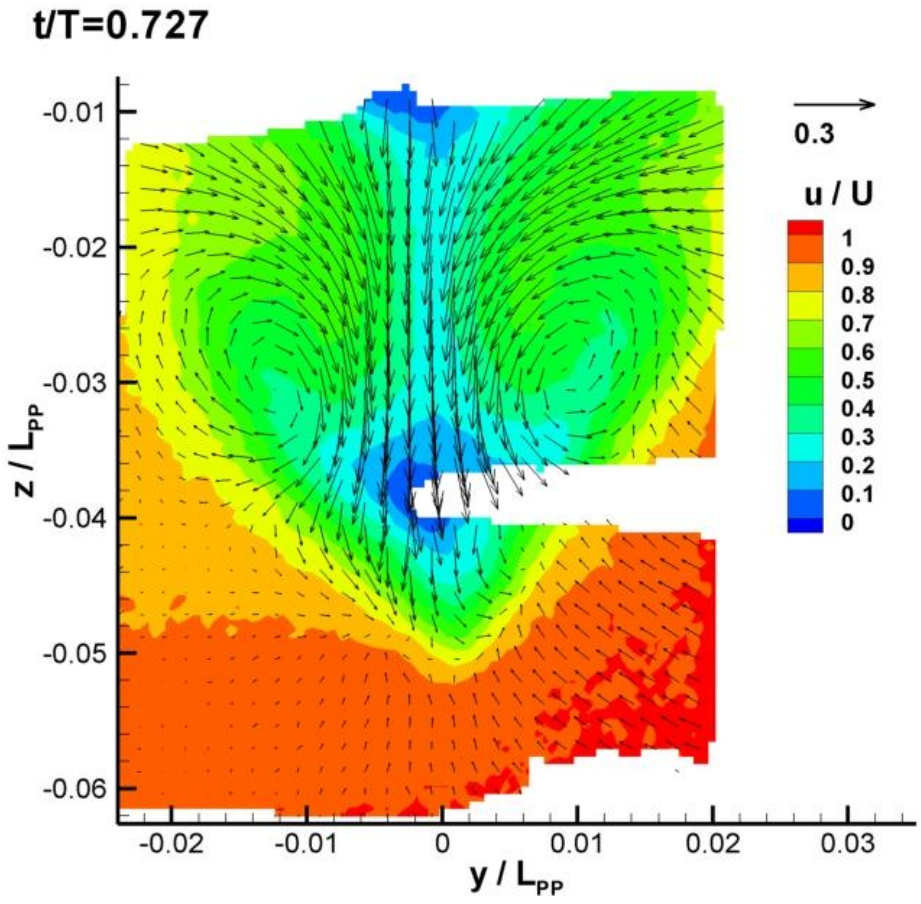


(b) Velocity distribution

Fig. 4-28 Velocity distribution (λ/L=1.6), t/T=0.574

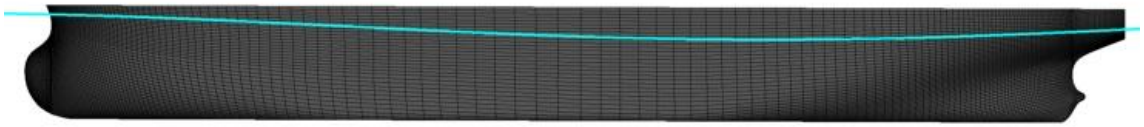


(a) Schematic view of wave and model ship

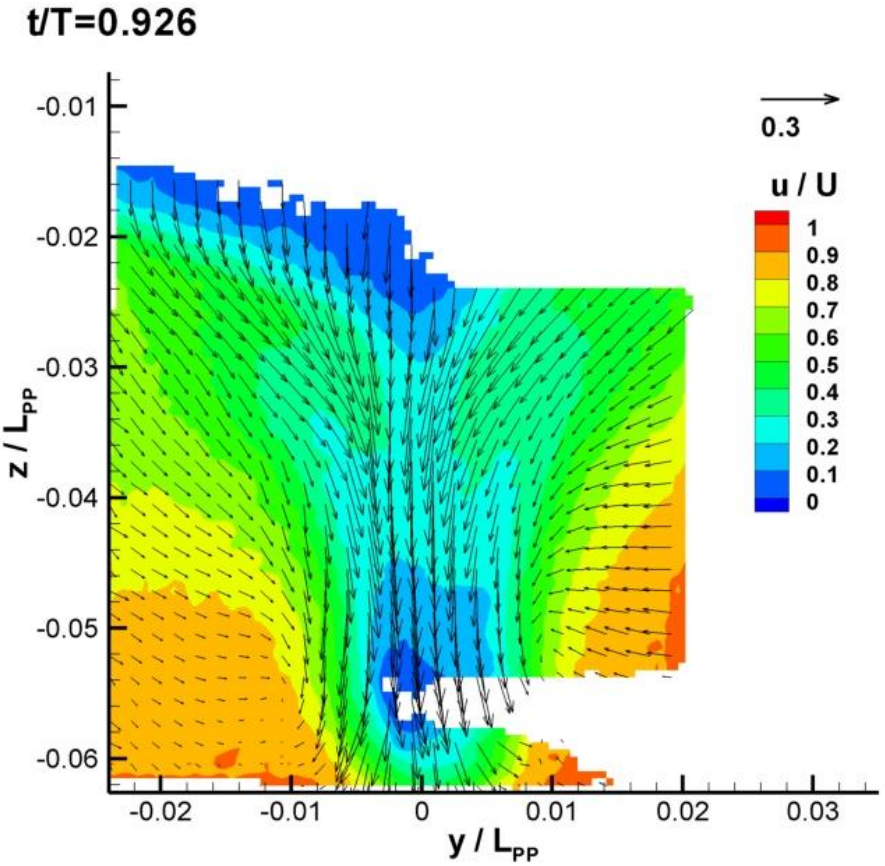


(b) Velocity distribution

Fig. 4-29 Velocity distribution (λ/L=1.6), t/T=0.727



(a) Schematic view of wave and model ship



(b) Velocity distribution

Fig. 4-30 Velocity distribution (λ/L=1.6), t/T=0.926

4.2 VELOCITY DISTRIBUTION AT PROPELLER PLANE IN BALLAST CONDITION

4.2.1 Velocity distribution at propeller plane in ballast condition

Fig. 4-31 shows the measurement results in calm water of ballast condition. In figures of measurement results, y(positive y is in starboard direction) and z(positive z is in upward direction) are measured from center plane and still water surface. In the figure, velocity components are shown in non-dimensional form using ship length L_{pp} and carriage speed U. For a numerical algorithm, the cross-correlation method was used. Finally, 32×32 pixel was selected as the inspection area and for the interrogation area, a 50% overlap was allowed between adjacent measurement areas. The shape of axial velocity contours is wider and longitudinal vortices are larger than those in full load condition. It is due to shallow draft and trim for ballast condition.

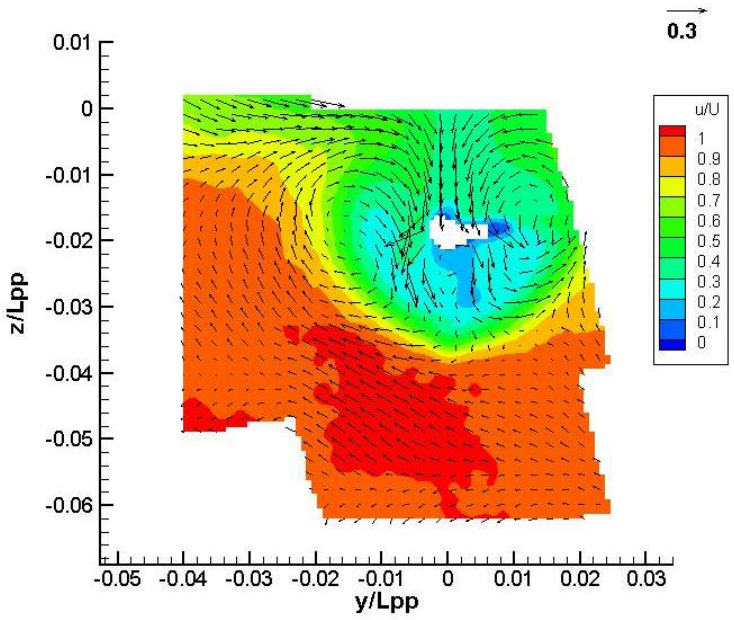


Fig. 4-31 Velocity distribution in calm water

4.2.2 Velocity distribution at propeller plane in ballast condition

Fig. 4-32 to Fig. 4-53 shows the velocity distribution for λ/L=0.6, 0.9, 1.5, respectively. The wake field is more complex than in calm water condition, as the wave changes the shape of the wake field over the encounter period. t/T shows the non-dimensional time using wave encounter period T. t/T=0 means the wave crest is at FP. From those figures, the shape of velocity distribution is changed by waves. The effect is larger in low velocity region. The fluctuation seems to be larger than that in full load condition due to the shallow draft. Fig.4-32 to Fig. 4-39 shows the velocity distribution for each phase for λ/L=0.6. Since the ship motion is small, pressure gradient effect and orbital velocity effect to the stretching of vortex sheet are dominant in the velocity distribution. So the axial velocity in outer invisid region is large due to the orbital motion velocity at wave crest.

The boundary layer thickness is changed by pressure gradient and the outer invicid flow. Near the propeller boss cap, the velocity fluctuation of low momentum fluid is larger than outer part and the phase of fluctuation is a little bit different from outer region. Fig. 4-40 to Fig. 4-47 shows the velocity distribution for each phase at propeller plane for λ/L=0.9. The motion is large, especially relative motion between the free surface and ship model is large. So, the part of propeller circle is in the air for some phases. The bilge vortices move up and down by the stern vertical motion. The vortices from the propeller boss part are also observed due to large vertical motion. The width of the boundary layer changes very largely. So, the thinner and thicker boundary layer can be observed compared with calm water due to the orbital motion and pressure gradient.

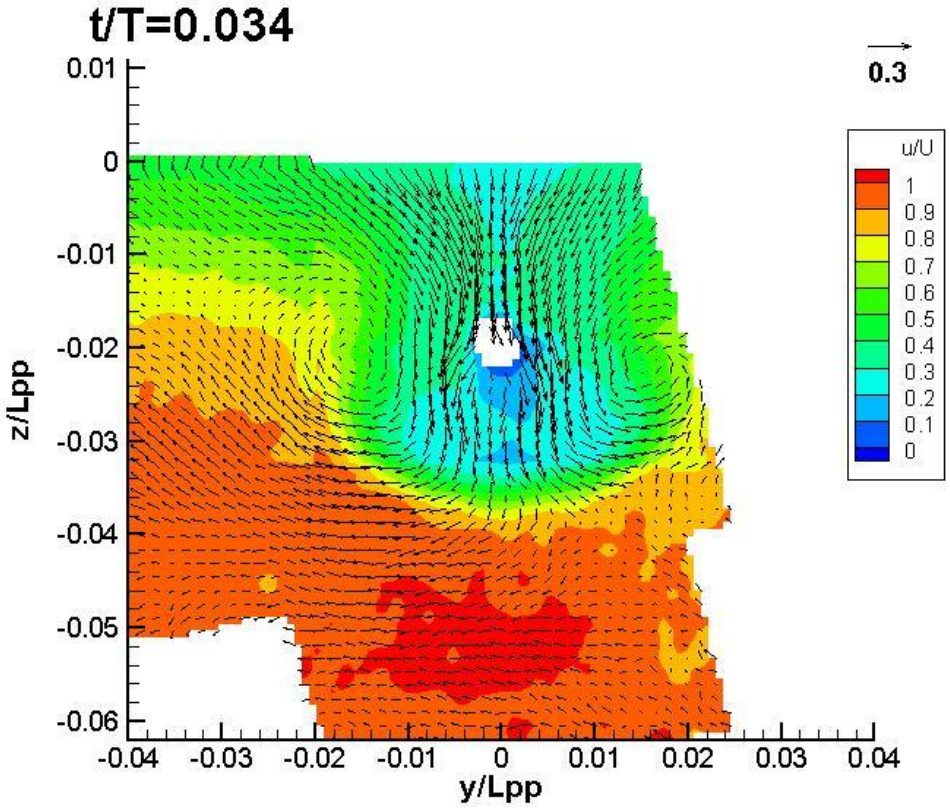
Fig. 4-48 to Fig. 4-53 shows the result for λ/L=1.5. The pitch and heave motion are large, but the added resistance and relative motion are small. So, the fluctuation is smaller than λ/L=1.5. But the phase velocity fluctuation inside the boundary layer seems to be different from the outside orbital velocity fluctuation due to the pressure gradient.

Note that it was difficult to maintain good uniform incident waves for a long period in one carriage run in present SPIV measurement. Therefore, the number of image pairs that can be taken in one carriage run was around 10-20. So, around 200 image pairs were taken by multiple carriage runs for one condition and one phase. But the numbers of images were not enough to get the fully converged mean flow. In addition to that, the low frequency surge motion due to the weak spring and mass system could not be completely adjusted to be 0, so the measured positions for same phase are a little bit different from the desired surge position. From these and the usual analysis, the uncertainty of velocity components are predicted around 5% of carriage speed near the center plane. Although the uncertainty is large, the wake distribution for the ballast condition in waves seems to be important to consider the propulsion performance in waves. So, the measurement data were presented in this study.

4.2.3 Velocity distribution at propeller plane, λ/L=0.6



(a) Schematic view of wave and model ship

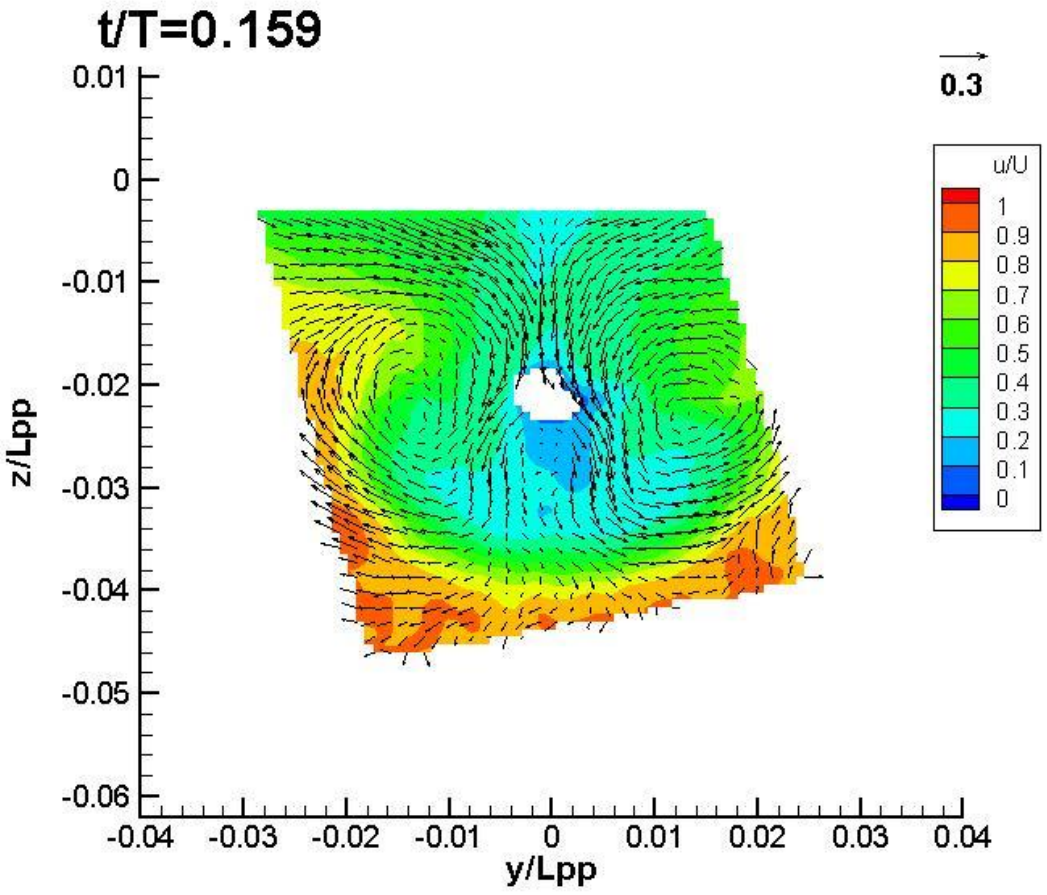


(b) Velocity distribution

Fig. 4-32 Velocity distribution (λ/L=0.6), t/T=0.034

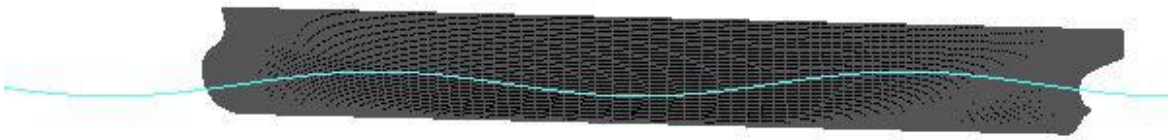


(a) Schematic view of wave and model ship

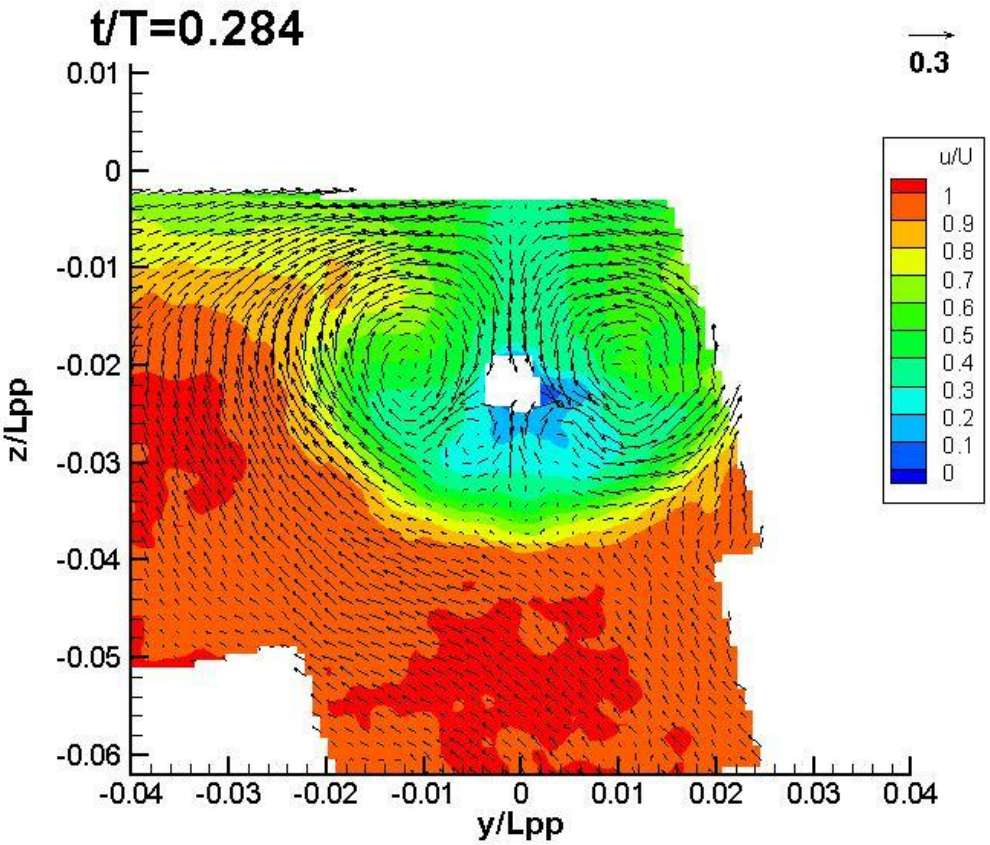


(b) Velocity distribution

Fig. 4-33 Velocity distribution (λ/L=0.6), t/T=0.159

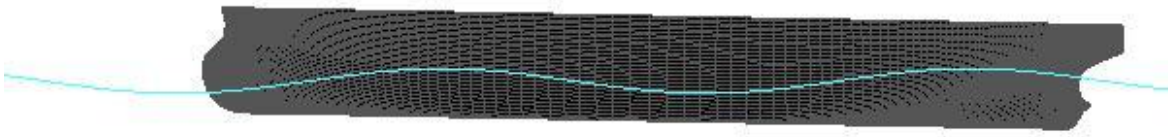


(a) Schematic view of wave and model ship

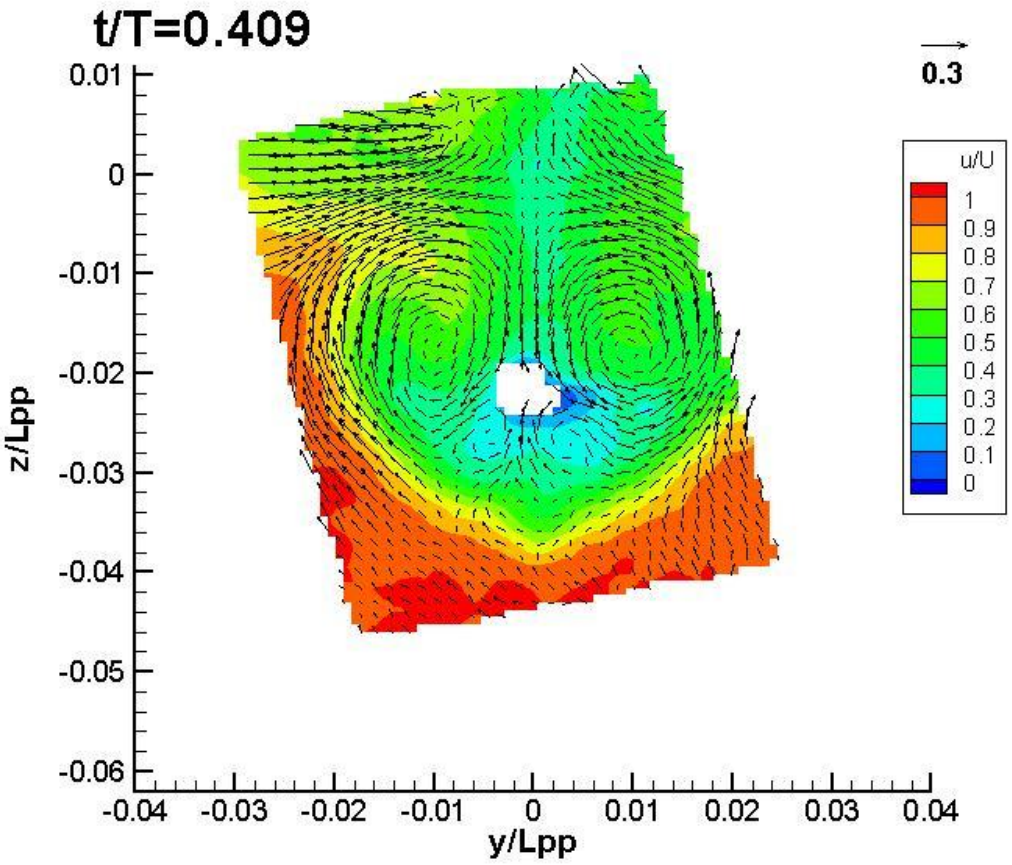


(b) Velocity distribution

Fig. 4-34 Velocity distribution (λ/L=0.6), t/T=0.284



(a) Schematic view of wave and model ship

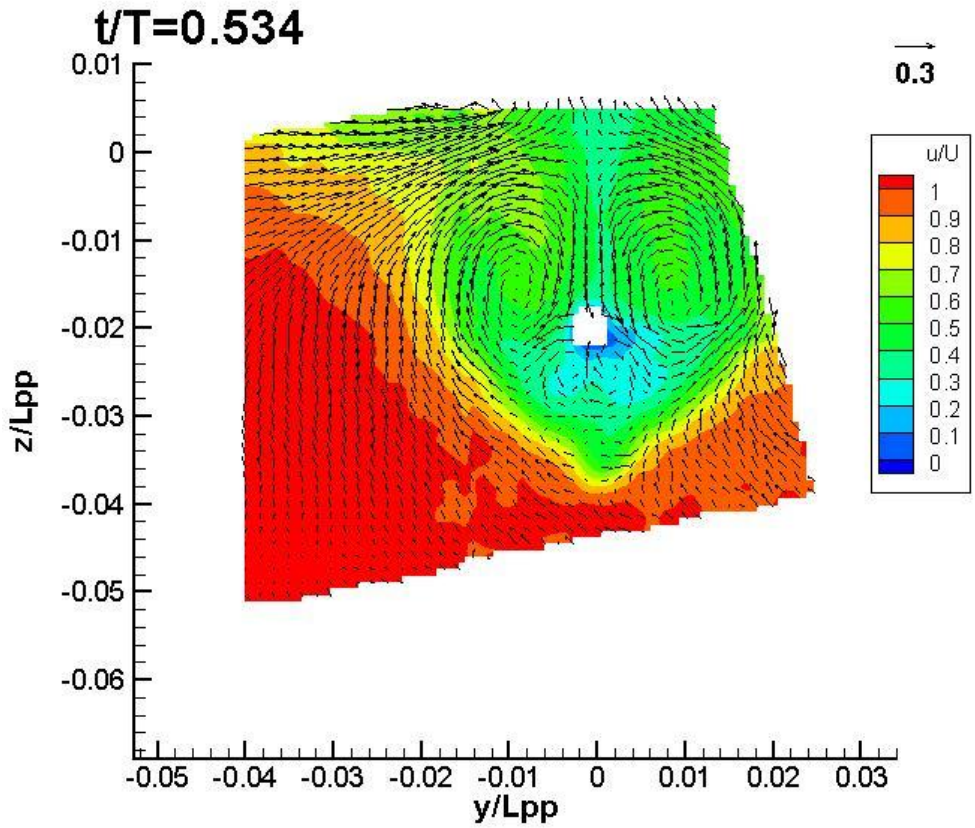


(b) Velocity distribution

Fig. 4-35 Velocity distribution (λ/L=0.6), t/T=0.409



(a) Schematic view of wave and model ship

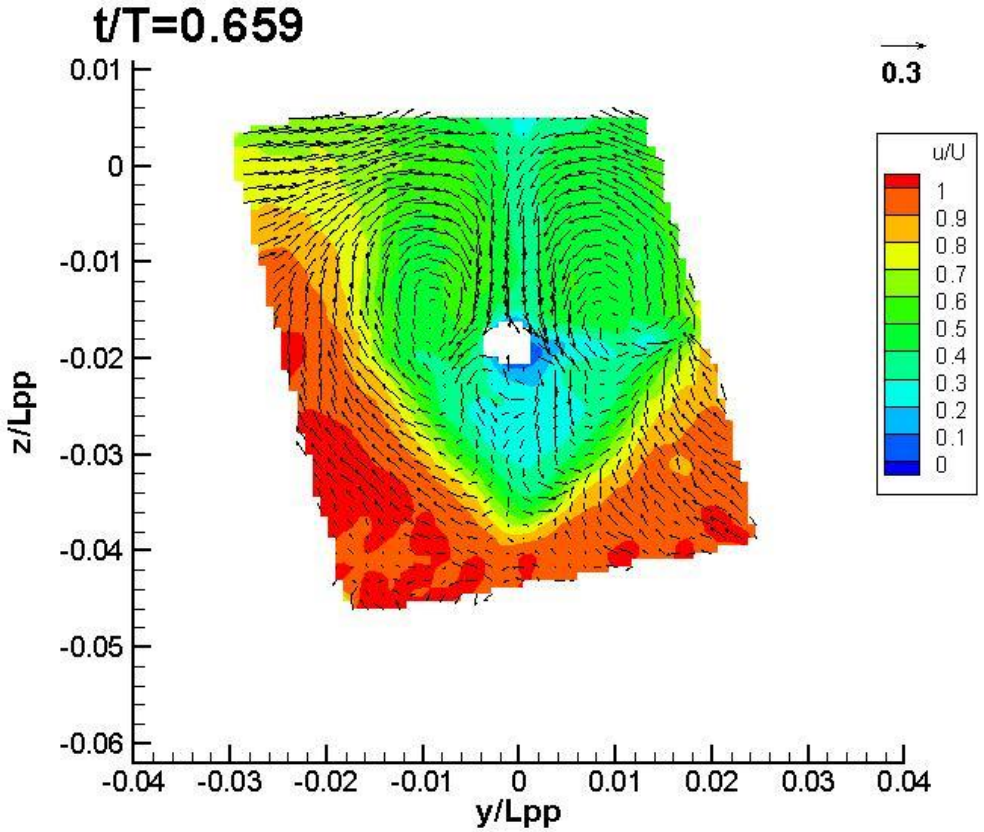


(b) Velocity distribution

Fig. 4-36 Velocity distribution (λ/L=0.6), t/T=0.534

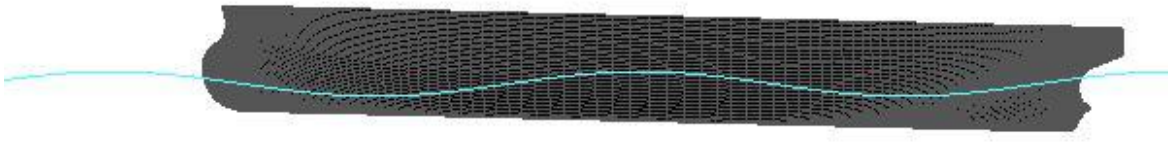


(a) Schematic view of wave and model ship

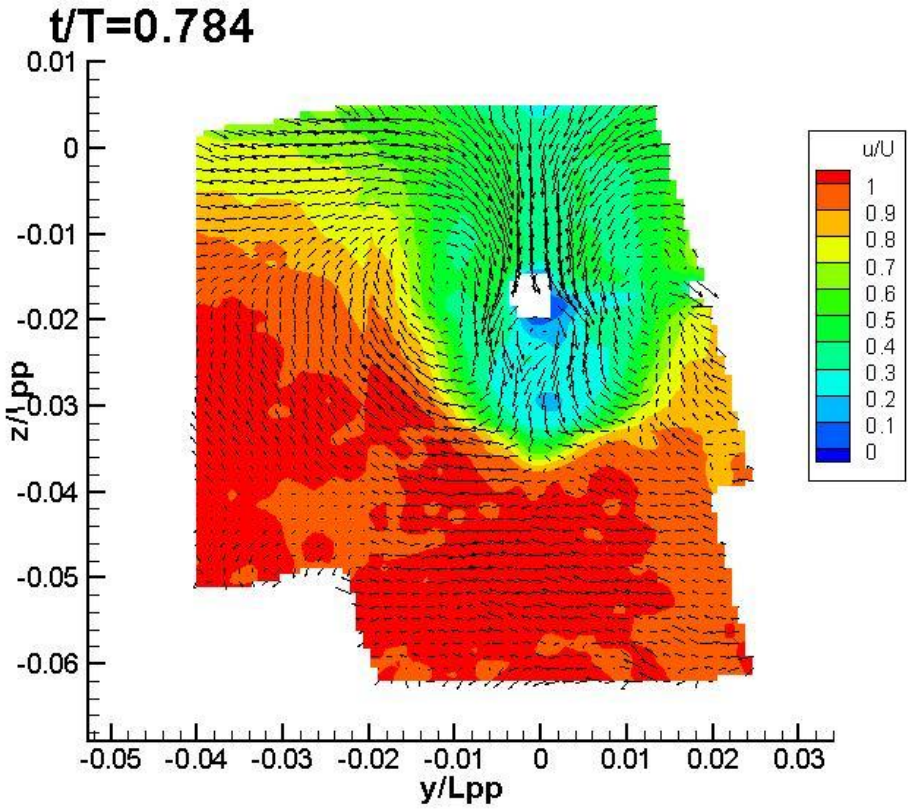


(b) Velocity distribution

Fig. 4-37 Velocity distribution (λ/L=0.6), t/T=0.659

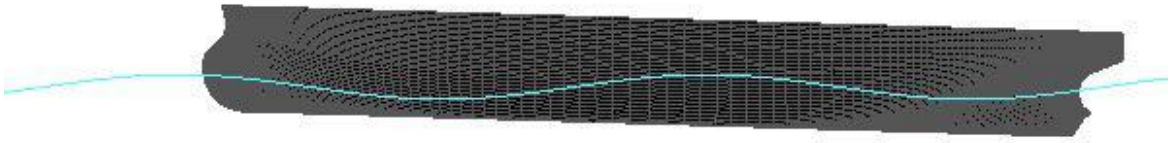


(a) Schematic view of wave and model ship

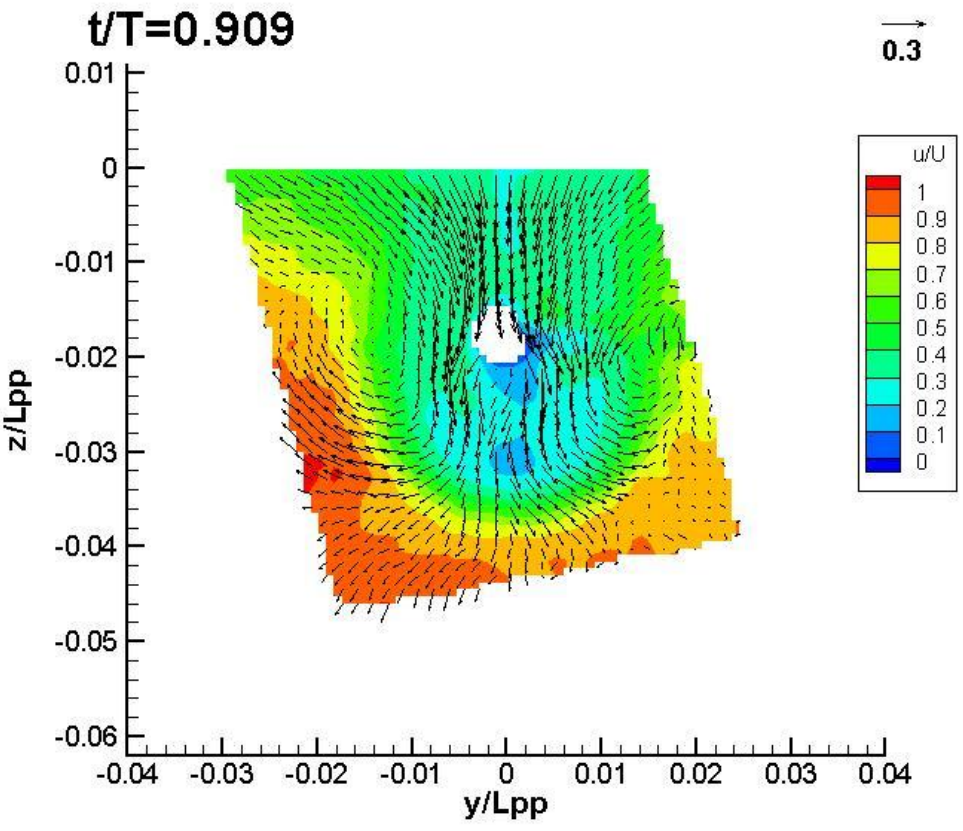


(b) Velocity distribution

Fig. 4-38 Velocity distribution (λ/L=0.6), t/T=0.784



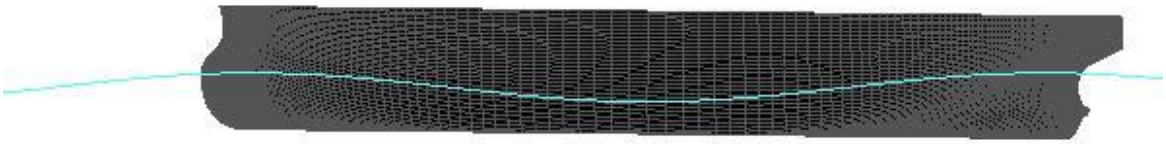
(a) Schematic view of wave and model ship



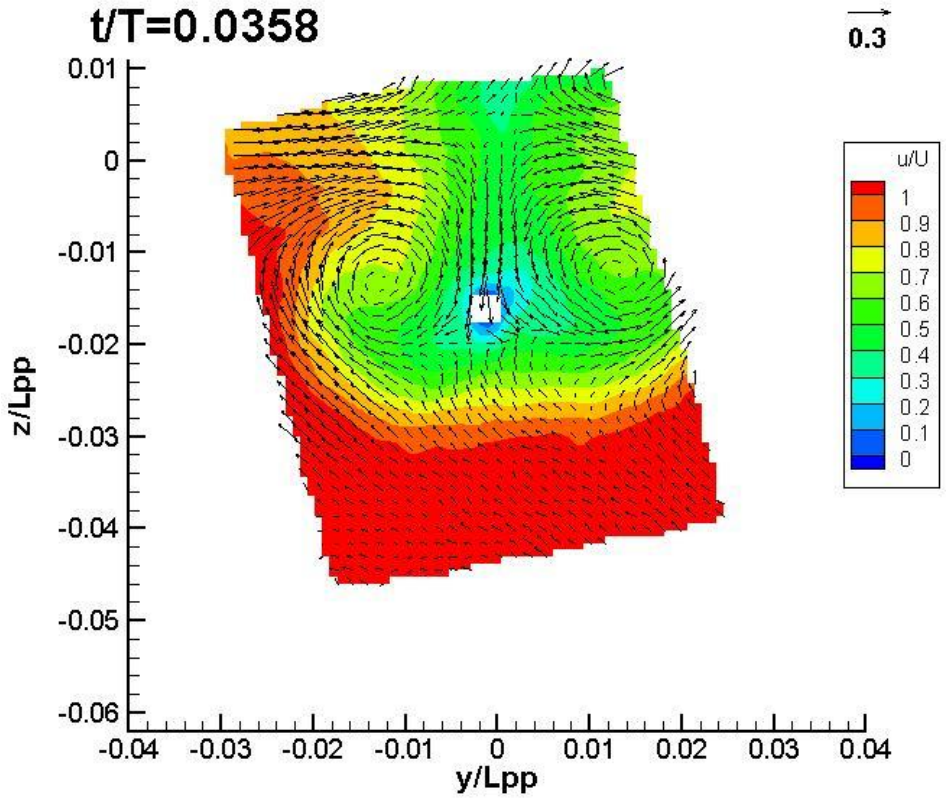
(b) Velocity distribution

Fig. 4-39 Velocity distribution (λ/L=0.6), t/T=0.909

4.2.4 Velocity distribution at propeller plane, λ/L=0.9



(a) Schematic view of wave and model ship

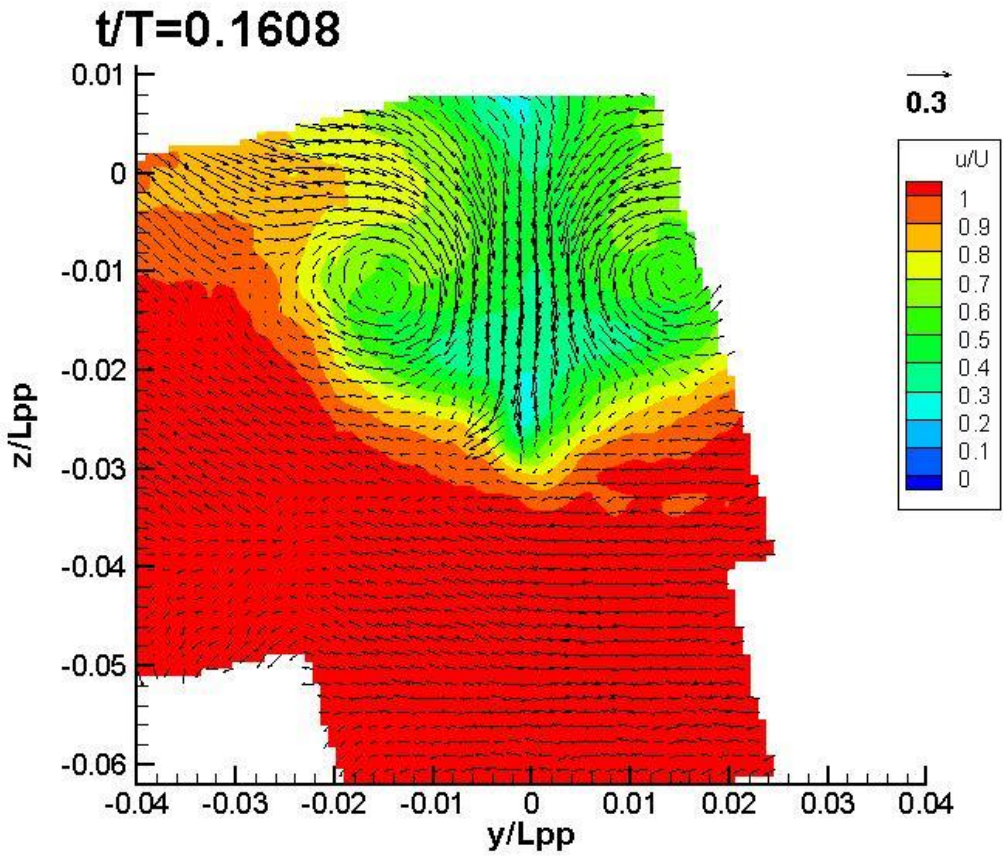


(b) Velocity distribution

Fig. 4-40 Velocity distribution (λ/L=0.9), t/T=0.0358

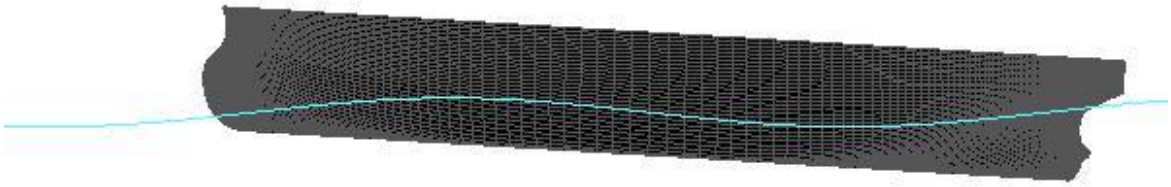


(a) Schematic view of wave and model ship

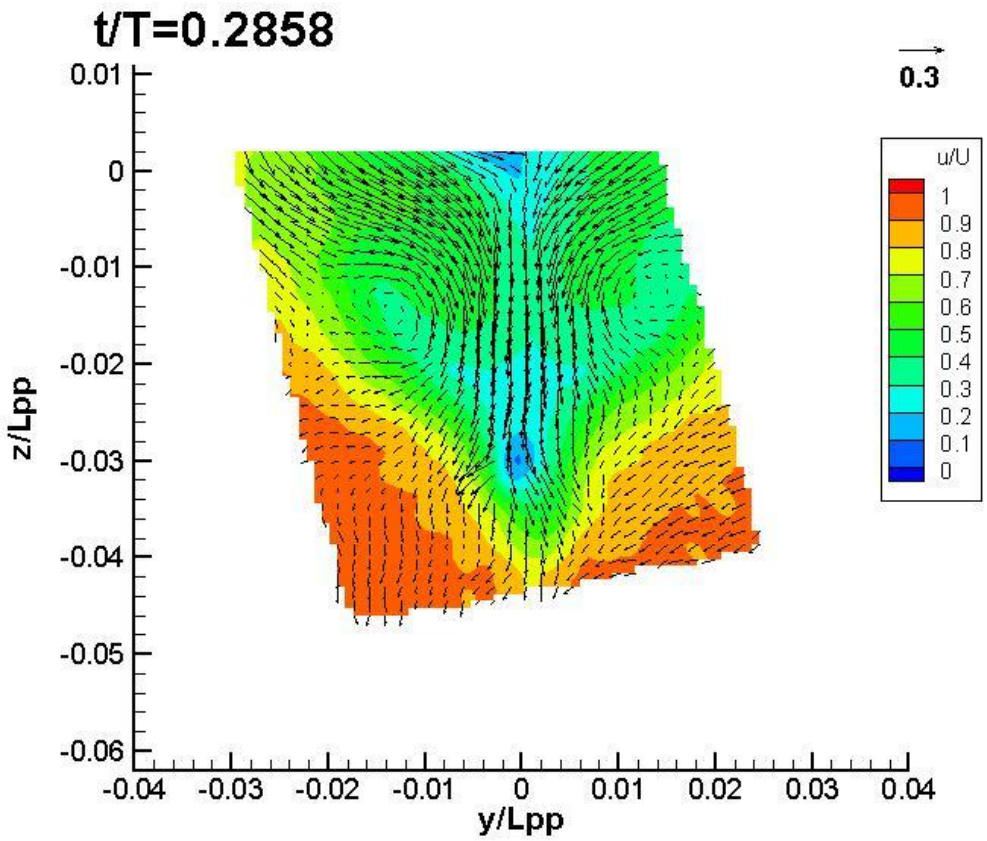


(b) Velocity distribution

Fig. 4-41 Velocity distribution (λ/L=0.9), t/T=0.1608



(a) Schematic view of wave and model ship

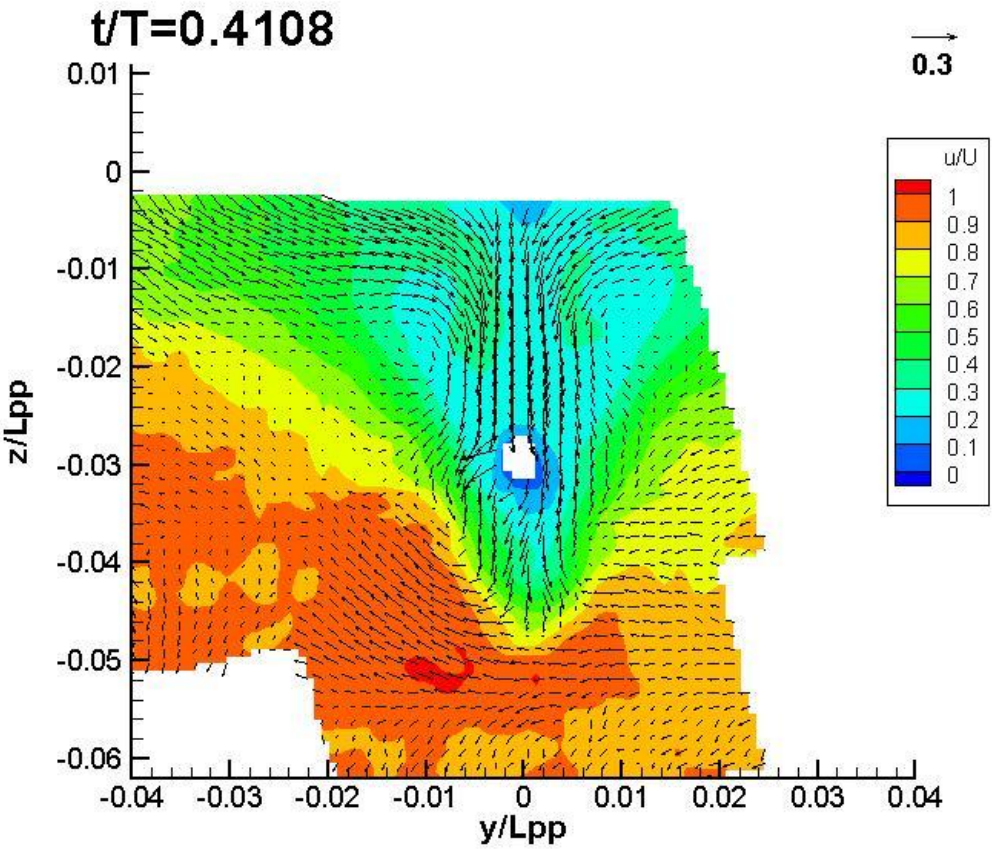


(b) Velocity distribution

Fig. 4-42 Velocity distribution (λ/L=0.9), t/T=0.2858



(a) Schematic view of wave and model ship

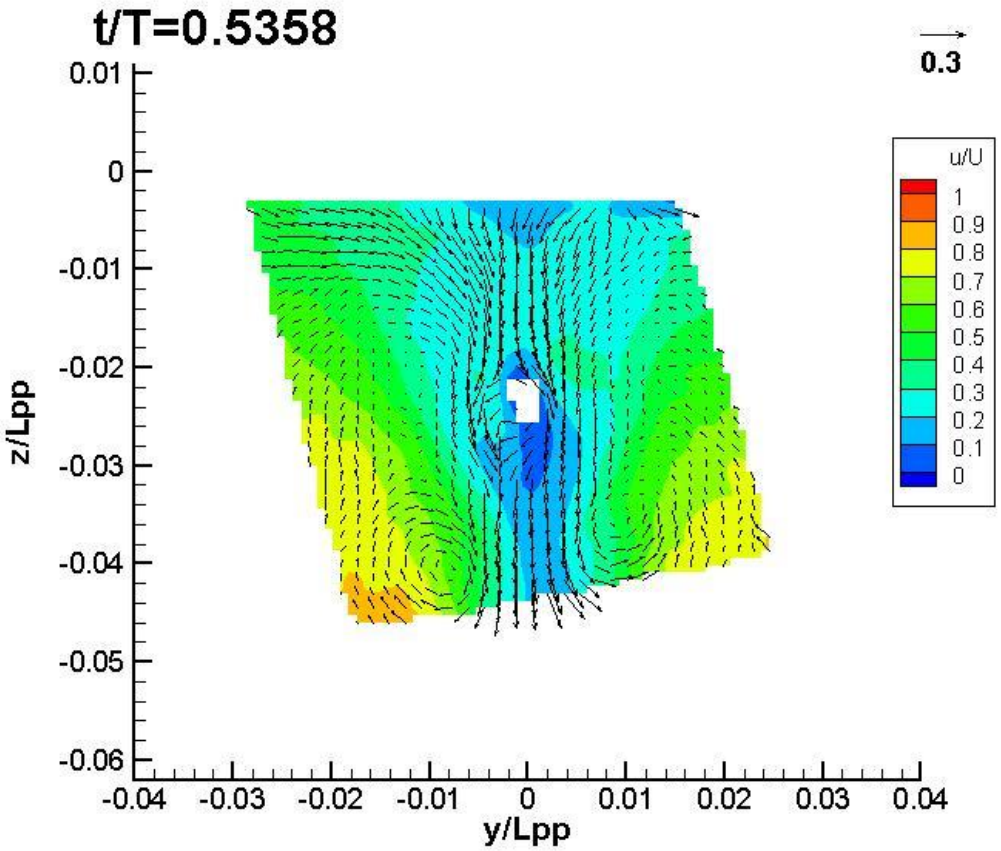


(b) Velocity distribution

Fig. 4-43 Velocity distribution (λ/L=0.9), t/T=0.4108

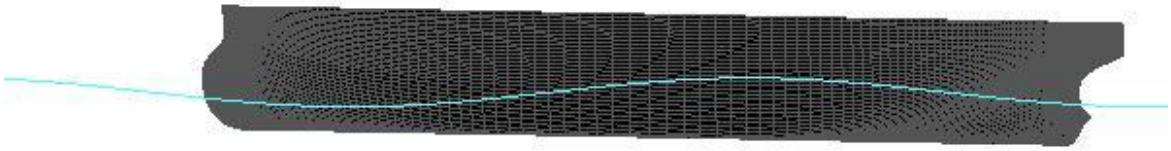


(a) Schematic view of wave and model ship

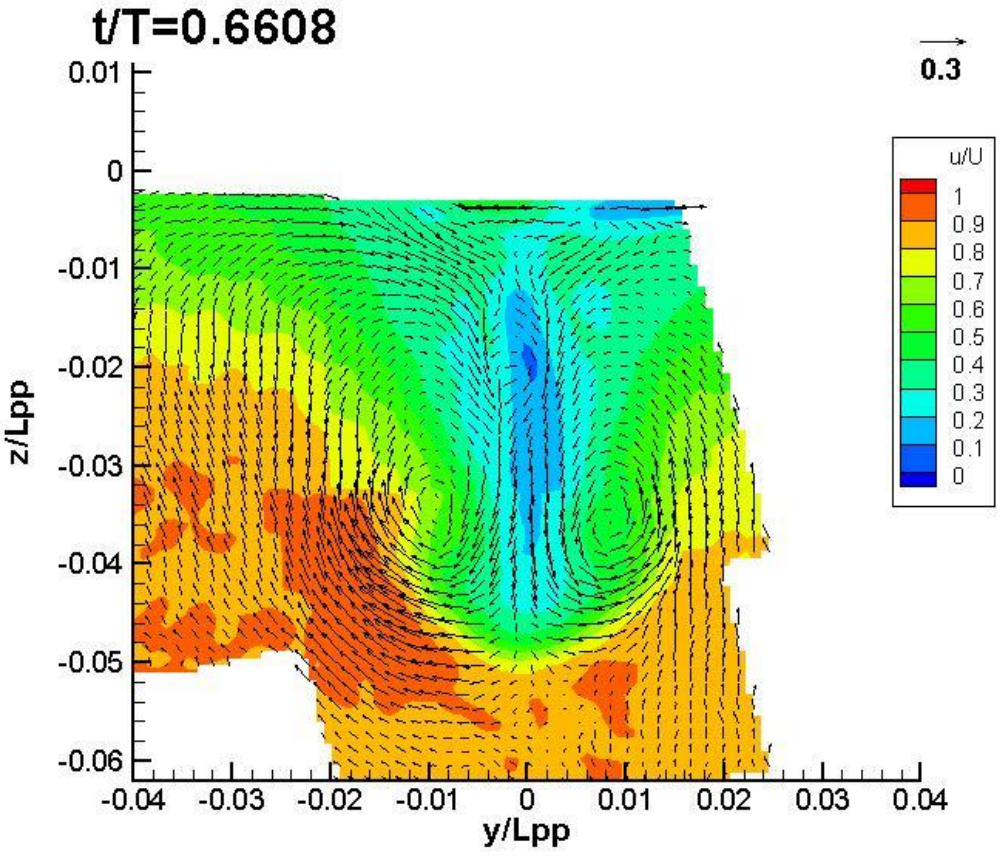


(b) Velocity distribution

Fig. 4-44 Velocity distribution (λ/L=0.9), t/T=0.5358

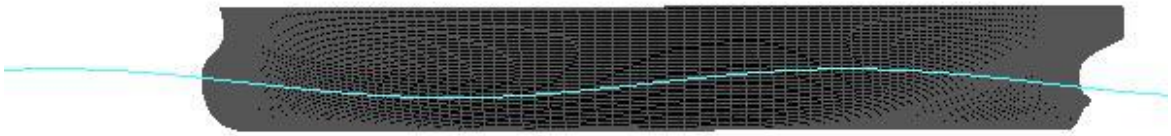


(a) Schematic view of wave and model ship

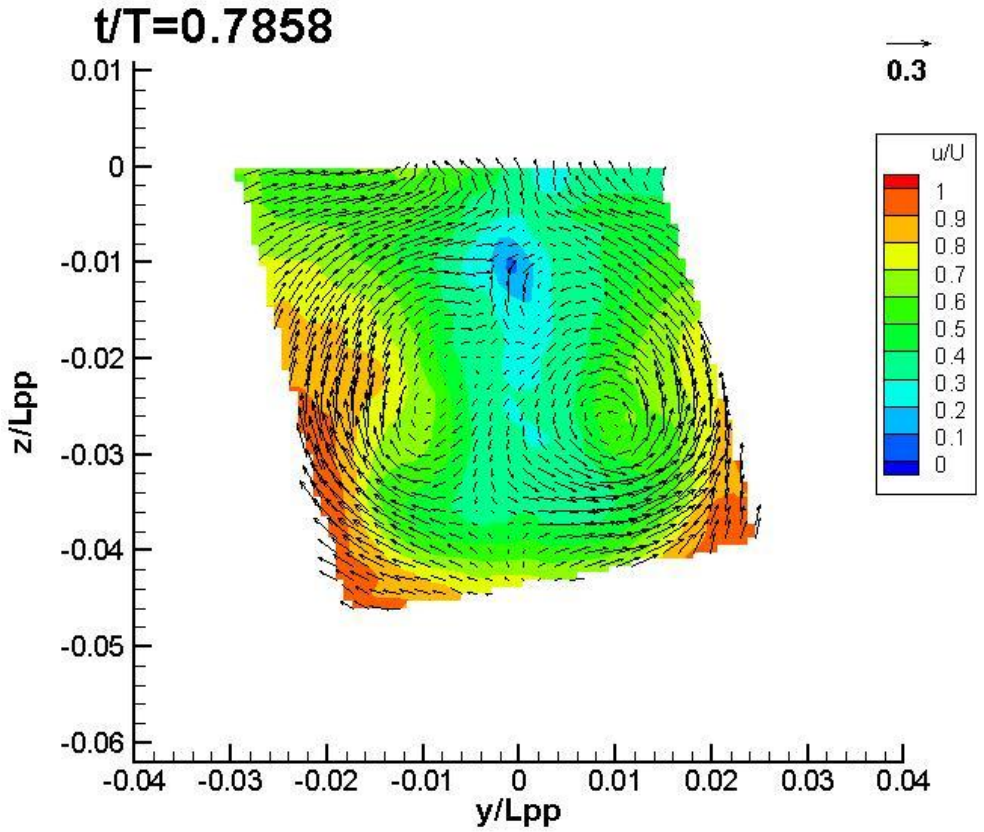


(b) Velocity distribution

Fig. 4-45 Velocity distribution (λ/L=0.9), t/T=0.6608

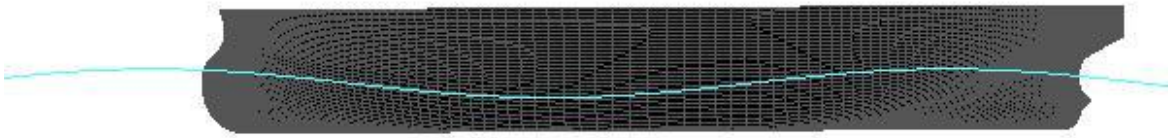


(a) Schematic view of wave and model ship

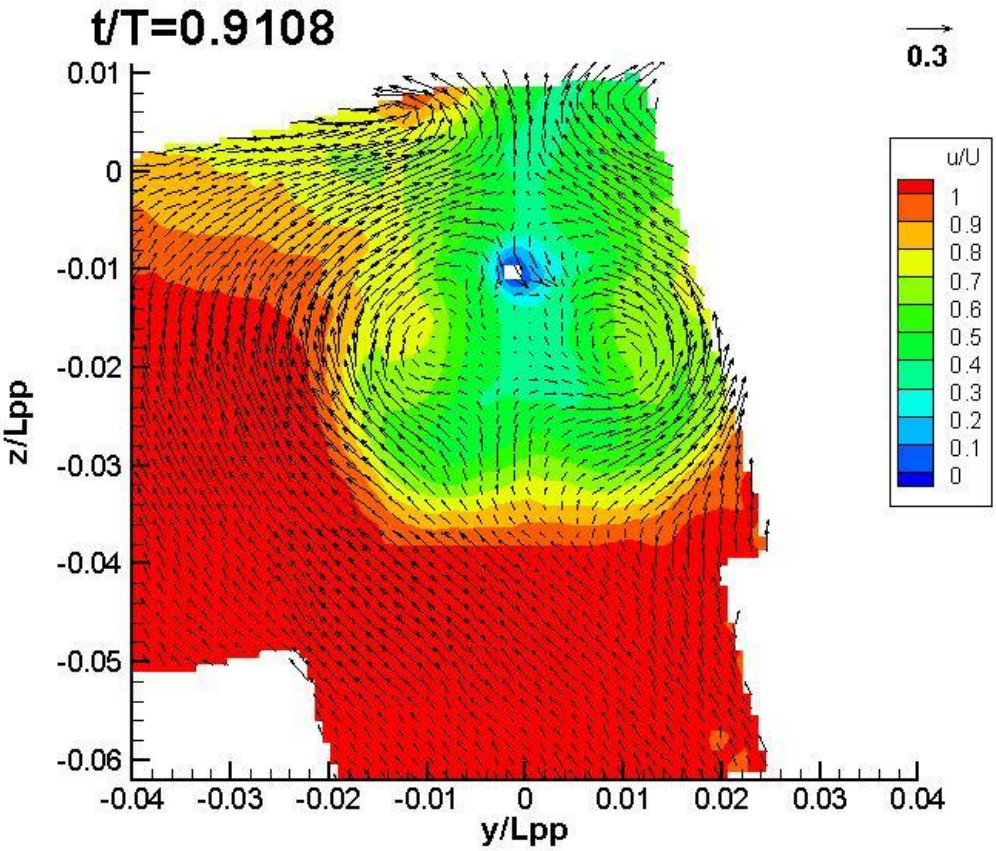


(b) Velocity distribution

Fig. 4-46 Velocity distribution (λ/L=0.9), t/T=0.7858



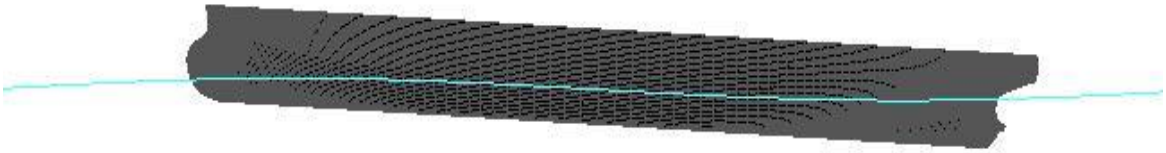
(a) Schematic view of wave and model ship



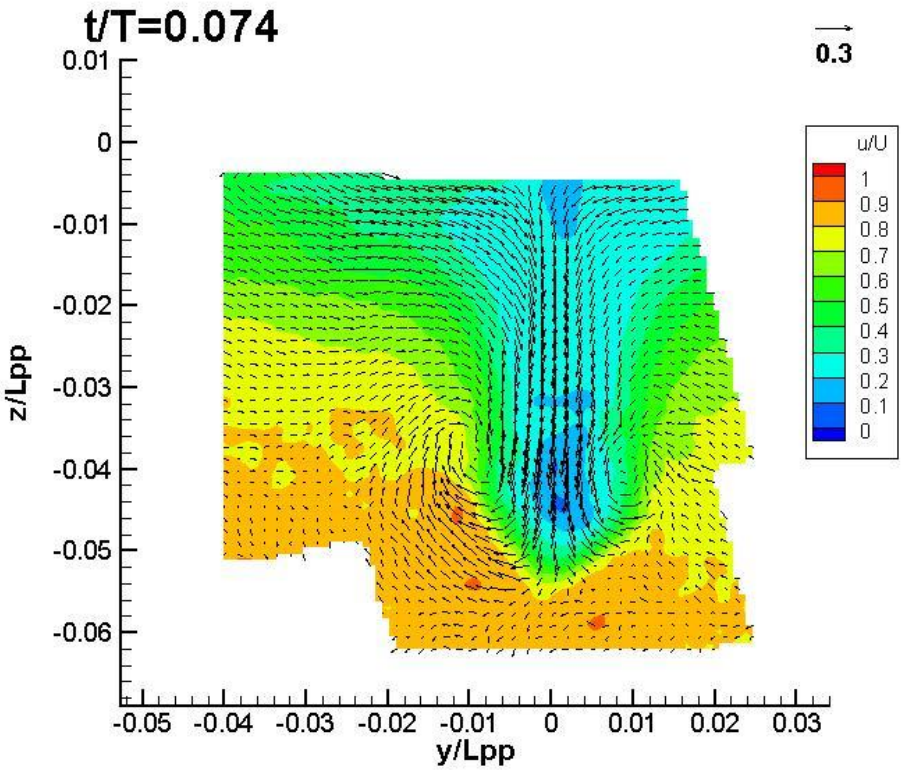
(b) Velocity distribution

Fig. 4-47 Velocity distribution (λ/L=0.9), t/T=0.9108

4.2.5 Velocity distribution at propeller plane, λ/L=1.5

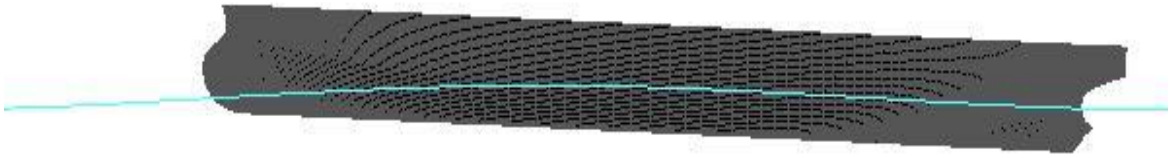


(a) Schematic view of wave and model ship

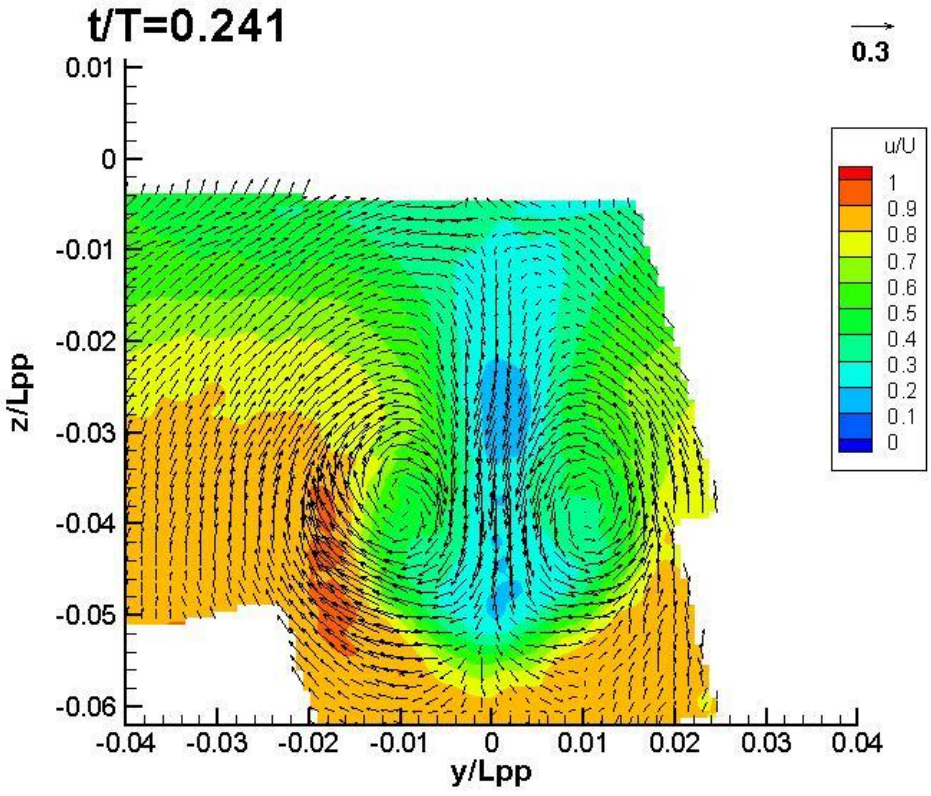


(b) Velocity distribution

Fig. 4-48 Velocity distribution (λ/L=1.5), t/T=0.074

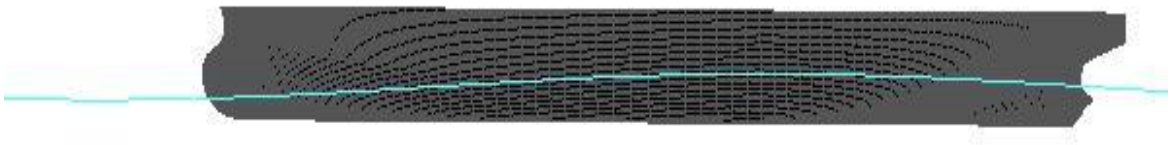


(a) Schematic view of wave and model ship

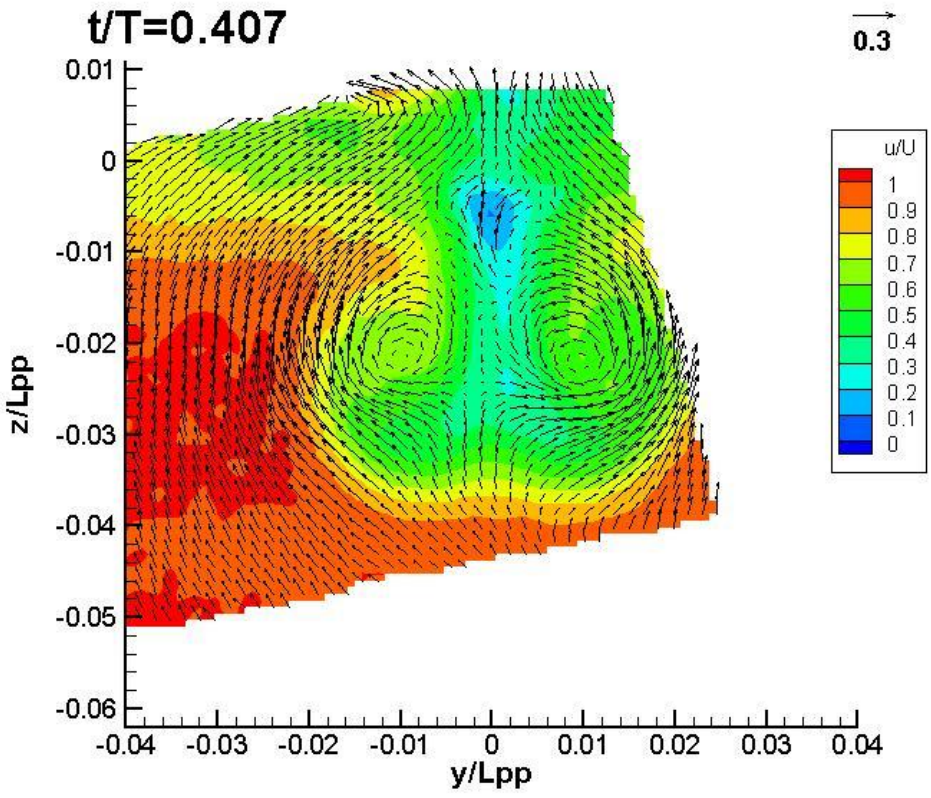


(b) Velocity distribution

Fig. 4-49 Velocity distribution (λ/L=1.5), t/T=0.241

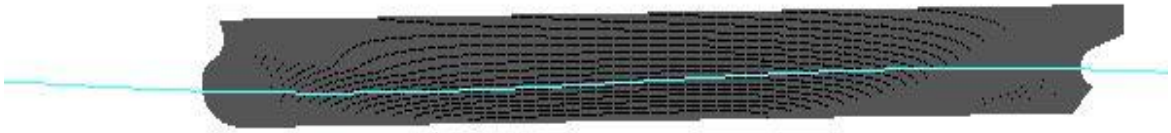


(a) Schematic view of wave and model ship

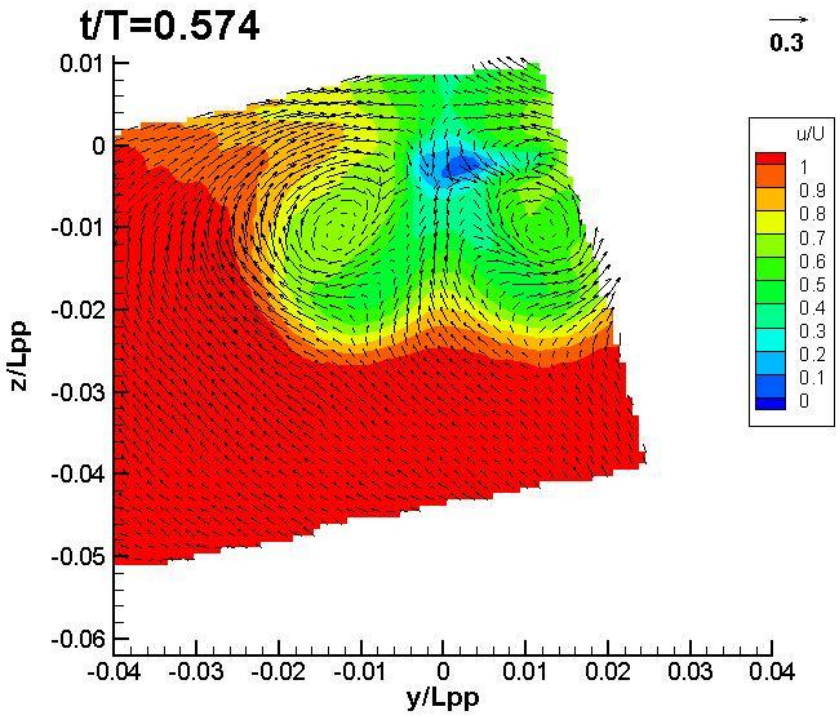


(b) Velocity distribution

Fig. 4-50 Velocity distribution (λ/L=1.5), t/T=0.407

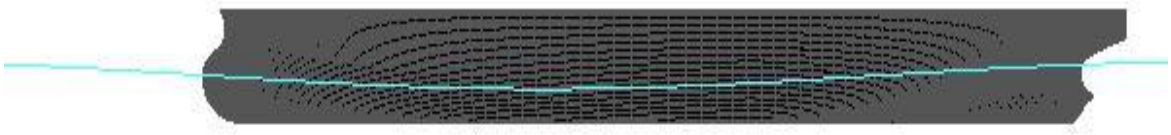


(a) Schematic view of wave and model ship

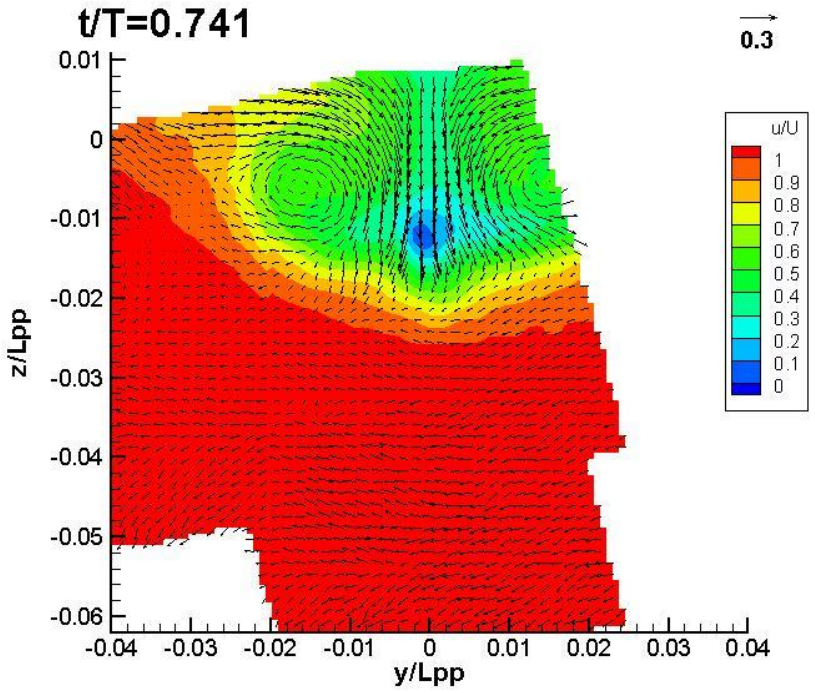


(b) Velocity distribution

Fig. 4-51 Velocity distribution (λ/L=1.5), t/T=0.574

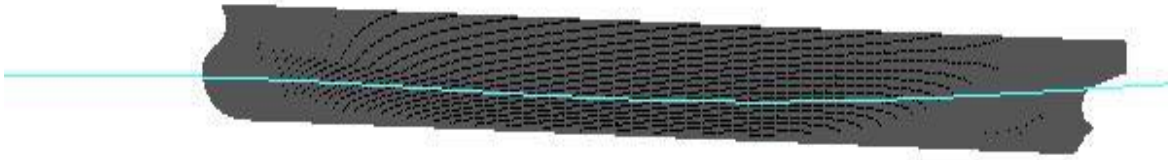


(a) Schematic view of wave and model ship

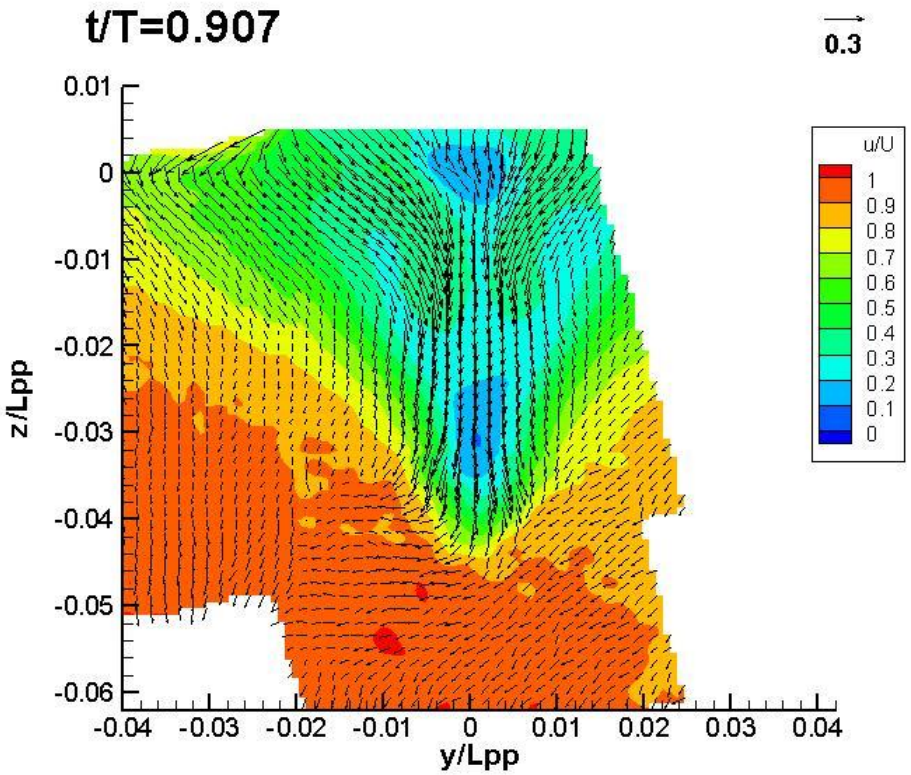


(b) Velocity distribution

Fig. 4-52 Velocity distribution (λ/L=1.5), t/T=0.741



(a) Schematic view of wave and model ship



(b) Velocity distribution

Fig. 4-53 Velocity distribution (λ/L=1.5), t/T=0.9071

CHAPTER 5: CONCLUSION AND FUTURE WORK

The motions and added resistance of KVLCC2 tanker under fully-loaded and ballast condition advancing at Fr=0.142 with fixed and free surge in head waves are validated for a wide range of wave length condition including very short waves. The verification, natural heave and pitch frequencies, effects of higher ship speed and the conditions for maximum added resistance and ship motions are investigated.

The velocity fields near the propeller plane were measured through the use of stereo-PIV System to investigate the effects of waves and ship motion to the propeller inflow velocity distribution for full form ship with large bilge vortices. Phase synchronizer, which is composed of a plate and a laser sensor, was developed and by using the heave motion, the phase averaged flow fields around moving ship could be measured.

Although the uncertainty of velocity measurement seems a little bit high due to the measurement position error due to the low frequency surge motion from weak spring and mass system, the velocity fields for three wave conditions were presented and the feature of the fluctuation was discussed. It can be used for CFD validation. It seems that the velocity fluctuation in the boundary layer has the different phase from the velocity outside the boundary layer due to the pressure gradient effect to low momentum fluid and the movement of bilge vortices.

The fluctuations of velocity distribution around propeller plane were measured using SPIV system with phase synchronizer. Due to the shallower propeller position than the full load condition, the interaction between boundary layer and free surface was large.

Although the uncertainty is considered to be large, the deformation of the velocity distribution shape due to wave and ship motion could be captured to understand the propeller inflow fluctuation in waves. The comparison between present EFD data and CFD result may be required to develop the accurate code to predict the self-propulsion performance.

For the future work : To investigate further these complex phenomena, it seems that the measurement in various cross section planes and with operating propeller is required.

References

Adegeest, L. J. M., (1995), "Nonlinear Hull Girder Loads in Ships", Ph.D. thesis, Delft University of Technology, Delft, Holland.

Calcagno, G., Di Felice, F.D., Felli, M., and Pereira, F., (2002), "Propeller Wake Analysis Behind a Ship by Stereo PIV," 24th ONR Symposium on Naval Hydrodynamics, Fukuoka, Japan, pp. 112-127.

Cotroni, A., Di Felice, F., Romano, G.P., and Elefante, M., (2000), "Investigation of the near wake of a propeller using particle image velocimetry," Experiments in Fluids, Vol. 29, pp. S227-S236.

Calcagno, G., Di Felice, F.D., Felli, M., and Pereira, F., (2002), "Propeller Wake Analysis Behind a Ship by Stereo PIV," 24th ONR Symposium on Naval Hydrodynamics, Fukuoka, Japan, pp. 112-127.

Di Felice, F., Romano, G., and Elefante, M., (2000a), "Propeller Wake Analysis by Means of PIV," 23rd ONR Symposium on Naval Hydrodynamics, Val de Reuil, France, pp. 493-510.

Di Felice, F. and De Gregorio, F., (2000b), "Ship Model Wake Analysis by Means of PIV in Large Circulating Water Channel," Proc. 10th Int. Offshore and Polar Eng. Conf., Seattle, WA, pp. 392-397.

Fu, T.C., Atsavapranee, P., and Hess, D.E., (2002), “PIV Measurements of the Cross-Flow Wake of a Turning Submarine Model (ONR Body-1),” 25th ONR Symposium on Naval Hydrodynamics, Fukuoka, Japan, pp. 154-166.

Gui., L., Longo, L., Metcalf, B., Shao, J., and Stern, F., (2002), “Forces, Moment, and Wave Pattern for Naval Combatant in Regular Head waves-Part 2: Measurement Results and Discussions,” Experiments in Fluids, Vol. 32, pp. 27-36.

Hirota K., Matsumoto K., Takagishi K., Yamasaki K., Orihara H., Yoshida H., (2005), “Development of bow shape to reduce the added resistance due to waves and verification of full scale measurement”, Proceeding of International Conference on Marine Research and Transportation, pp63-70.

Kim, Y.H., (1998), “Added Resistance and Power of a Frigate in Regular Waves”, Proceedings of 3rd ICHD, Seoul, pp. 209-215.

Longo, J., Gui, L., and Stern, F., (2004a), “Ship Velocity Fields,” PIV and Water Waves, Advances in Coastal and Ocean Engineering, World Scientific.

Longo, J., Shao, J., Irvine, M., Gui, L., and Stern, F., (2004b), "Phase-Averaged Towed PIV Measurements for Regular Head Waves in a Model Ship Towing Tank," PIV and Water Waves, Advances in Coastal and Ocean Engineering, World Scientific.

Longo, J., Yoon, H.-S., Toda, Y.,Stern, F., (2006), “Phase-Averaged 3DPIV/Wave Elevations and Force/Moment Measurements for Surface Combatant in PMM

Maneuvers," *Proceedings of 26th Symposium on Naval Hydrodynamics* Rome, Italy, 17-22, September.

Mizokami S, Yasukawa H, Kuroiwa T, et al, (2001), "Wave loads on a container ship in rough seas", J Soc Nav Archit Jpn 189:181–192. (in Japanese)

Matsumoto, K., Naito, S., Takagi, K., Hirota, K. and Takagishi, K., (1998), "BEAK-BOW to reduce the Wave Added Resistance at Sea", Proceedings PRADS '98, The Hague, pp. 521-526.

Nakamura, S.., R, Hosoda. and S, Naito.,(1975), "Propulsive Performance of a Container Ship in Waves", *J of KSNAJ,* Vol.158

Naito, S., Kodan, N., Takagi, K. and Matsumoto, K., (1996), "An Experimental Study on the Above-Water Bow Shape with a Small Added Resistance in Waves", JKSNAJ, No. 226, pp. 91-98.

O'Dea, J.,Powers, E., Zselecsky, J. (1992), "Experimental determination of non-linearities in vertical plane ship motions". Proceedings of 8th International Conference on numerical ship hydrodynamics, Busan, Korea.

Ogiwara, S. and Yamashita, S., (1996), "On Resistance Increase in Waves of Short Wavelength", JKSNAJ, No.225, pp. 37-46.

Paik, B.G., Lee, C.M., Lee, S.J., 2004. PIV analysis of flow around a container ship model with a rotating propeller. Experiments in Fluids 36, 833–846.

Sadat-Hosseini, H., P, M. Carrica., H, Kim., Y, Toda. and F, Stern., (2010), "Urans Simulation and Validation of Added Resistance and Motions of the Modern Commercial Oil Carrier KVLCC2 with Fixed and Free Surge Condition, " *Proceedings of CFD Workshop 2010, Gothenburg, Sweden,2010.*

Sadat-Hosseini, H., Wu, P.-C., Carrica, P.M., Kim, H., Toda, Y. and Stern, F., (2013), "CFD verification and validation of added resistance and motions with fixed and free surge in short and long head waves, " *Ocean Engineering*, Vol.59, No.1

Tsukada, Y., Hinatsu M., Hasegawa, J., (1997) "Measurement of Unsteady Ship Wakes in waves" KSNAJ Vol.228, pp. 15-20.

Ueno, M., Tsukada, Y., Tanizawa, K.(2013), "Estimation and prediction of effective inflow velocity to propeller in waves", *Journal of Marine Science and Technology*, Vol.18, issue3

Wu, Ping-Chen.,(2013) "A CFD Study on Added Resistance, Motions and Phase Averaged Wake Fields of Full Form Ship Model in Head Waves" Doctor thesis, Osaka University Japan.

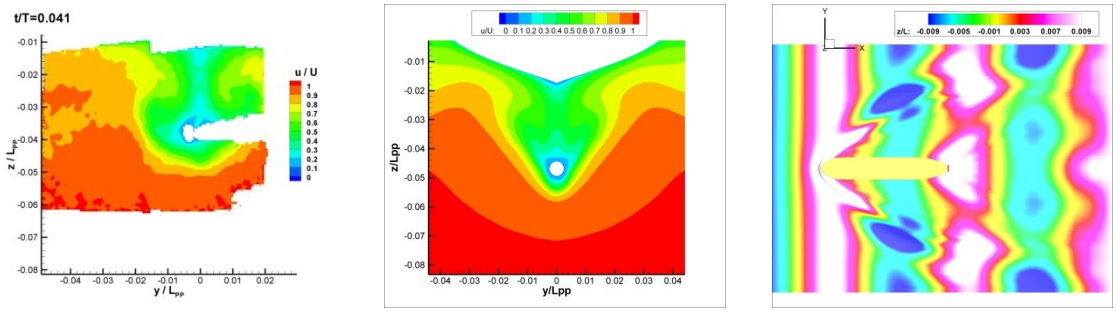
Acknowledgement

Foremost, I would like to deep express my sincere thanks to my advisor Prof. Yasuyuki Toda for the continuous support of my Ph.D study and research, for his patience, motivation, enthusiasm, and immense knowledge. His guidance helped me in all the time of research and writing of this thesis. And also, He has provided insightful discussion about the research and all experiments. I am very grateful for his guidance. I could not have imagined having a better advisor and mentor for my Ph.D study. Besides my advisor, I would like to thank my thesis committee member: Prof. Kazuhiko Hasegawa, Prof. Kiyoshige Matsumura and Prof. Hiroyoshi Suzuki for their encouragement, insightful comments, and good questions. My sincere thanks also goes to Prof. Yugo Sanada, Dr. Ping Chen Wu in IOWA University and Yoshiki Hayashi, Keiske Akamatsu, Hiroshi Okawa and my labmates in Japan. I really thank to their big help and effort. Especially, I really thank to Dr. Wu. I was able to compare EFD and CFD for good his data successfully. And also, Hayashi, Akamatsu and Okawa, we were working together in towing tank for a long time. I shall never forget your kindness and hard working as long as I live. I would like to thank my Korean Prof. Gyoungwoo-Lee and Daehwan-Cho, for strictly advice and warm encouragement when I was big depressed. Also, I appreciate to Dr. Jooshin-Park, Dr. Oksok-Gim and Dr. Kukhyun-Song for their support and big cheer up and I would like to thank my friend of Osaka University doctor course student, Minsun-Lee, Sanghoon-Lee, Kyounggun-Oh, and Daejin-Yoon. Lastly, I am deeply thankful to my family for all their love, support, sacrifices and encouragement. Whenever my mother raised me who is in a delicate state of health. Without them, this thesis would never have been written. This last word of acknowledgement I would like to dedicate this thesis to my wife Hwajoo and daughter Hnabyeol, for their love, big patience and understanding. I love you and thank you.

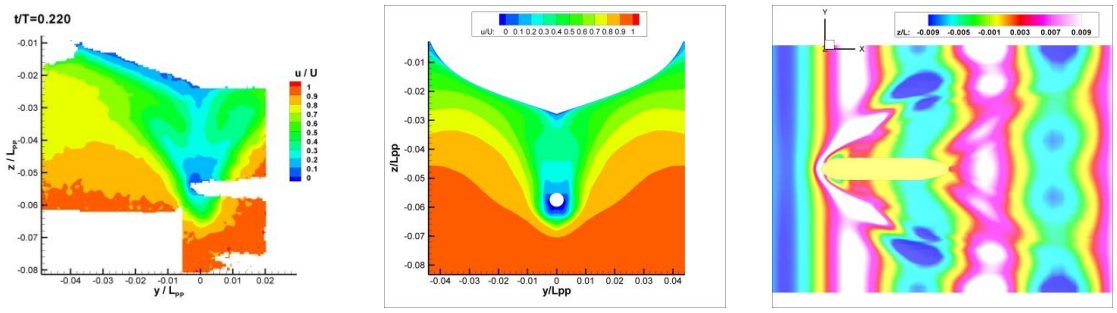
Appendix (1)

- Comparison of EFD and CFD result with wave pattern (Fully-loaded condition)

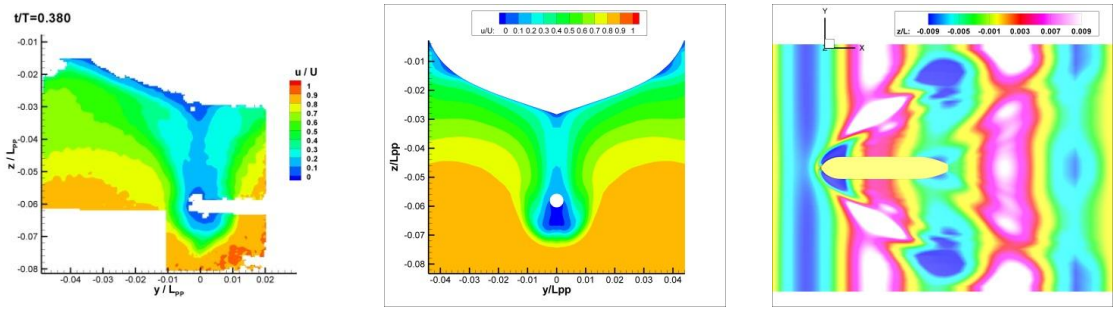
- CFD result are provided with Dr. Ping Chen wu IOWA Uni.



(a) EFD: t/T=0.041, CFD: t/T=0.06699



(b) EFD: t/T=0.220, CFD: t/T=0.22775



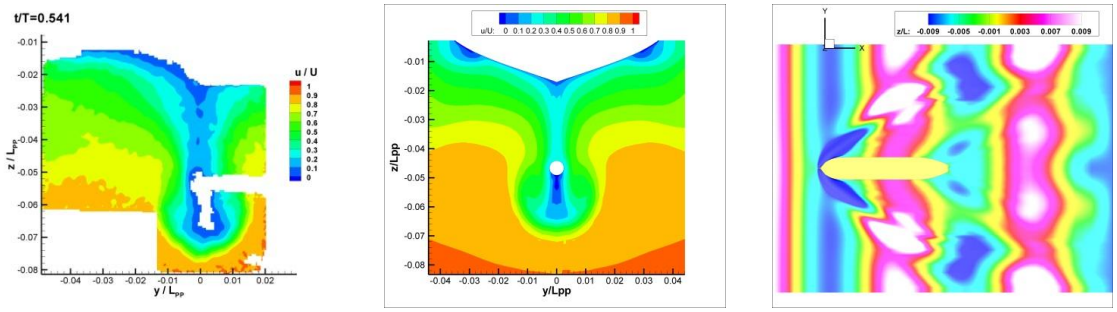
(c) EFD: t/T=0.380, CFD: t/T=0.38852

λ/Lpp = 1.1

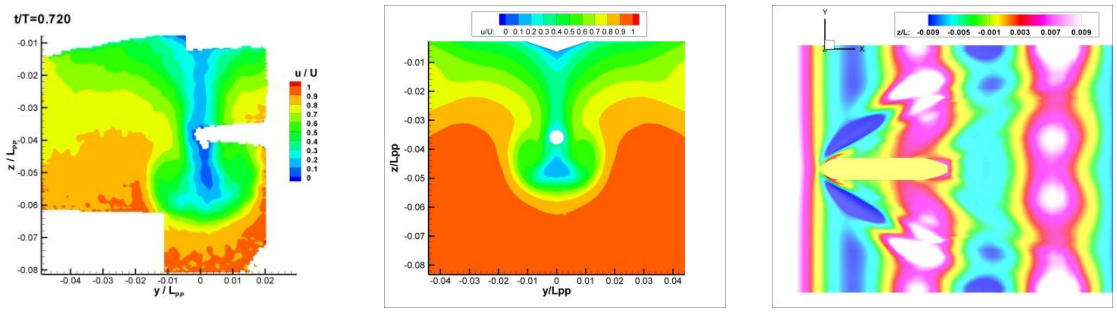
Appendix (2)

- Comparison of EFD and CFD result with wave pattern (Fully-loaded condition)

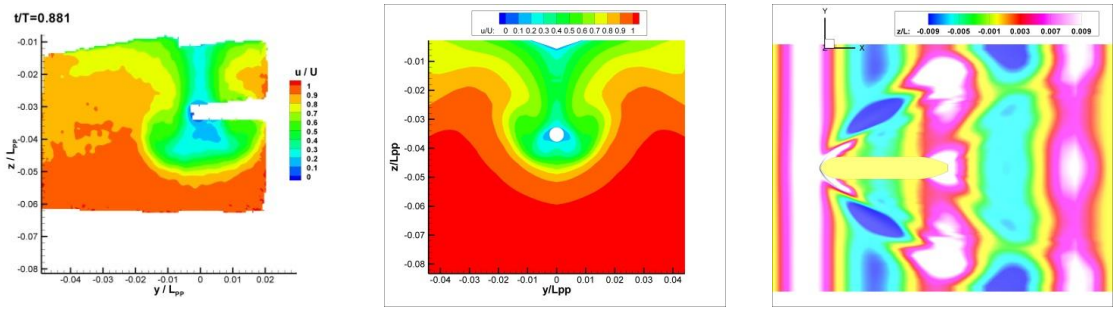
- CFD result are provided with Dr. Ping Chen wu IOWA Uni.



(d) EFD: t/T=0.541, CFD: t/T=0.56268



(e) EFD: t/T=0.720, CFD: t/T=0.72344



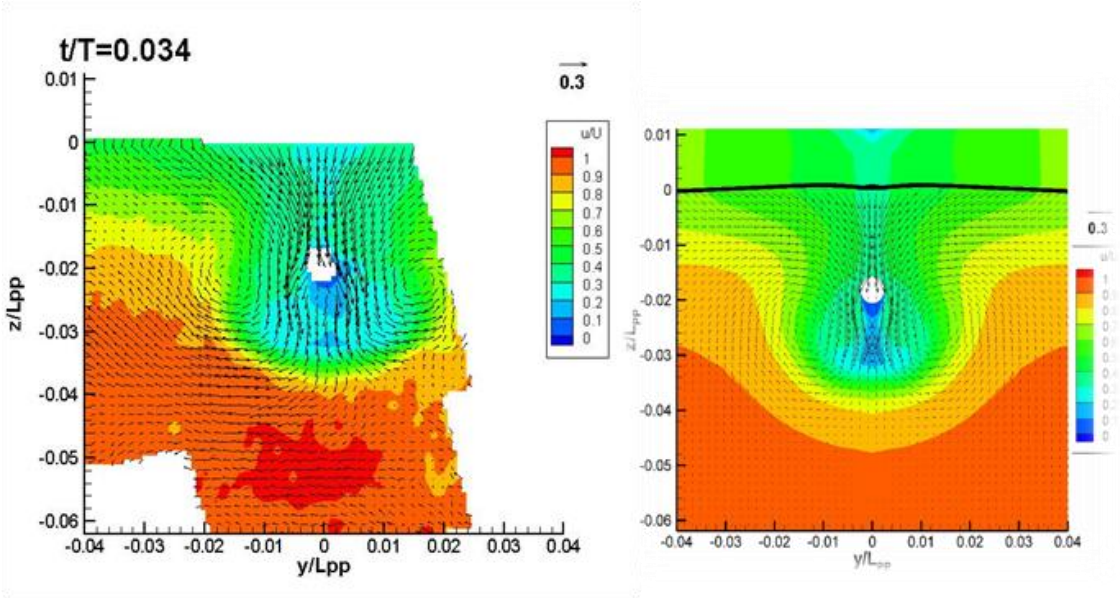
(f) EFD: t/T=0.881, CFD : t/T=0.88421

λ/Lpp = 1.1

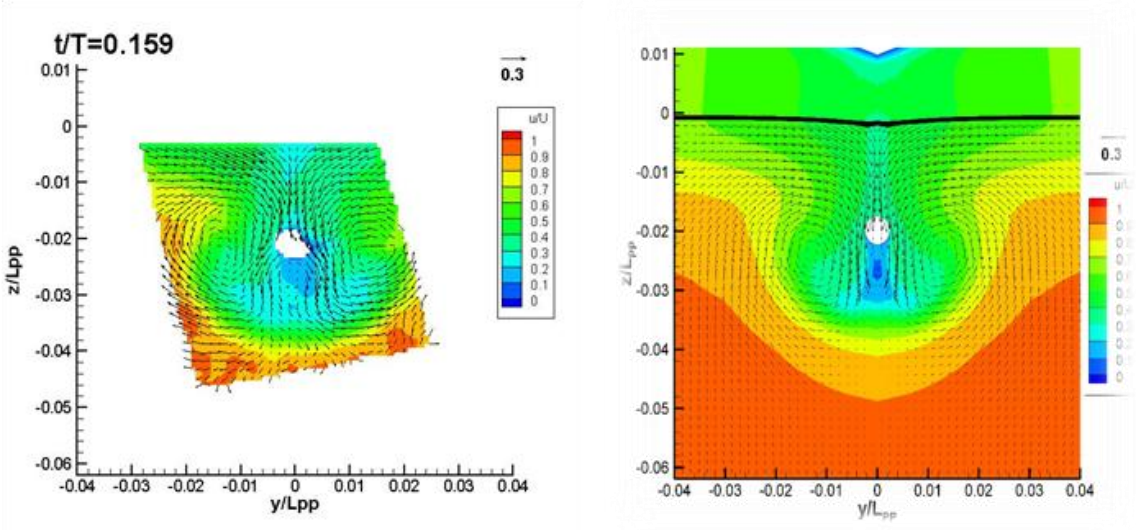
Appendix (3)

- Comparison of EFD and CFD result with wave pattern (Ballast condition)

- CFD result are provided with Dr. Ping Chen wu IOWA Uni.



(1) λ/L= 0.6 (EFD) t/T= 0.034 (CFD) t/T=0.04

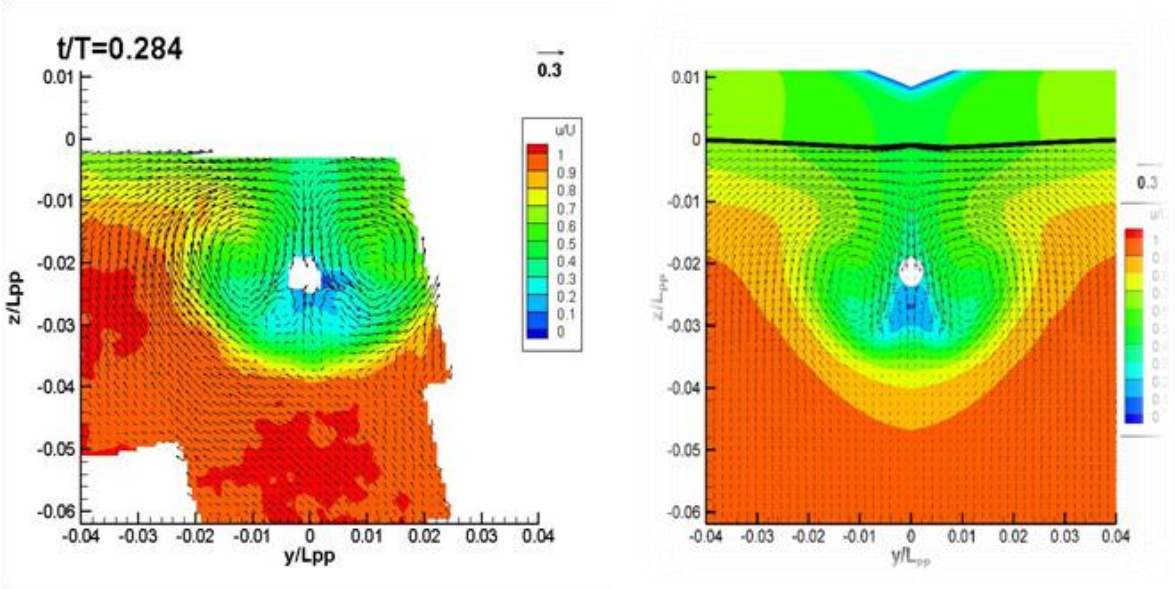


(2) λ/L= 0.6 (EFD) t/T= 0.159 (CFD) t/T=0.16

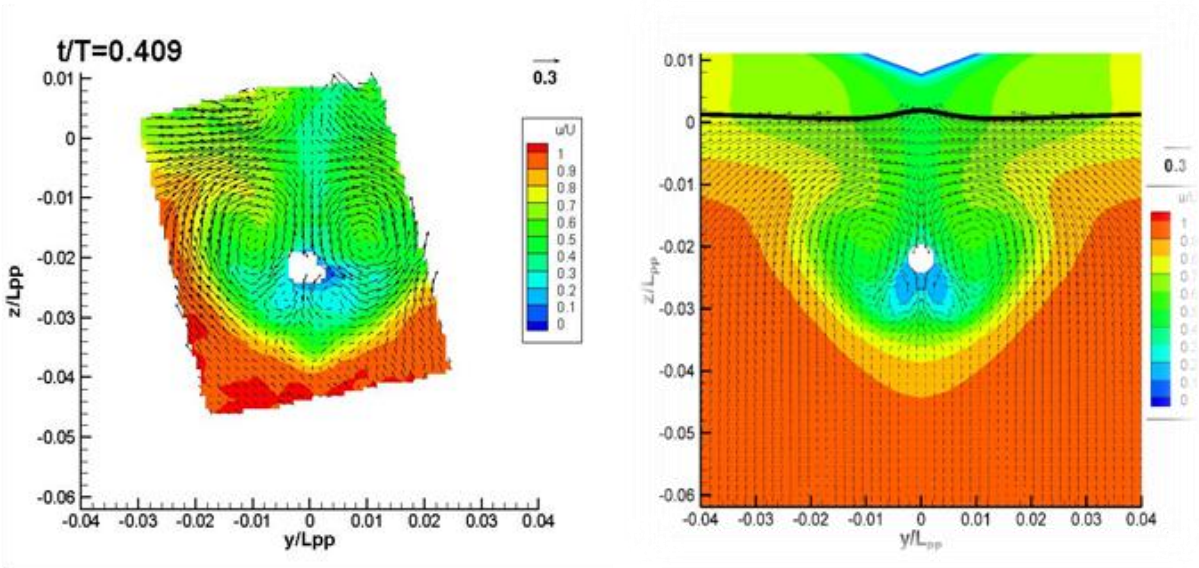
Appendix (4)

- Comparison of EFD and CFD result with wave pattern (Ballast condition)

- CFD result are provided with Dr. Ping Chen wu IOWA Uni.



(3) λ/L= 0.6 (EFD)t/T= 0.284 (CFD)t/T=0.28

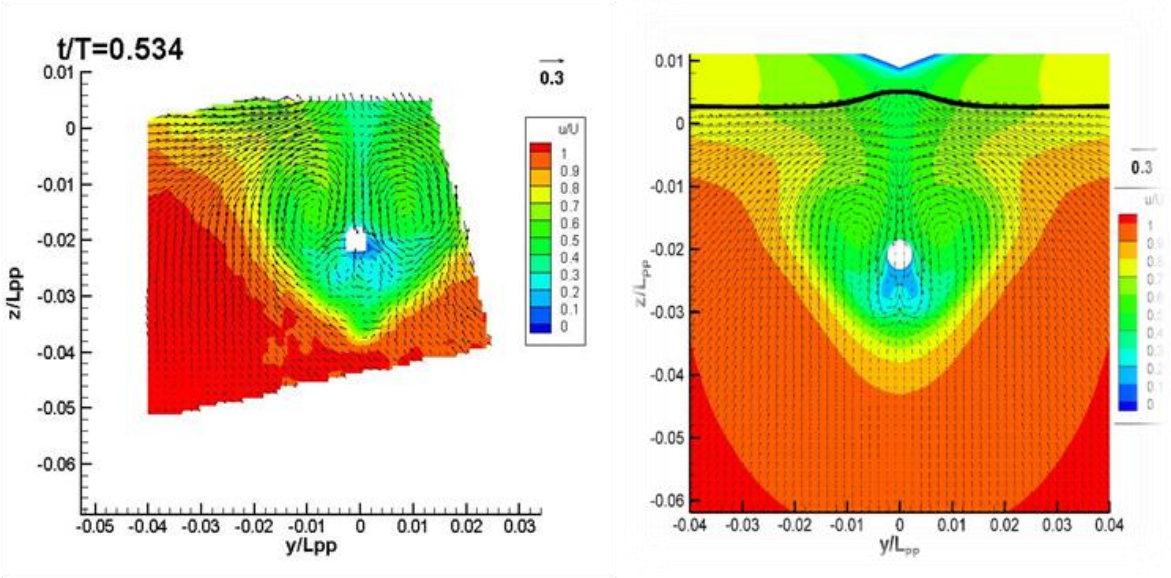


(4) λ/L= 0.6 (EFD)t/T= 0.409 (CFD)t/T=0.40

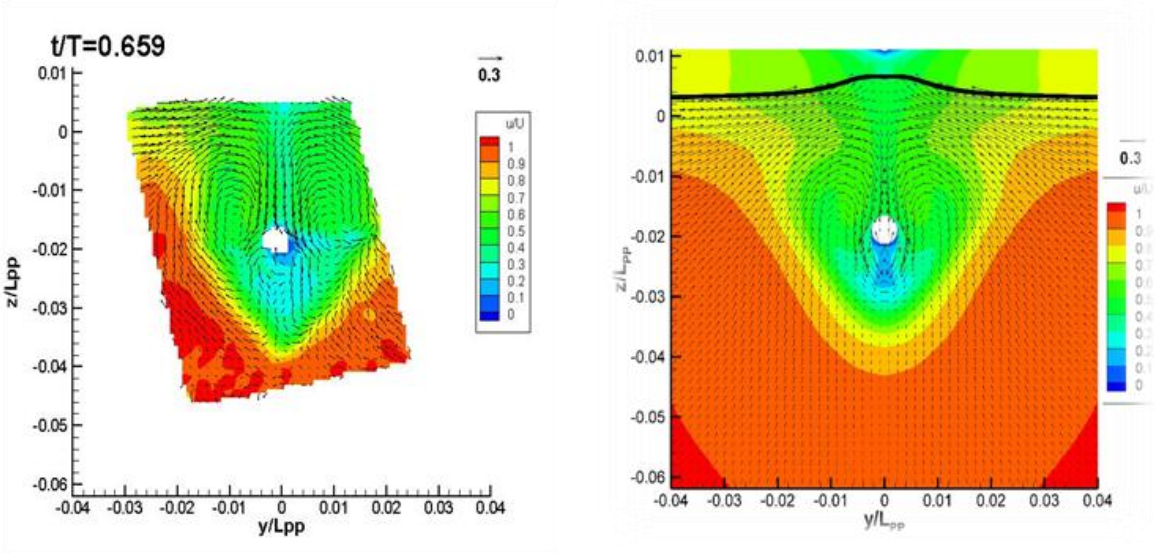
Appendix (5)

- Comparison of EFD and CFD result with wave pattern (Ballast condition)

- CFD result are provided with Dr. Ping Chen wu IOWA Uni.



(5) λ/L= 0.6 (EFD) t/T= 0.534 (CFD) t/T=0.54

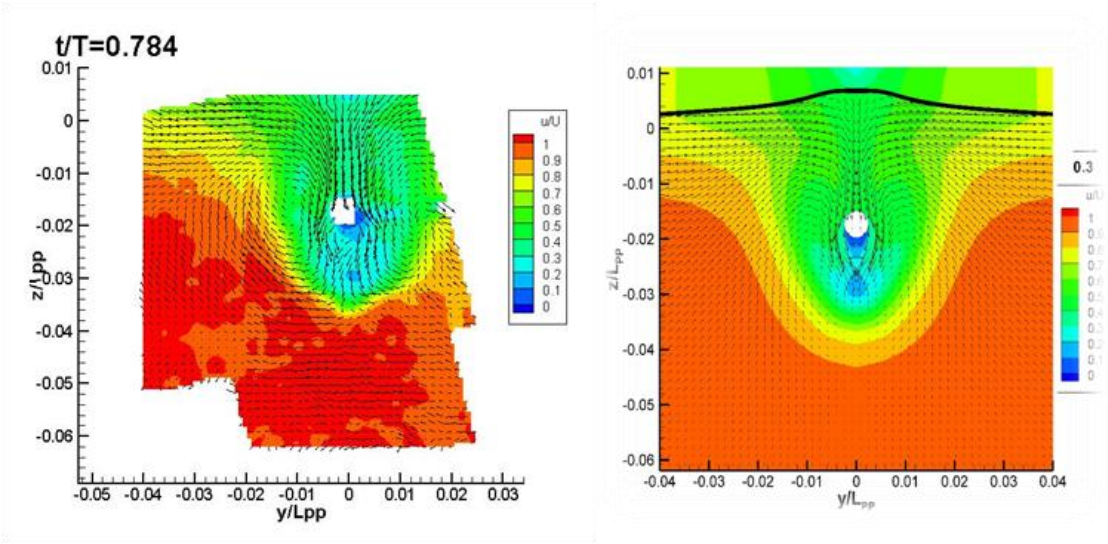


(5) λ/L= 0.6 (EFD) t/T= 0.659 (CFD) t/T=0.66

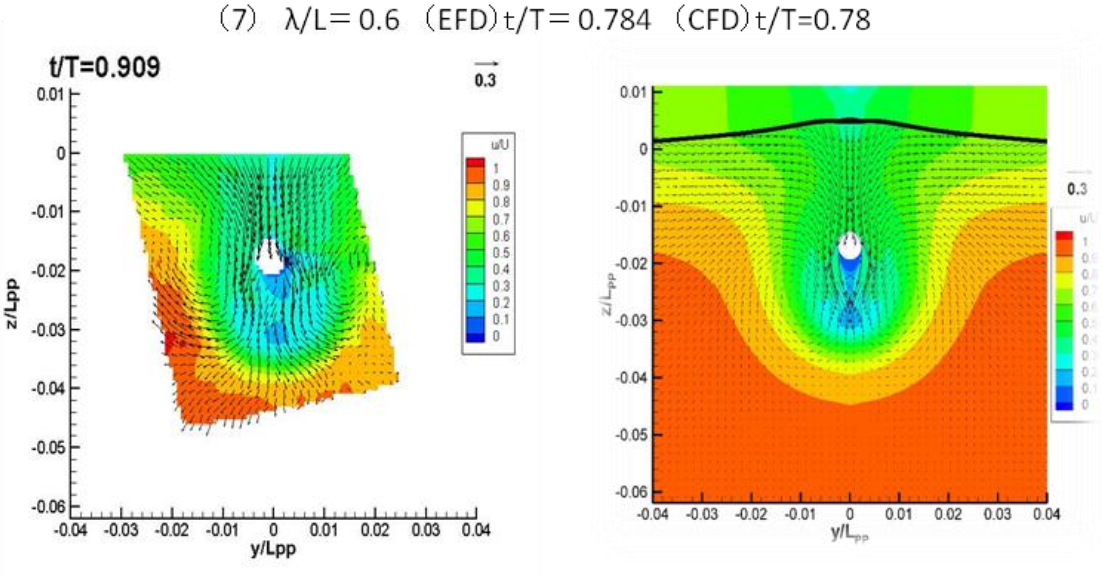
Appendix (6)

- Comparison of EFD and CFD result with wave pattern (Ballast condition)

- CFD result are provided with Dr. Ping Chen wu IOWA Uni.



(7) λ/L= 0.6 (EFD) t/T= 0.784 (CFD) t/T=0.78

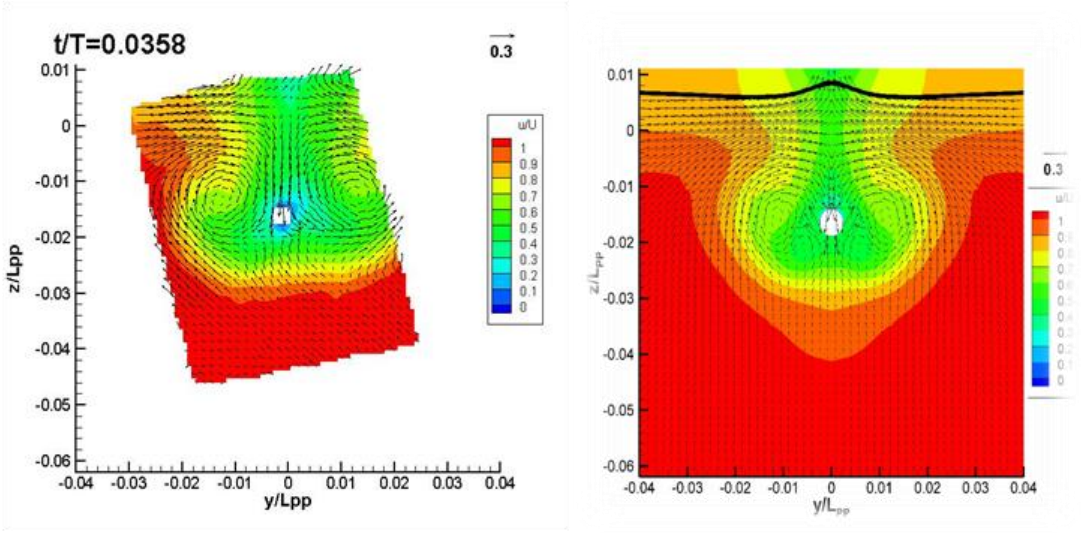


(8) λ/L= 0.6 (EFD) t/T= 0.909 (CFD) t/T=0.90

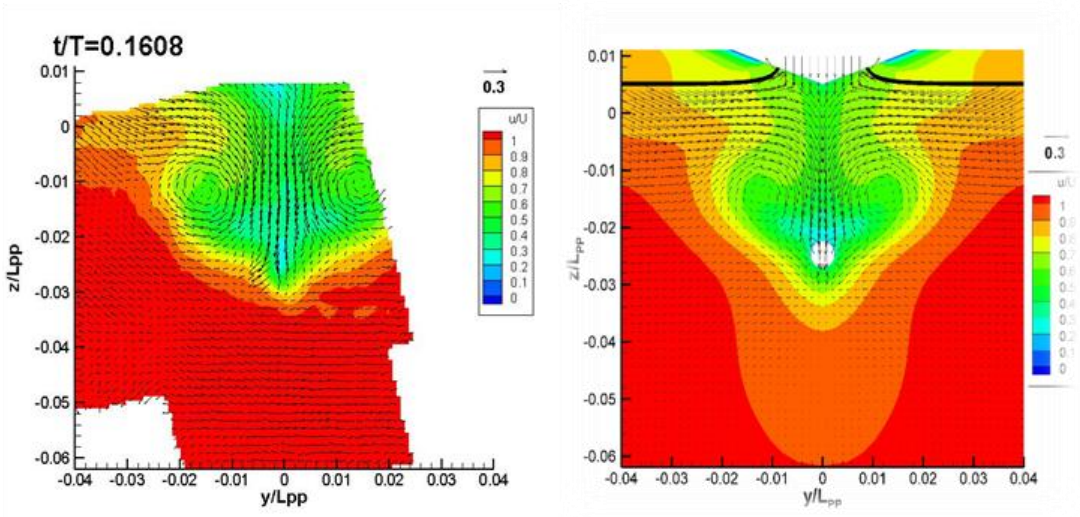
Appendix (7)

- Comparison of EFD and CFD result with wave pattern (Ballast condition)

- CFD result are provided with Dr. Ping Chen wu IOWA Uni.



(1) λ/L= 0.6 (EFD)t/T= 0.909 (CFD)t/T=0.90

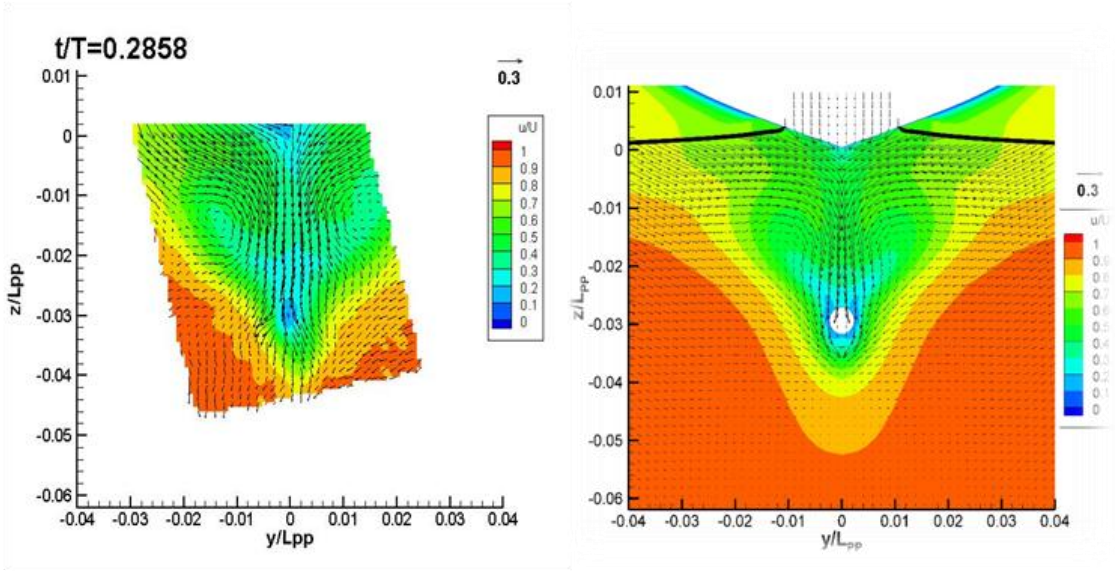


(1) λ/L= 0.9 (EFD)t/T= 0.1608 (CFD)t/T=0.1667

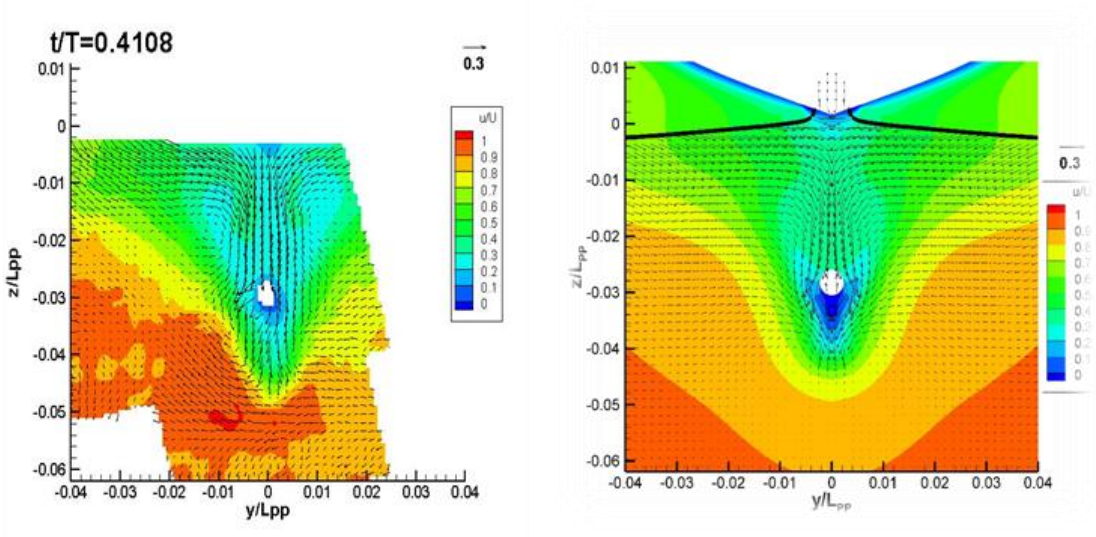
Appendix (8)

- Comparison of EFD and CFD result with wave pattern (Ballast condition)

- CFD result are provided with Dr. Ping Chen wu IOWA Uni.



(3) λ/L= 0.9 (EFD)t/T= 0.2858 (CFD)t/T=0.2878

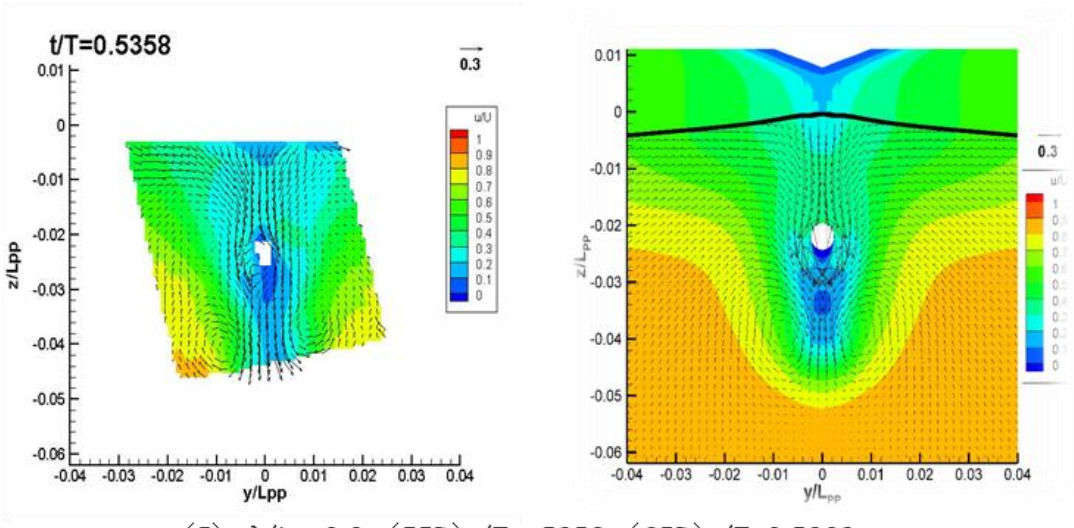


(4) λ/L= 0.9 (EFD)t/T= 4108 (CFD)t/T=0.4090

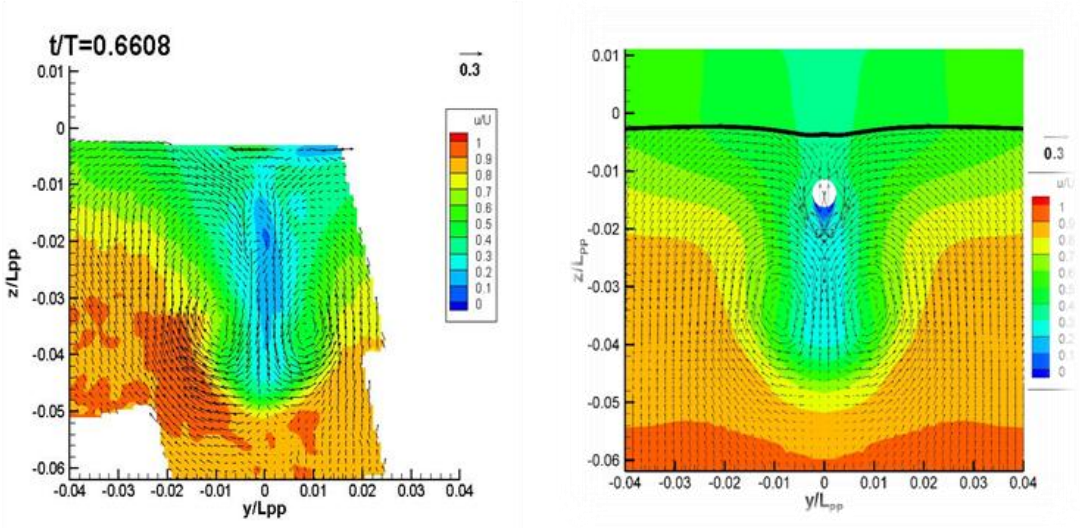
Appendix (9)

- Comparison of EFD and CFD result with wave pattern (Ballast condition)

- CFD result are provided with Dr. Ping Chen wu IOWA Uni.



(5) λ/L= 0.9 (EFD)t/T= 5358 (CFD)t/T=0.5303

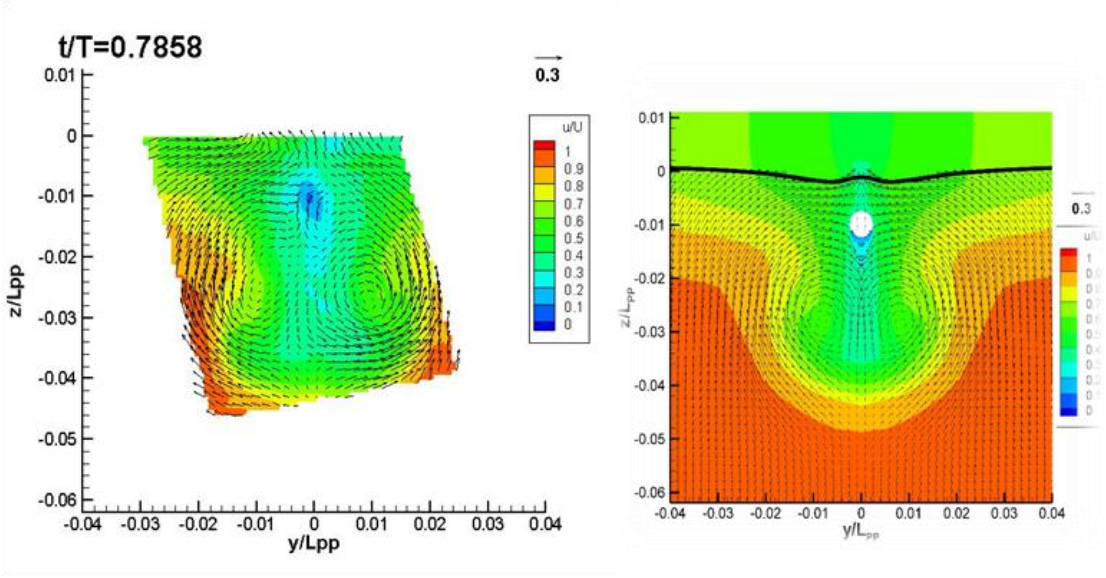


(6) λ/L= 0.9 (EFD)t/T= 6608 (CFD)t/T=0.6666

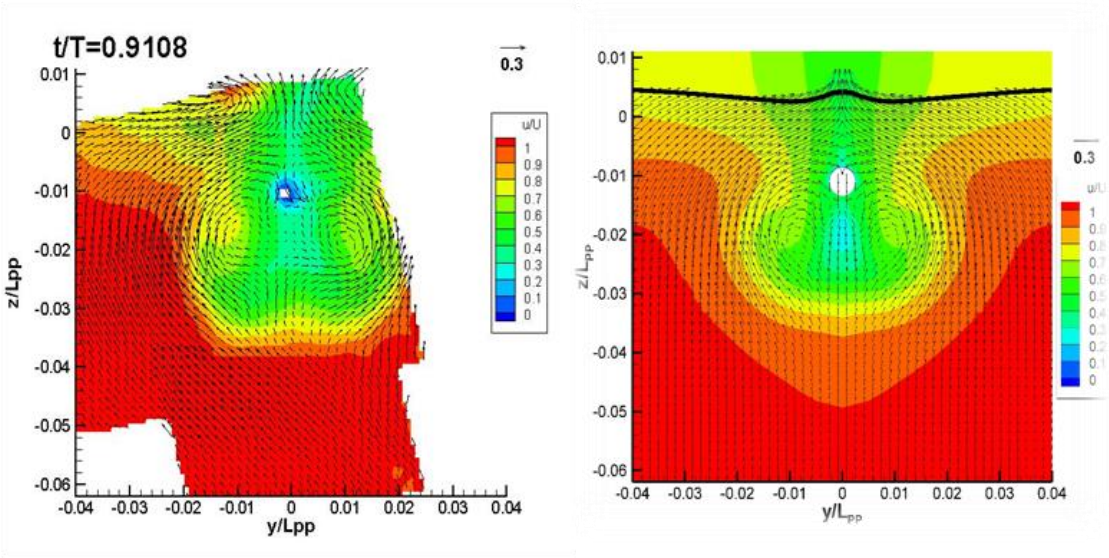
Appendix (10)

- Comparison of EFD and CFD result with wave pattern (Ballast condition)

- CFD result are provided with Dr. Ping Chen wu IOWA Uni.



(7) λ/L= 0.9 (EFD)t/T= 7858 (CFD)t/T=0.7878



(8) λ/L= 0.9 (EFD)t/T= 9108 (CFD)t/T=0.9090

List of publication

- Sadat-Hosseini, H ., P,M.Carrica., **Kim Ho**., Y, Toda., and F. Stern., (2010)
  " Urans Simulation and Validation of Added Resistance and Motions of the Modern Commercial Oil Carrier KVLCC2 with Fixed and Free Surge Condition."
  Gothenburg 2010 : Proceeding of the Workshop on Numerical Ship Hydrodynamics, Vol. II ,(2010)

- **Kim Ho**., Y. Hayashi., S.Oshita., R.Inoue.,K. Akamatsu., and Y, Toda., (2012)
  " Phase-Averaged SPIV Flow Field Measurement for KVLCC2 Propeller Plane in Waves."
  Proceeding of the 6th Asia-Pacific Workshop on Marine Hydrodynamics September 3-4.

- Wu, P-C., **Kim Ho**., Y. Hayashi., S. Oshita., and Y, Toda., (2012)
  " Added Resistance and Phase Averaged wake field of KVLCC2 model ship in waves."
  Proceeding of the 2th East Asia International Student Symposium on Marine Sciences(EAISS2012)

- **Kim, Ho**., Y. Hayashi., O. Syo., K. Akamatsu., and Y. Toda.,(2012),
  "Phase-Averaged 3D-PIV Flow Field Measurement for KVLCC2 Propeller Plane in waves / Full load".
  Proceedings of JASNAOE conference, Vol. 15

- H.Okawa., **Kim, Ho**., K. Akamatsu., and Y. Toda.,(2013),
  "Phase-Averaged Stereo-PIV Flow Field Measurement for KVLCC2 Model in waves/ Ballast ".
  Proceedings of JASNAOE conference,

- **Kim, Ho**., Y. Hayashi., O. Syo., K. Akamatsu., and Y. Toda.,(2014),
  "Phase-Averaged SPIV Flow Field Measurement for KVLCC2 Propeller in waves ".
  2014 ISOPE in Korea ., 2014.4

- K. Akamatsu., **Kim, Ho**., H.Okawa., and Y. Toda.,(2014),
  "Phase-Averaged Stereo-PIV Flow Field Measurement for Ballast condition of KVLCC2 in waves ".
  2014 ISOPE in Korea.: 2014.4

Journal Papers

- Sadat-Hosseini, H., Wu, P.-C., Carrica, P.M., **Kim Ho**., Toda, Y. and Stern, F., (2013),
  "CFD verification and validation of added resistance and motions with fixed and free surge in short and long head waves, " Ocean Engineering, Vol.59, No.1

Curriculum vitae

Educations

Doctoral Course, Naval Architecture and Ocean Engineering 2009 – present

Osaka University–Suita, Japan

Adviser : Dr. Yasuyuki Toda

Areas of research: Experimental fluid dynamics, ship hydrodynamics.

Current topic: Phase – Averaged SPIV flow field measurement for KVLCC2 propeller plane in wave

Master of Science, Naval Architecture and Ocean Engineering

Mokpo National Maritime University – South Korea

Adviser: Dr. Gyoungwoo–Lee

Areas of research: Experimental fluid dynamics, Analysis of flow field

Current topic: PIV Application for flow analysis of floating offshore structure with vertical plate

Bachelor of Science, Naval Architecture and Ocean Engineering

Mokpo National Maritime University – South Korea